Overview of the status of the FAIR Project

Dr.- Ing. J. Henschel, Technical Director & FAIR Project Lead; Dr. P. Spiller, SPL SIS 100; Dr. H.Simon, SPL SFRS; Dr. K.Knie, SPL PLinac;Dr. I. Koop, SPL CR; Dr. D.Prasuhn, SPL HESR; Dr.H.Reich Sprenger, SPL Commons; Dr. A.Brauening Demian, APPA; Dr. H.Gerl, APPA; Dr. W.Mueller, CBM; Dr. L.Schmitt, PANDA
[1]GSI, Darmstadt, Germany;.

Summary

The construction of FAIR is one of the four strategic objectives of FAIR GmbH & GSI GmbH in Darmstadt as illustrated in figure 1.

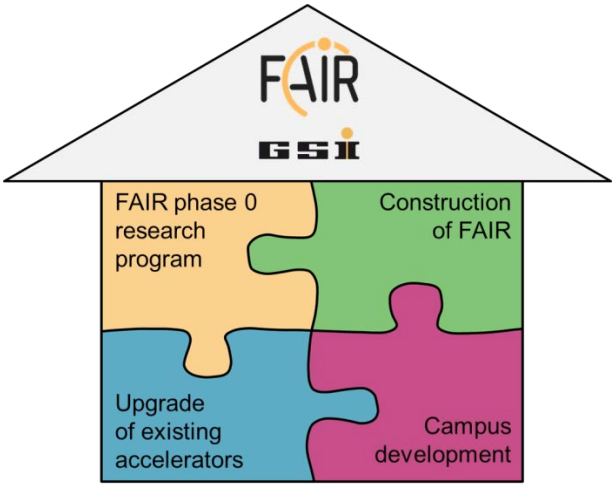

Figure 1: Strategic objectives of GSI & FAIR

For the progress in the FAIR Project the following core activities are worth to mention.
The rework of the complete Project planning after the major review in 2015 was finished on time in late 2016, resulting in the resource loaded and integrated project master time schedule. All three, now integrated areas, Accelerator, Civil construction and the Experiments are progressing according to the expectations documented in this plan.

Most remarkable is the progress in the area of civil construction so far. The target to start preparation work on site was reached already late in 2016. Currently all "connection" tasks from the GSI premises to the FAIR construction site are under execution ("GAF Gebäude Anbindung FAIR").
The enhancement of the SIS 18 (new coverage for increased radiation protection, a supporting wall, and the opening to the FAIR site), the main transformer stations north & south and the preparation of the remaining foundations are in execution. All preparatory and regulatory work for the area north (SIS100 Tunnel & CBM) is on target schedule. All work is aiming towards the start of the excavation of the tunnel 110 in summer 2017.

As remarkable as the progress of the civil construction, the continuity in the design and procurement of the accelerator components has to be highlighted. After the finalization of the new planning setup late 2016, the resources needed for the work packages were identified and committed. The balancing of the resources down to every single name was successfully executed until end of Q1 2017 in a first run. As a result a resource loaded and executable plan is now present, documented and the foundation of the work currently being executed.
The final step to a complete planning rework was done with the major rework on cost. All opportunities and potential threads were re-evaluated and documented. The FAIR Project Risk- and Opportunity report documents the results.
The progress in the experimental areas is as remarkable as the above mentioned ones. All four pillars are in intensive planning work and currently consolidating the procurement activities.
The focus for the remaining year 2017 can be summarized as follows. The major and most visible task will be the start of the excavation of the SIS100 tunnel.
The major contracts closed late 2016 / early 2017 with the In-kind Partners, namely BINP Institute Novosibirsk Russia, CEA and CNRS France and GSI Germany are in ramp up and execution as envisioned. Contract with Industrial partners are alike in status & progress.
The last "Mega-tender" with a value of not less than 30 M€ will be the main Cryogenic plant. Alongside with the planned increase of procurement activity this tender is planned for release during 2017. The award is targeted for late this year. With this tender, the last major component of the machine is in procurement.

Status of the FAIR Project

The Report of the FAIR project status is subdivided in the overview of the six SubProjects (SIS 100, SFRS, PLinac, CR, HESR, and Commons), FAIR Site & Buildings, and the four experimental areas, according to the organizational structure on site.

FAIR Accelerator Subprojects

The progress of the subprojects SIS100, Super Fragment Separator, Proton-Linac and p-bar Target, Collector Ring, High Energy Storage Ring and the cross functional sub-

DOI:10.15120/GR-2017-1

project Commons is documented in the following overview. The activities, progress and current status of civil construction works for the FAIR Project and the experimental areas are made transparent also.

SIS100

The subproject SIS100 owns the responsibility of two major tasks. The primary one is the design and build of the Synchrotron SIS100.
He secondary one is the enabling of the existing Synchrotron SIS18 as injector for FAIR and the connection between the GSI facility and the FAIR buildings.

SIS100
Major progress has been achieved in contracting of new components for SIS100 and developing FOS (First of Series) devices towards serial-production.
After the successful manufacturing and cold testing of the FOS superconducting dipole magnet, the serial production of 110 magnets has been released. The manufacturer, BNG, has just completed its move of the production line to a new dedicated building and released the production of the steel for the yokes and the superconducting coils. Starting in summer this year, one sc. dipole magnet will be delivered per week to GSI for cold testing. Therefore, the set-up of the team for series testing of the dipole magnets over the three years production time is currently in progress.
The manufacturing of the superconducting quadruple magnets in Dubna has progressed with the first two integrated units, consisting of two quadruple magnets, a steerer- and a sextupole magnet. In parallel, the preparation for cold testing of these units is progressing. The set-up of the dedicated NICA-FAIR superconducting magnet test facility could be completed end of November 2016.
The design of the quadrupole modules has been conducted together with industrial partners. The tendering of manufacturing and integration, which is one of the biggest technical efforts for the FAIR accelerators, was launched recently.
The status of design and manufacturing of the radiofrequency systems, used for acceleration and compression of the beam has progressed well. After successful completion and testing of the FOS bunch compression cavity, the series production of the remaining eight cavities has been launched. The design and manufacturing of the FOS acceleration cavity was finalized together with the industrial partner. The cavity undergoes presently an intensive FAT (Factory Acceptance Test) including ramping with targeted machine cycles.
The procurement of several other SIS100 components has been launched. The goal is to complete the procurement according to functional section. All major components of the injection system, the injections kicker modules and the injection septum magnets have been tendered and awarded. As next large system, the components of the extraction system shall be procured, starting with the electrostatic extraction septum in summer 2017.
The local cryogenics system is one of the most complex and unique technical systems of SIS100. Especially the bypass lines, bridging the warm sections of SIS100, differ from conventional cryogenic transfer line by the integrated superconducting bus bar system. A FOS bypass line has been manufactured and delivered. Although the FOS bypass line has been accepted, the internal design had to be further improved for serial production. The design of the overall local cryogenics system, including the end boxes, current feed boxes and all bypass lines segments is progressing very efficient.

SIS18
To finalize the SIS18upgrade program and to enable the execution of major civil construction measures, the machine operation has been interrupted in 2017. In order to prepare SIS18 for the fast cycling FAIR injector operation, in the early project phase of FAIR, an upgrade program has been defined, involving all major technical subsystems. Most of the upgrade program has been successfully implemented trough the last decade. The missing technical items will be completed in the course of 2017. This involves
a) The completion of the new dipole power converter for fast ramping with a ramp rate of 10 T/s, the installation of the missing two of three new MA (magnetic alloy) acceleration cavities.
b) Manufacturing and installation of the IPM (ionization beam profile monitor) system.
c) The manufacturing and installation of a new large bipolar dipole magnet for linking the existing facilities to the transfer line to SIS100.
To cope for the operation with significantly increased average beam intensities, beside the machine upgrade, the SIS18 tunnel construction is presently undergoing a major modification. The so called GAF (Gebäude-Anbindung an FAIR) civil construction project has been launched at the end of 2016 and shall be completed in January 2018. The project involves
a) an enhancement of the soil shielding on top of the SIS18 tunnel, requiring a support structure to cover the additional load.
b) A enhanced air management system.
c) A fire protection system based on Nitrogen flooding.
d) A reinforcement wall at the Northern arc of SIS18.
e) The opening and modification of the Eastern building wall in the experimental hall, generating the interface to the FAIR tunnel 101.
Another major ongoing activity which needs to be completed in 2017 is the retrofit of the accelerator control system. The new control system architecture, including the new timing system, replaces the old VMS based controls hardware and will be implemented and tested for the first time for the re-commissioning of SIS18. The successful completion of this effort is demanding and crucial for the machine operation in 2018. In parallel, upper level controls software, required for generating the set-values for all devices based on physics models and parameterized algorithms, will be completed. This software has

DOI:10.15120/GR-2017-1

been developed in collaboration with CERN, based on the LSA (LHC Software Architecture) over the last decade and is presently tested at commissioning of the CRYRING accelerator at GSI.

Super Fragment Separator

The last six months can be characterized as a period of major targets reached for the progress of the Super Fragment Separator (Super-FRS) development.
In the frame of assembling the ATB ("Along the beamline") List several missing components, in particular the insulating vacuum for cryogenics and cables, were identified. To each element a Work Package was assigned together with a work breakdown structure (PSP Code).
The review of the expected costs was done for all elements of the ATB Elements. In particular the now defined design for the superconducting (SC) dipole magnets, the improvement in the definition of the Local Cryogenics work Package, the robot handling in the Pre-Separator, and the full inclusion of the magnet test facility construction and operation.
The scheduling structure of the sub-project was adapted and embedded into the Integrated Master Schedule structure of the FAIR project. To this aim, three important achievements were reached:
Renewed scheduling for each work package. in addition to the all technical element listed in ATB, also project-related activities were identified and assigned to the new Work Packages. Examples given are: Digital-Mock-Up, Experiment Interface, and Civil Construction Interface. All technical components and project activities were scheduled in individual project-plans according to the work package structure.
The scheduling of the installation of Super-FRS components was established. Side constraints from civil construction as well as common systems were included. The planning yields three time windows for installation of the technical components. The installation scheduling was optimised according to the available of these time frames, which determine the critical path of the Super-FRS machine. The readiness of all three branches of the Super-FRS is given in the overview plan. Since each branch serves different experiments, they could be operated independent of the availability of the other two branches. The timeline for the stepwise implementation of the three branches will be subject of the forthcoming reports.
The overview plan, so called Level-2 plan, was reworked. The plan includes mirror images of the relevant milestones and activities from the Civil Construction plan, from the procurement plans, and from the central FAIR Commissioning plan.
For each activity the assignment of work necessary to carry out the activity was rechecked and defined. The assignment of work was attributed to individual human resources. The mitigation of appearing resource conflicts in the overall project was addressed with the "resource balancing" activity in Q1 2017.

The design phase for the two pre-series SC Multiplets was completed. In December 2016 the Final Design Review (FDR) was successfully concluded which includes in particular also a Quality Control Plan. The Production Readiness Review (PRR) for the Short Multiplet is scheduled for Q2 2017 and for the Long Multiplet in Q4 2017. The existing technical risks in particular the cooldown procedure with a major impact on the schedule will be vastly reduced there. Procurement of most important components like SC wire and yoke steel was initiated. Specimen of some subsystems were built (e.g. quarter yoke of quadrupole magnet, beam tube including cleaning process and μr measurements, coil impregnation, sextupole coil, steerer support structure).
All technical documentation required for the tender of the standard SC dipole magnets were finalized and approved (including detailed specification, Conceptual Design Report (CDR), 3D model and 2D definition drawings). In the meantime all necessary tender documents are established and it was agreed on the criteria for the awarding of the contract.
The beam instrumentation for the LEB has been agreed on with the respective NUSTAR experiments. The Conceptual Design Report (CDR) for the SC magnets of the low-energy Buncher/Spectrometer is in preparation by the magnet experts from VECC Kolkata, India.
The cryogenic system including the 3 satellite boxes and the connecting cryo transfer lines were delivered to the CERN magnet testing facility; the installation is going to be finalized and commissioning of the system is in preparation. The last missing parts to complete the cryogenic system are the magnet interfaces, i.e. the so called cryo jumper lines. The tender of those is currently ongoing.
The construction of the support frame for the radiation resistant dipole magnet was finalized. However, during testing the remote alignment capability it was realized that the required moments of torque are too high. This lead to the action, that the corresponding gears were revised, which is almost completed right now.
The FAT for the First of Series (FoS) x-slit system was completed successfully.
It was agreed that the media connection board required for remote handling in the Pre-Separator will be developed by GSI. The design phase of a prototype board is running.
The FAIR IKC for the time-of-flight (ToF) detectors including the contract documentation was established.
The FAIR IKC for the Delta-E detectors (MUSIC) including the contract documentation was established and it was sent to our collaboration partner.
The Detailed Specification of the Plastic detectors was finalized and approved.
The Detailed Specification for the SC dipole vacuum chamber is finalized and in the approval process.
The Detailed Specification for the Focal Plane Chamber (which will contain all Super-FRS beam instrumentation parts) is close to be finalized. It is planned to prepare and award the in-kind contract still in 2017.

DOI:10.15120/GR-2017-1

The preliminary design of the target chamber and its plug inserts are progressing. The FDR for the plug guidance system was accepted in December 2016 and a full scale mock-up is under preparation. The PDR for the target chamber itself is expected for summer 2017.
It was decided to modify the preliminary design of the shielded transport flask in such a way that all components which have to be transported from the target area of Super-FRS to the Hot Cell complex can be handled by one common flask. In particular this required increasing slightly the cross section of the flask and thus also the docking ports on the Hot Cell roof. A corresponding change request concerning civil construction was established and approved.

Proton-Linac & p-bar Target

As the responsibility for the p-bar Target and the Proton-Linac is allocated to the same Subproject leader, Mr. Klaus Knie, both contents are getting reported in one section.

Proton Linac

According to the baseline schedule the finalization of installation and commissioning of the pLinac was not expected to be earlier than 2025. This fact can endanger the schedule of HESR and PANDA commissioning. Therefore, the construction of the p-Linac building was re-evaluated and subsequently rescheduled to an earlier time. Now the p-Linac will be fully available in 2023 according to this measure.
The contract with our collaboration partner has been signed. The proton source build is close to completion. The first phase of commissioning has been started; an ion-current of 70 mA has been produced, which is close to the design value of 100 mA already. The construction of the low energy beam transport (LEBT) is in progress.
The first Klystrons provided by our collaboration partners passed the FAT successfully.The production of the first-of series-modulator in-house is in progress.
After the very successful power RF tests of the ladder RFQ prototype the design of the full size RFQ, is close to completion.
The layout of the CH and CCH cavities is nearly finished. The production of the internal quadrupole triplets for the CH cavities is delayed due to minor changes in the layout of the cavities.

p-bar Target

An ANSYS working group has been successfully established. Simulations for target, collimators and beam dump are in progress. An experiment at the HiRadMat facility at CERN is in preparation. It is planned to test the mechanical stability of different potential materials for the pbar target and to do a benchmarking of our simulations.
The work on the target station and the alignment system for the magnetic horn is progressing.

Collector Ring

The TDR for the CR is finally ready. 50% of specifications have been approved. The technical design of the full ring has been performed for 80%. The most critical issues: dipole production is still not started; technical design of the vacuum system requires proof-of-principle experiments.
Component status:
a) RF debuncher: readiness – 25%. The first of series RF debuncher is delivered to FAIR. SAT is ongoing.
b) Stochastic cooling: readiness - 22%. The Pick-up prototype of stochastic cooling system is under development.
C) All other CR components (magnets, power supply, diagnostic, vacuum...): readiness – started
Presently 35 BINP experts are working on the CR project. All BINP experts are busy partially from 5 % to 50 % working time for CR project. Totally it corresponds to 11.95 FTE.

High Energy Storage Ring "HESR"

The production of the HESR is in full swing. All deliveries are according to plan. Schedule, Content and Budget is on target. The HESR components are in intermediate storage close to the FAIR site and will be relocated to their final storage area in 2017.

Commons

The status report for the subproject Commons follows the major technical systems used in all other subprojects.
The Subproject Commons takes the responsibility for the major technical systems (listed .psp numbers according Work Breakdown Structure (WBS)):

.psp 2.3. (High Energy Beam Transport (HEBT))
.psp 2.14.1 (Electric Power (EP))
.psp 2.14.8 (Cryogenics (CY))
.psp 2.14.10 (Controls (CO))
.psp 2.14.12 (Transport and Installation (TI))
.psp 2.14.xx (smaller work packages, will not be reported in detail)
.psp 2.3 High Energy Beam Transport (HEBT)

Magnets:
After the first pre-series dipole magnet had successfully passed the SAT Ab in March 2016, the second pre-series dipole magnet was delivered by the end of September 2016. In the meanwhile the dipole magnet passed the SAT Ab and the series production of in total 51 dipole magnets started. At the beginning of March 2017 the first

DOI:10.15120/GR-2017-1

two series dipole magnets passed the FAT. These dipole magnets will be delivered to GSI/FAIR at the end of March. At the same time series dipole magnet number three and four will be ready for the FAT.

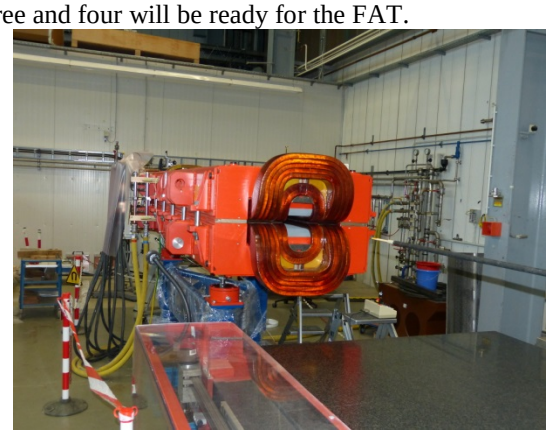

Figure 2: dip13_0 during magnetic measurement at GSI

The magnets of batch2 and 3 (22 dipole, 166 quadrupole, 92 steerer magnets) will be built by the Budker Institute of Nuclear Physics (BINP), Novosibirsk, Russia. While most of the magnet types are currently in the final design phase, stamping lamination and production of yokes of the standard 18Tm quadrupole magnets has already started.

Power Converters:
The power converters for HEBT quadrupole and steering magnets will be mainly built by the Indian company ECIL (Electronics Corporation of India Limited, 152 for quadrupole and 44 for steering magnets). In November 2016 two prototype quadrupole power converters were delivered.

Beam Instrumentation:
The day zero beam instrumentation of the HEBT lines foresees resonant transformers (RT), fast current transformers (FCT), and particle detector combinations (PDC) for intensity measurements and secondary electron emission grids (SEM-Grid) (see figure 3), multi-wire proportional chambers (MWPC) and scintillator screens (SCR) for the determination of the transverse beam profile.
Prototypes of all these instruments have been tested successfully during the GSI beamtime 2016. In addition, the beam loss monitor (BLM) has demonstrated its capability for future requirements.

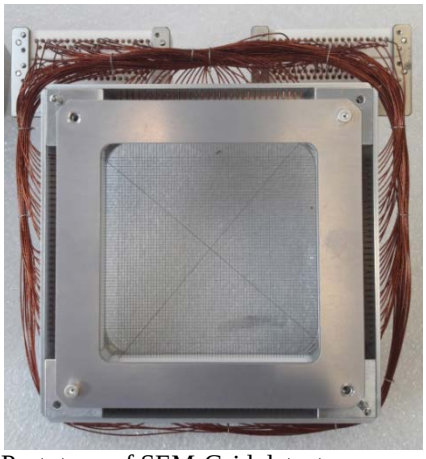

Figure 3: Prototype of SEM-Grid detector
After all prototypes passed the tests, the production of RT, FCT, PDC, SCR, and MWPC started. The purchasing of SEM-Grids and Beam Loss Monitors will follow soon.
Moreover, significant progress was achieved with regard to the auxiliary components related to beam instrumentation detectors.

Vacuum chambers:
The vacuum chambers for the dipole magnets of batch1 will be built. Based on the experiences made with three prototype vacuum chambers which were accepted as prototype only in June 2016, several remedial measures were taken for the series production.

Power Connection to FAIR:
The Technical Department CSEP has successfully supported FAIR Site & Buildings (FSB) in the procurement process and negotiations with energy providers. The construction of the new FAIR transformer fields north and south is on time-schedule (see figure 4). Necessary preparatory work by FAIR S&B was completed in time. Orders for 3 of 4 main items (buildings, transformers, high-voltage cables) have been placed.. The work on the transformer field north has started in February 2017 and will be finished by the end of the year. The work on the transformer field south has started in March 2017. No specific completion date in 2018 required.

Figure 4: FAIR transformer field north

DOI:10.15120/GR-2017-1

Power converters Cables and Machine cable management

PSP-structure and MSP-plans for all technical departments have been created. Cable costs for delivery, cable-laying and assembly were determined on the basis of information provided by the technical departments. Measures have been taken to update the existing data in completeness and quality.

A new work package "coordinating function for cable procurement and cable routing" was established to merge all accelerator related cable data. The aim of this task is to create a complete cable data base, appropriate to go into procurement processes for accelerator cables in synergy with FSB standards for cable planning and purchase.

Cryogenics (CY)

The Technical department Commons Cryogenics (CSCY) is responsible for the GSI and FAIR wide cryogenic helium cooling of superconducting magnets. CSCY is presently operating a prototype test facility (PTF) , a series test facility (STF), the Helium Supply Unit and two more Cryo plants for R3B GLAD magnet testing and for the cooling of the CRYRING electron cooler solenoid. The main customers at FAIR are the SIS100 and the Super-FRS with a total helium inventory of about 8 tons, and CSCY serves additionally small consumers like the final focusing system of APPA and the large scale experiments CBM/HADES and Panda. In addition the department is responsible for the so-called local cryogenics belonging to SIS100 and Super-FRS respectively. In the following different resent activities will be highlighted:

Helium Supply Unit (HeSu):

The HeSu is a liquefier with a decant station, a mobile Dewar parking station and a warm gas recovery system with campus wide helium return lines. The HeSu was taken into operation in 2015 and has delivered more than 7,000 l of LHe to users onside the campus so far. The main purpose is the cryogenic testing of FAIR prototypes. It has a liquefaction capacity of approximately 25 l/h for pure helium gas and 17 l/h in purification mode. A picture of the installation is shown in figure 5. Part of the HeSu project was in addition a universal cryostat for the testing of FAIR components, in particular SIS100 beam pipe vacuum chambers. The universal cryostat has a more than 4 m long cold testing area with an actively cooled table. Two views of the universal cryostat are shown in figure 6. Several different cooling schemas are realized:

(a) LN_2 shield cooling and LHe 4 K cooling with Dewars (using the HeSu)

(b) LHe cooling only, with a boil-off cooling of the shield using again Dewars

(c) connection to the universal connection box of the STF, see below. The planned and realized overall budget for the HeSu, including the universat cryostat and a campus wide recovery system was 1.75 M€.

Figure 5: Helium Supply Facility (HeSu)

Figure 6: Universal cryostat for FAIR components testing

Cryogenic Infrastructure for the Series Test Facility (STF):

The series test facility for SIS100 dipole serial magnet testing was taken into operation in 2015 and continuously running in 2016 for the testing of the first of series (FoS) dipole magnet, but additionally for the test of the SIS100

DOI:10.15120/GR-2017-1

main current leads, for the SIS100 local current leads, for SIS100 cryopumps and for the site acceptance test (SAT) of the first parts of the local cryogenics for SIS100 arrived at GSI in summer 2016. The STF has an overall cooling capacity of 1.5 kW @ 4 K equivalent is equipped with four test benches for magnet testing and one universal connection box. Up to now the plant has about 10,000 h of operation. A picture of the STF cryogenic infrastructure is shown in figure 7.

Figure 7: Serial Testing Facility (STF) in operation

Procurement of the FAIR Cryo Plant CRYO2:

For FAIR one central cryo plant will be installed serving the helium cooling capacity for SIS100, Super-FRS, CBM and HADES. In the first step a 19 kW @ 4 K equivalent cryo plant will be installed, including a campus wide 1.6 km long distribution system. Two industrial studies concerning the cryo plant layout were performed in 2014 and afterwards the specification was progress continuously adapted to future user requirements. According to the present civil construction time schedule the procurement phase is currently in preparation: The specification is under final approval, the budget is released and the official announcement will take place in the second quarter of 2017. Depending on the time for the negotiation with the suppliers, the contract is planned to be signed end of 2017. According to the present time schedule the plant installation will take place in the second half of 2021 and the commissioning will be performed until the end of 2022.

Control Systems (CO)

The activities of the accelerator Controls Department is fully focussed on the development and implementation of the accelerator control system for FAIR.

During the past 6 months significant progress has been made on all control system subprojects. The design of the standard equipment controllers (SCU) for FAIR power converters and many other systems, of which more than 1200 units will be needed, has been successfully completed and production and assembly of the first batch (100 units) has been finalized. Several components of the newly developed White Rabbit protocol-based high precision time and event distribution system, backbone of real-time control in the control system for the full facility, has been further developed and already installed in as a prototype test system for the CRYRING machine. Electronic timing receiver boards (FTRN) in several form factors (PCe, VME, PMC, uTCA), both GSI in-house developments as well as Slovenian in-kind contribution projects are under development. Schematics design and board layout has been checked and prototypes have been produced or are presently under production for test and evaluation. Significant progress has been made in development of the fundamental underlying control system software frameworks for accelerator equipment control (FESA), communication middleware, databases, physics modelling of the machines and beam lines (LSA) as well on user interfaces graphical control room applications. On the industrial controls side, vacuum control with the industrial control SCADA-based UNICOS framework has been developed, installed, commissioned and is presently under testing at. The vacuum bake-out of several sections of the CRYRING has been already successfully tested in the last 2 months, shortcomings and problems being identified and are being addressed in the ongoing development. In respect of cryogenic controls, several cryogenic sensors and actuators have been tested as a sound base for the cryogenic controls system design. Subsequently technical and functional specification documents for the control system of the upcoming tendering of the FAIR central cryo-plant have been worked out and are presently under formal approval.

In January 2017, the IT hardware base of the accelerator control system, both used for development and tests of the new system as well as for operation with the existing GSI accelerators, have successfully been relocated to the new FAIR computing center building, the Green IT Cube (see figure 8). While presently a full row of 14 racks are equipped, the setup is arranged and designed for future extensions to control the full scope of the FAIR accelerator facility.

DOI:10.15120/GR-2017-1

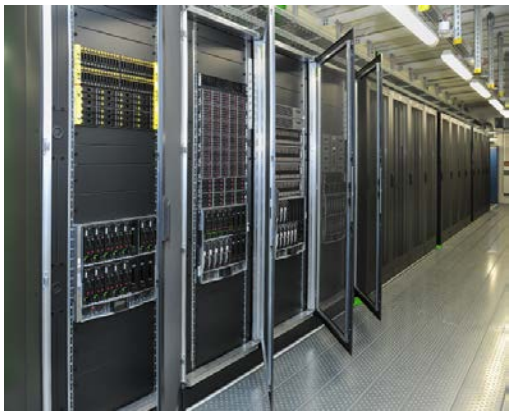

Figure 8: Relocation of accelerator controls hardware to the Green IT Cube

Following the agreed project strategy of the control system subproject, the full control system architecture was implemented at the new CRYRING machine, being used as test-bench for FAIR. During the last 6 months numerous tests have been performed in order to identify bugs and limits. Finally the control system was already used for commissioning the CRYRING local injector with beam and the injection into the CRYRING storage ring itself. Presently a new release of the control system stack is being prepared for beam operation in May. In parallel, the control system team is fully engaged in providing the FAIR control system already for the upcoming beam time of the existing GSI machines in 2018 and 2019. These two applications to existing machines will greatly reduce the time and risk during commissioning of the FAIR machines.

Transport and Installation

Numerous workshops on the topic of accelerator installation have been carried out since Q3/2016, resulting in the creation of dedicated additional work packages and corresponding detailed installation plans.

An overall concept for the intermediate storage of FAIR components is in progress. Measures have been taken to use existing Campus Facilities according increasing requests for adequate component testing and storage. The overall need for intermediate storage leads to leasing of external storehouse areas. Presently the storage of HESR components delivered by Forschungszentrum Jülich (FZJ) is ongoing (see figures 9 and 10).

Figure 9: Unloading of one HESR dipole magnet (weight: 35t) at the site of an external storehouse

Figure 10: Remote positioning of an HESR dipole magnet for intermediate storage.

Engineering /Mechanical Integration

For visualization of beam lines, buildings and technical building services and for facilitation of coordination tasks and test processes of web-based tool, the Kisters 3D viewer, was implemented. This tool allows work package leaders, subproject leaders and management to receive a general review about the content. Independently of CAD tools the configuration of the beam lines will be shown in connection to their position in the buildings. This view can be used on any web-connected unit like computers or mobiles independently of any licence structure. The content will be updated regularly once in a month by the person in charge of DMU group.

Figure 11 shows the screenshot of the Kisters 3D viewer with the detail of the HEBT beam lines and buildings.

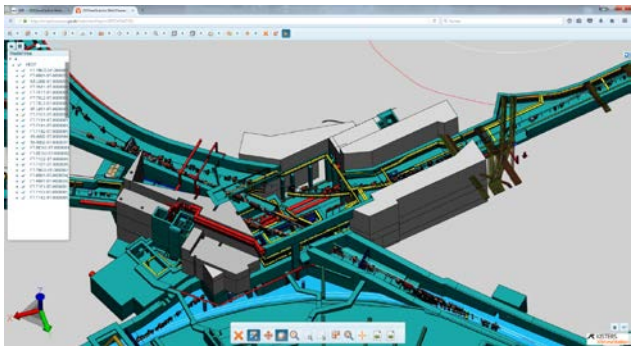

DOI:10.15120/GR-2017-1

Figure 11: Screenshot of that based Kisters 3-D viewer with HEBT

FAIR Site & Buildings

The approval for the tendering and subsequent award of civil works for the construction area North by the BMBF is given mid-September 2016. The reorganization of the S&B department is completed. The development of a staffing plan of S&B department is also completed.
The civil works execution plan for the FAIR project is divided into construction area North and construction area South. The contractual schedules with the civil design companies will be adapted accordingly to next steps. Detailed scheduling of civil work packages is currently progressing in cooperation with the civil designers.
An overall time schedule including defined periods for installation of machine components was developed as part of the integrated project master time schedule.
The tenders for groundwater lowering, trench sheeting and excavation in the construction area North are in the negotiation phase. The award of this contract is planned in Mai 2017. Subsequently it is planned to start site works in July 2017. The tender process for the SIS 100 shell construction works is progressing as per plan aiming at contract award in 4th quarter 2017.
The overall project civil construction permission is issued since 2014 for the entire facility. Some construction permissions for the buildings have to be revised as part of the design process (e.g. for the north and south electrical substations). The revised applications are scheduled in line with the civil construction schedule.

FAIR Experimental Areas

Major developments for the experimental areas of CBM, APPA, NUSTAR & PANDA are described in the following chapters.

APPA
Work on design and construction of the experiment components proceeds as planned. Special attention is devoted to the components which will already be used in the FAIR Phase-0 for experiments. Especially the installation and commissioning of the CRYRING at ESR is a main collaboration activity with strong support from on-site specialists. The realization of the ultra-high vacuum in the ring started according to the planning. The performance of the local injection is continuously improved. The electron cooler was reassembled, cooled down to Liquid-He temperature and demonstrated his superconductivity. In addition, the new FAIR control system is getting implemented and tested in the ring. The next test with beam is planned for May 2017, when also the first training for accelerator operating team with the new control system will take place. The time scheduling and the installation plans of the subprojects were improved in an additional effort by the collaborations.
Within the reporting period, APPA completed and submitted one TDR (Beam line matching section for Plasma physics experiments) to FAIR for the ECE evaluation. A second TDR, Gas-Jet Target for CRYRING, is presently in the stage of internal review and will be submitted soon to FAIR for evaluation.
Concerning the In-kind contracts listed in the previous section the Detailed Technical Specifications and time lines have been defined and are currently in the process of internal collaboration approval and FAIR management check.

CBM
CBM experiment: The CBM magnet has been contacted. The silicon tracker (STS), RICH, time-of-flight (TOF), and muon (MUCH) detector systems have approved TDRs, are in the engineering design phase, and full sized pre-series chambers are verified in test beam campaigns. The STS, as most complex detector project, will structure the production readiness reviews in three parts (sensor, electronics, integration) planned for 2017 and 2018. A cooperation with JINR, which builds 4 silicon tracker planes using the same technology as CBM to augment the BM@N tracking system, will help to widen the manufacturing competence. The photon detector of the RICH is in an advanced stage, 2/3 of the photo multipliers are tested. The RICH readout is a joint CBM, HADES, and PANDA development. This detector component has a modular design and will be used in the context of the HADES experiment at SIS-18 starting 2018. The production of the first batch of TOF chambers will start in April this year.
The PSD detector also has an approved TDR, is already in production phase. The STS, RICH, TOF, and PSD activities at BM@N/JINR, STAR/RHIC and HADES/SIS-18 constitute the CBM FAIR Phase-0 activities which will gain early operational experience for these detectors and generate valuable physics data.

NUSTAR
For all experimental set-ups of the NUSTAR pillar, the list of components and associated Work Breakdown Structure code (PSP Code) was refined and re-confirmed. An intense activity was devoted to the improvement of the time scheduling of the sub-project, which was matched to the Integrated Master Schedule of the FAIR project. For each experiment, the milestone defining the completeness of each component necessary for the installation of the experimental set-up was mirrored in an overview plan, the Level-2 plan. This allowed also the creation of a devoted Installation plan. The time range available for installation is established in the plan of the Civil Construction. Two time windows define the time range available for the assembly of components. The allocated time slot for the installation of NUSTAR experiments is in some cases too early with respect to the foreseen beam availability. The beam availability is scheduled in only one plan (Commissioning plan) for the whole FAIR pro-

DOI:10.15120/GR-2017-1

ject. For this reason, it is foreseen to re-schedule the experiment installation starting backwards from the Commissioning plan. This would be advantageous for some of the experimental groups which could profit from experimental activities at the upgraded GSI facility and other laboratories.
Work has continued on the detailed technical specifications for several In-Kind and Collaboration Contracts. The TDR for the common NUSTAR data acquisition system has been submitted and further TDRs are expected in the next six months. Work on NUSTAR detection systems, electronics, data acquisition and associated infrastructure is proceeding according to the internal planning. Focus is on readiness for FAIR Phase-0 experiments from 2018 onwards. The CDR for the LEB magnets has been updated and the present version is currently under evaluation by internal experts.

PANDA
Electromagnetic Calorimeter (EMC): The first-of-series of 16 modules of the Target Spectrometer Barrel EMC is under construction and is planned to be completed in summer 2017 after the delayed delivery of the PCBs needed for the mounting of readout chips.
The delivery of the high-purity PWO base material funded by Russia has started and will be completed by May 2017. The first two samples showed excellent quality and are stored for further processing. The crystal producer has produced crystals of a pilot series, which show very good quality.
The mass production should resume as soon as possible, to prevent delays. The Forward Endcap EMC is currently under construction in Bonn and Bochum and will be fully assembled until mid 2018. The module design of the Backward Endcap EMC has been revised and is complete now. A full readout chain successfully has been tested with beam.
Superconducting Solenoid Magnet: The PANDA solenoid magnet has been assigned to BINP Novosibirsk (RU) and a collaboration contract for the construction of the complete magnet was signed in March 2017. Work has started and the next step will be a plan review in summer 2017. In addition to the construction contract a service contract for the complete field mapping of the magnet on-site at BINP is being drafted.
Barrel DIRC: The TDR of the Barrel DIRC, was submitted in September 2016. In fall 2016, further test-beam measurements were done with a plate shaped design of the radiator. The detailed analysis of the result is presented in an addendum to the TDR being submitted in April 2017 along with the start of the review of the TDR by ECE.
Luminosity Detector: The Luminosity Detector TDR has received comments from an internal review in 2015, which were addressed in further R&D work during 2015/16. The resulting enhanced version of the TDR was reviewed anew and is now approved for submission to FAIR. A full-scale prototype of the core sensor component, will be tested in summer 2017.
Time-of-Flight (ToF) Detectors: The technical design of the Barrel ToF Detector is based on Silicon Photomultipliers and thin scintillator tiles. The Forward ToF consists of more conventional large area scintillator bars read out by photomultiplier tubes. The TDRs of these detectors were submitted to an internal review at the beginning of 2017. The TDR of the Barrel ToF Detector was approved for submission to FAIR in March 2017, the Forward ToF TDR is supposed to follow soon, at the latest by June 2017.
Infrastructure: Currently the detailed planning of the infrastructure of the PANDA experiment is being brought to the next level of detail in the context of the execution planning of the PANDA hall along with all technical services and the routing of cables and pipes. The experiment infrastructure comprises support structures, rails, gas distribution, electrical power distribution and cooling supplies. In addition, there are service networks and the controls infrastructure.

DOI:10.15120/GR-2017-1

Concept for content and structural quality assurance of CAD models for integration into the DMU models of accelerators developed

L. Heyl[1], *C. Will*[1],
[1]GSI, Darmstadt, Germany.

The sublimation of the CAD models, prepared by GSI and by the collaboration partners, to a high-quality overall model is only possible by consequent structuring. Therefore the qualitative properties of the individual models have to be considered before integration.

As a virtual image of the accelerator systems and their structural embedding, a synthesis of CAD models of buildings, technical building equipment and accelerator systems has been developed in the DMU group, which is part of Engineering Mechanical Integration (ENMI). These CAD models allow the visualization of the components, interfaces and the media supply. Furthermore, transports and assembly tasks can be planned based on the model.

The models have been created using CATIA as CAD program and are based on the ion optical layout and the information of the specialist groups. The product data management functionality of SAP has been used for managing models and drawings.

PDM is defined as "the management of the product and process model with the objective of generating unique and reproducible product configurations" [1]. It provides an increase in productivity due to reuse of models, a considerable time advantage by a fast information access, an improvement of co - operation within and outside the organization and a reduction of throughput times. [2]

Modern PDM functionality (such as implemented in the PLM-systems SAP-PLM, Enovia V6, Oracle Agile or PTC Windchile) ensure, that changes to models, which have already passed an approval cycle, are displayed with a changed revision level. In addition, the structure of models, the designation of parts and the reuse of components are managed.

The contents of the CAD accelerator models have been updated not only by the adaptation of models created by GSI, but also by the integration of CAD models of external collaboration partners. For these models, if not created by CATIA, the STEP format will be used as a system-independent exchange format for 3D CAD models.

To integrate these models into the CATIA SAP, the Enterprise Connector (EnCo) from CENIT is used at the GSI Helmholtz Center.

For integration, EnCo checks the clear identification of the models consisting of the model number and the revision status, as well as the designation. If this information matches with already existing data, the already integrated data are reused.

As changes in the content of the system, which have not been indicated by the change of the revision status, cannot be detected, this will lead to an alienation of the information.

At the latest during the integration of individual models into the overall system of the 3D model of the accelerator systems, erroneously structured data sets lead to a considerable time overload due to the necessary manual reworking. Not all external collaboration partners use a PDM system for managing CAD models and drawings. It is also possible, that the STEP-converters from different CAD-systems cause errors during converting process.

In the DMU group a method has been developed to scan the structural, the content and the orientation-relevant properties of the models. This method is used to check designation, structure, positioning, orientation, completeness and volume of the model components. With this information the Macro identifies the already in SAP stored components and exchange them in the new models.

In the second step, a program checks whether the drawing number of the components of the model matches the supplied drawings. Possible errors can be remedied using the results log. So the EnCo can store the new models and drawings in CATIA SAP correctly. A faulty data exchange can be avoided.

At the same time, the recording of the scan results and a traceable documentation of the made modifications are carried out. The structural agreement between the model and the drawing set is examined and data integration is facilitated.

Based on this concept, the model structures, that are specific to the supplier, can be tested and, if necessary, corrected.

References

[1] M. S. R. Eigner, Product Lifecycle Management – Leitfaden für Product Development und Life Cycle Management, Berlin, Heidelberg: Springer Verlag, 2009.

[2] "Solid System Team PDM Definition," Solid System Team / Worksline, 2017. [Online]. Available: http://www.solid-system-team.de/pdm/smap3d-pdm/pdm-definition.html. [Accessed 26 04 2017].

DOI:10.15120/GR-2017-1

Design studies for Cryogenic Current Comparators (CCC) at FAIR

F. Kurian[1#,2,3], M. Schwickert[1], T. Sieber[1], R. Stolz[4], T. Stöhlker[1,2]
[1]GSI, Darmstadt, Germany; [2]Helmholtz Institute, Jena, Germany; [3]Friedrich-Schiller University, Jena Germany,
[4]IPHT Jena, Germany

For beam intensity measurement in the FAIR accelerator facility, development work for an advanced Cryogenic Current Comparator (CCC-XD) system is ongoing in association with the collaborating partners at TU-Darmstadt, FSU- Jena, CERN-Geneva and IPHT-Jena [1]. There are four major components for the CCC-XD, a suitable cryostat and cryogenic environment, a superconducting beam current to readout current transformer with superconducting shield, a SQUID readout and data acquisition. While the design of a universal cryostat which fulfils the special boundary conditions given in the FAIR beam lines has been worked out, some of its components still undergoing optimization. The focus in this phase of the development lays on the readout using the shield and SQUID which will be described herein.

Optimization of the CCC Design for FAIR

There are obviously contradictory needs for the CCC implementation at FAIR: First of all, the beam installation restricts the size of the cryostat and thus the dimensions of the CCC. Secondly, since the CCC should cope with larger dimensions given by large beam tube diameters (160 mm) of FAIR beam lines which. But as already shown before [2], a larger diameter of the magnetic shield reduces the magnetic shielding factor of the CCC. At the same time, given by the requirement of a compact cryostat with separated insulation vacuum, a minimum possible outer diameter of the shielding has to be achieved. This also limits the sensitivity of the CCC which was approved by simulations.

To ensure minimum temperature fluctuations on the liquid helium surfaces, which were previously shown to cause large drifts in the CCC output signal [3], the thermal load had to be minimized even though a room temperature UHV beam tube needed to be introduced as a 'warm-hole' through the cryostat. The cross-sectional view in figure 1 shows the recent design of the cryostat. Besides a stable operation at FAIR, it also has to provide easy access to all internal parts to allow exchange of CCC components during future development work. Therefore, the isolation vacuum chamber consists of a stainless steel frame with Aluminum windows, which can easily be removed and thus the CCC mounted and serviced in the cryostat.

All these factors led to the development of new concepts for the CCC without magnetic core and with reduced dimensions of the superconducting magnetic shield described in the next section.

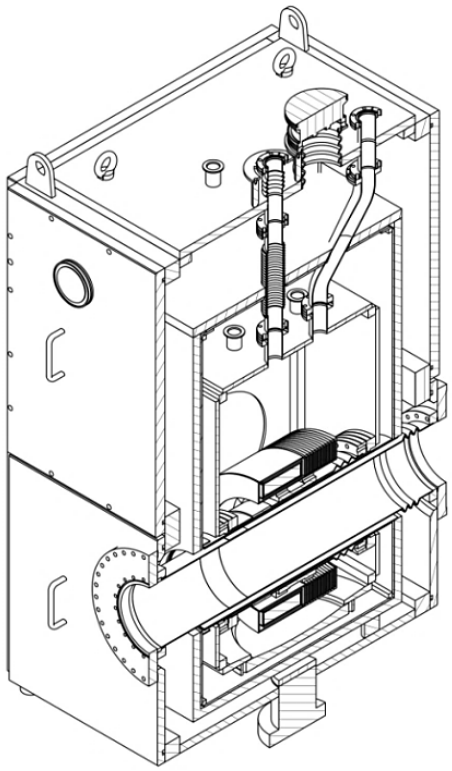

Figure 1: Cross-sectional view of the schematic design of the new CCC system for FAIR

Radially Stacked Magnetic Shield for CCC

For the operation of CCC system as a standard diagnostic instrument in FAIR beam lines, large baseline drifts (long term drifts as well as instantaneous drifts) due to temperature fluctuations has to be minimized. Hence, in order to characterize both types of drifts, detailed experiments on the magnetic shield are still in progress. Preliminary results show clear indications that the high permeability ring core (which acts as a flux concentrator and enhances the magnetic field coupled to the sensor unit) is the main source of the drifts.

In order to achieve better current resolution through enhanced field attenuation and removal of temperature fluctuations of the ring core, which is additionally a source of strong Barkhausen noise, a radially stacked design of magnetic shield is proposed. In this scheme, unlike the magnetic field pickup by the pickup coil, the magnetic shield itself acts as the single turn pickup coil. The superconducting screening current will in this case be inductively coupled to a next generation dc-SQUID with an inductance matched to the shielding. The magnetic shield is radially stacked and thus improves the attenuation factor and reduces dimension at the same time.

DOI:10.15120/GR-2017-1

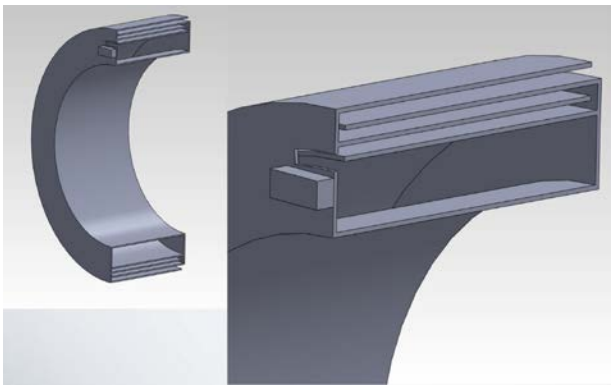

Figure 2: Radially stacked meander CCC.

This new implementation of the CCC is planned to be tested in the new cryostat, which will in installed in the Cryring@ESR storage ring. Depending on the performance compared to the classical solution, application in the FAIR facility is foreseen.

References

[1] T. Sieber, F. Kurian, M. Schwickert et. al, "Optimization studies for an advanced Cryogenic Current Comparator System for FAIR", Proceedings of IBIC 2016

[2] H. De Gersem, N. Marsic, F. Kurian, T. Sieber et al. "Finite-element simulation of the performance of a superconducting meander structure shielding for a cryogenic current comparator", Nucl. Instrum. Methods Phys. Res., Sect. A, 840:77 86, 2016

[3] F. Kurian, "Cryogenic Current Comparator for Precise Ion Beam Current Measurements", PhD thesis, Goethe University, Frankfurt am Main, March 2016

DOI:10.15120/GR-2017-1

Vacuum acceptance test of ferrites for UHV applications

P.M. Suherman, M.C. Bellachioma, J. Cavaco, C. Kolligs
GSI, Darmstadt, Germany.

Introduction

In the last several years, the activities of the vacuum lab, as part of the CSVS (Common System Vacuum System) Division at GSI, have been mainly focused on assisting the realisation of the FAIR project. These mostly involve the vacuum acceptance test for some components used for the FAIR project, such as outgassing rate measurements, leak tests, and residual gas analysis. In addition, the vacuum lab also conducts the fabrication of NEG coatings on vacuum chambers for HESR (High Energy Storage Rings) [1]. This report presents some results obtained from the vacuum acceptance tests of different types of ferrites.

Vacuum Properties of Various Ferrites

The vacuum properties of different types of commercial ferrites (Table 1) have been investigated, as part of a request from SCBC (Stochastic Cooling Beam Cooling) Division, GSI Darmstadt. One of the ferrites is foreseen to be used in the Palmer pick-up and kicker for the CR (Collector Ring).

Table 1: Different Types of Ferrites

No.	Types	Temperature treatment (in a vacuum oven)	Sample Condition
1	Type A1	300 °C, 3 h	Cleaned, as-fired, Not ground
2	Type B	300 °C, 3 h	Cleaned, as-fired, ground
3	Type C	-	As received, as-fired, ground
4	Type D	-	As received, as-fired, ground
5	Type A2	-	As received, as-fired, ground

Figure 1 shows the temperature dependent outgassing rates of the ferrites over the bake-out cycles. The bake-out temperatures in this experiment (80 °C and 150 °C) were chosen based on the demand from the SCBC Division. It was assumed that the temperature of the future setup will increase to such values ((80 °C and 150 °C) during operation.

The results showed that all of the unbaked (as-received) ferrites were not suitable for UHV (ultra-high vacuum) applications due to high outgassing rates (> $1x10^{-10}$ mbar.l/s.cm^2 at room temperature), especially for use at higher temperatures. Even with longer pump down times, the outgassing rates were still slightly higher than the required value. The extrapolated outgassing rate at room temperature after one week pump down time for Type A1 ferrite, for example, was about $1.6x10^{-10}$ mbar.l/s.cm^2.

After bake-out cycles, the outgassing rates of the ferrites were in a marginal acceptance value. The outgassing rates might be improved more significantly with higher bake-out temperature (e.g. 250 °C for 24-48 hours).

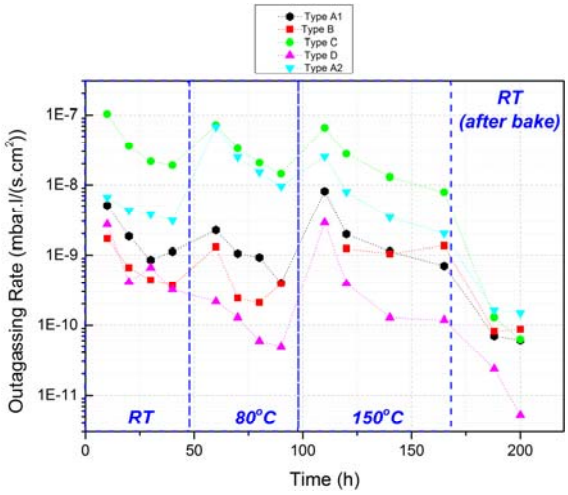

Figure 1: Time dependent outgassing rate of different ferrites over the bake-out temperature ranges.

The RGA (residual gas analysis) scans for all the ferrites at room temperature and after bake-out temperature did not show any concern of contamination or any unwanted chemical elements. Figure 2 shows the RGA scan of one of the ferrites at room temperature after 24 hours pump down.

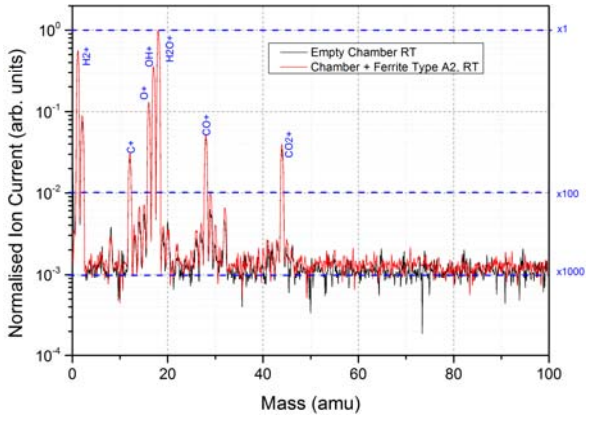

Figure 2: Normalised ion current of the RGA spectra of the empty chamber and the chamber loaded with Type A2 ferrite (as-received, no thermal treatment) after 24 hours pump down.

References

[1] M.C.Bellachioma et. al. GSI Scientific Report 2013.

DOI:10.15120/GR-2017-1

High precise 3D measurements with laser tracker through optical glass under cold-vacuum conditions

A. Junge[1], V. Velonas[1], K. Knappmeier[1], T. Miertsch[1], I. Pschorn[1], C. Schröder[2], F. Walter[3], B. Zielbauer[4],
GSI, Darmstadt, Germany.

Applying an already existing procedure to monitor a cold mass component for deformation and movements with regard to a cryostat covers not all the desired needs. The procedure relies on a combination of two instruments, a theodolite and a laser tracker. The observer performs optical measurements through different optical media which is air, an optical glass and vacuum. The optical glass is mounted on the integrated viewport on the cryostat and represents the window between air and vacuum. The results by using this procedure are very accurate (absolute position of the target is less than ±0.1 mm). The disadvantage is that the yielded results are only 2D and not 3D. This is because of the missing distance between the theodolite and the targets. To overcome this problem a direct replacement of the theodolites by the laser tracker is suggested in order to measure directly a distance contemporaneous with the angles on the targets/spherical mounted reflector (SMR) as shown in Figure 1.

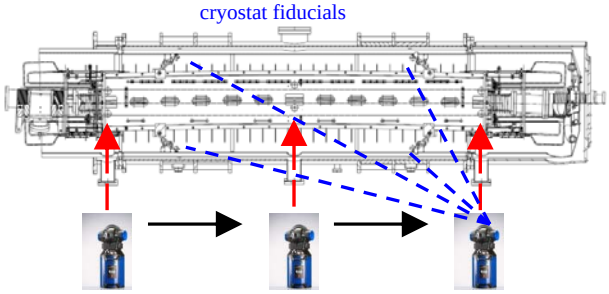

Figure 1: The suggested concept where the theodolite is replaced by the laser tracker

First tests showed that measurements through uncoated optical glass are disturbed by reflection. The laser beam is reflected diffusely on the glass. The superposition of the different laser beams cannot be interpreted by the laser tracker. Therefore a coating of the glass, adapted to the wavelength of the laser tracker, is imperative. The used (coated) optical glass has an actual thickness of 15.10 mm. Its coplanarity is better than 0.01 mm. The surface flatness of both window sides was specified as 1.5 lambda PV (peak to valley) or better.

Before verifying measurements inside a vacuum chamber this coated glass was used for measurements at common conditions on air. The beam transmits the media air, glass and air again. The repeatability of focusing a target behind the glass was about ±0.005 mm in 3D. A comparison of observations accomplished through glass and without it showed range and angle errors. With the aim of error compensation the physical effects which act on the beam were analysed.

Measuring through a glass blank, laser tracker observations are disturbed by several physical effects. Therefore a new complex mathematical model was developed for the calculation of a 3D position behind a coplanar glass by its pseudo observations. As a difference to conventional laser tracker measurements, there is the need to measure the front plane of the glass to define its normal, which is needed for the computation of the angle of incidence. Further the plane gives the distance from laser tracker source to the glass front. Furthermore the value of the glass thickness needs to be known and must be given with an accuracy of ±0.01 mm. By applying this mathematical model the absolute 3D point accuracy is about ±0.015 mm.

Afterwards measurements inside a vacuum chamber were accomplished. Now the laser beam transmits the media air, glass and vacuum (Figure 2). The repeatability of focusing the targets inside the vacuum was ±0.005 mm. Using the mathematical model the absolute 3D point accuracy for measurements inside the vacuum chamber is identical with the measurements through air-glass-air about ±0.015 mm.

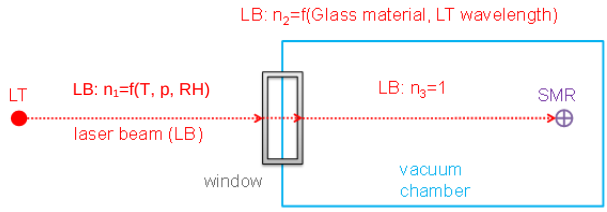

Figure 2: Splitting the distance in separate parts regarding the refractive index of the different optical media

Under cold vacuum conditions (90 K) additional test were performed. Through a second port the observation of the laser tracker was contemporaneous checked by a further independent instrument (theodolite). The investigations showed that the mathematical model works correct under cold-vacuum conditions. 3D point accuracy of 0.01-0.03 mm can be achieved by a laser tracker system.

Absolute 3D Measurements through an optical glass with laser trackers are possible as long as the suitable glass material and coating has been chosen. The mathematical model must be used as a post processing method to eliminate or reduce different errors that yields to absolute coordinates of points measured behind the glass. [1]

References

[1] V. Velonas et al, „Measuring through glass window with laser tracker under cold-vacuum conditions: Investigations and results“, IWAA 2016

[1] alignment@gsi.de
[2] c.schroeder@gsi.de; [3] f.walter@gsi.de; [4] b.zielbauer@gsi.de

DOI:10.15120/GR-2017-1

Development of new projectiles for future FAIR experiments

A. Adonin and R. Hollinger
GSI, Darmstadt, Germany

The upcoming FAIR facility will provide wide opportunities for investigations and research in different branches of science including antiproton physics, bio and material research, nuclear astrophysics and many others. Some of the FAIR experiments require improved quality and intensity of ion beams for certain ion species as well as the new projectiles as primary ion beams. To fulfil these requirements the tests on Terminal Nord with high current VARIS ion source have been performed in 2016.

Seven elements were tested in various operation modes and under different conditions. For three elements (O_2, Mg and Mo) the goal was to improve the performance and another four elements (Al, V, Zr and Ru) have never been performed from high current ion sources before. The main results of the tests are summarized in Table 1. For middle-heavy elements (V, Zr, Mo and Ru) the performance has been tested for various ion charge states optimizing for highest particle current and stability of operation.

Table 1: Ion beam currents achieved with VARIS ion source in front of the RFQ for various charge states and operation modes, using different auxiliary gases.

Element	Provided ions	Duty cycle	Beam current	Auxiliary material
O_2	$^{32}O_2^+$	2 Hz	3.5 mA	V-cathode
Mg	$^{24}Mg^+$	2 Hz	3.5 mA	He-gas
Al	$^{27}Al^+$	2 Hz	2 mA	O_2-gas
V	$^{51}V^+$	2.7 Hz	2.3 mA	O_2-gas
	$^{51}V^{2+}$	2.7 Hz	4.5 mA	–
Zr	$^{90}Zr^{2+}$	1 Hz	8 mA	N_2-gas
	$^{90}Zr^{3+}$	2 Hz	6 mA	He-gas
Mo	$^{98}Mo^{3+}$	2 Hz	5 mA	He-gas
Ru	$^{102}Ru^{2+}$	2 Hz	9 mA	He-gas
	$^{102}Ru^{3+}$	2 Hz	5 mA	–

Plasma generation processes in vacuum arc ion source define a certain distribution of ion charge states in plasma and in extracted beam, respectively. This distribution depends mainly on plasma density and could be changed by tuning the ion source parameters or by changing the operation duty cycle. Normally the ion source is optimized for maximum production efficiency and the distribution maximum is situated on the desired ion charge state. However during the ion source optimization for highest beam current in front of the RFQ the maximum of this distribution could be shifted to higher charge states reducing the production efficiency. The situation could be improved by adding to the plasma a small amount of proper auxiliary gas. Due to varied energy- and charge-exchange schemes in ion source plasma the maximum of the distribution could be returned to the desired ion charge state further increasing the beam intensity (Fig.1). Moreover admixture of the auxiliary gas in most of the cases leads to a more stable vacuum arc and results in noise reduction of the beam pulse and improved pulse-to-pulse repetition. On Figure 1 the influence of auxiliary gas on charge state distribution as well as on the production efficiency for Zr^{2+} and Ru^{2+} ions is demonstrated.

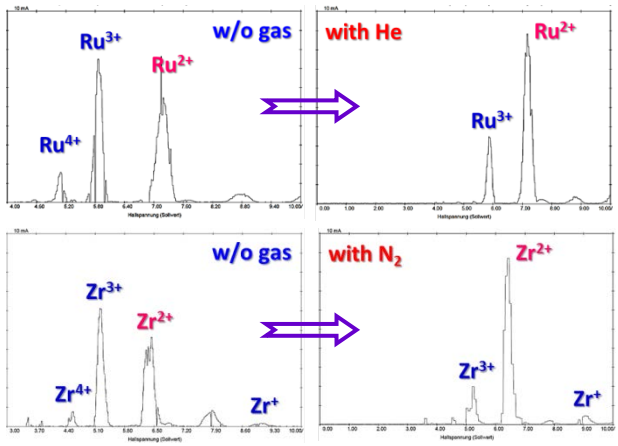

Figure 1: Optimization of the spectrum and production efficiency for desired ion charge state by using auxiliary gas on example of Ru (*upper*) and Zr (*lower*).

Summing up, the production of O_2^+ ions was the most efficient using V-cathodes. It showed very good performance also with 2 Hz repetition rate. Magnesium has shown very good pulse-to-pulse stability. The production efficiency was optimal using helium as auxiliary gas. Aluminium showed average performance with noisy beam pulses and pulse-to-pulse instabilities even with auxiliary gases. Situation became worse by increasing the duty cycle. In contrast to Al vanadium showed extremely good performance also with 2.7 Hz (maximum requested for FAIR experiments) operation. Oxygen is a proper gas for production of V^+ ions. Also one could tune the ion source for production of V^{2+} ions. In this case no gas is necessary. Operation is very stable with the same particle current as for V^+. The highest particle current for zirconium has been achieved with Zr^{2+} ion beam. However the stable operation was possible only with 1 Hz. Switching to charge state of 3+ notably improved pulse-to-pulse stability and allowed higher repetition rates but at the cost of particle current. The similar situation was with ruthenium. Molybdenum has shown much better stability and higher particle current with 3+ charge state compare to 2+.

As the conclusion, four new projectiles from high current ion sources have been developed for FAIR experiments. Operation with three elements has been notably improved. As next steps further performance optimization for considered elements for 2.7 Hz operation as well as tests with Si and Nd are planned.

DOI:10.15120/GR-2017-1

DOI:10.15120/GR-2017-1

SIS18 upgrade and SIS100 status report

P. Spiller, U. Blell, L. Bozyk, T. Eisel, E. Fischer, P. Hülsmann, H. Kollmus, P. Kowina, H. Klingbeil, H.G. König, J.P. Meier, A. Mierau, C. Mühle, C. Omet, D. Ondreka, I. Petzenhauser, I. Pongrac, V. Plyusnin, N. Pyka, P. Rottländer, C. Roux, A. Schuhmann, J. Stadlmann, K. Sugita, P. Streicher, S. Wilfert

GSI, Darmstadt, Germany

SIS18 Upgrade

In order to prepare SIS18 for the operation as fast cycling FAIR injector, a technical upgrade has been conducted and almost completed. This upgrade program has been defined in the early project phase of FAIR [1]. It follows a recipe to control the dynamic residual gas pressure during beam operation and involves almost all major technical subsystems [2]. Most of the upgrade program has been successfully implemented through the last decade. The still missing technical items will be completed in the course of 2017. This involves a) the completion of the new dipole power converter for fast ramping with a ramp rate of 10 T/s, the commissioning of the last two of three new MA (magnetic alloy) acceleration cavities, b) the manufacturing and installation of the IPM (Ionization beam Profile Monitor) system and c) the manufacturing and installation of a new large bipolar dipole magnet for linking the existing facilities to the transfer line to SIS100. Since SIS18 will also be the driver for a major experimental program in the FAIR phase 0, further technical improvements, machine developments and maintenance measures are continuously conducted from institutional funds. E.g. a new cavity is under preparation for smoothing the micro spill structure of slowly extracted ions [fig.1] [3].

Figure 1: A UNILAC single resonator cavity is under modification for smoothing the micro spill structure.

The planned machine developments will provide further insight into critical phaenomena showing up at high current operation or low charge state, heavy ion operation and will enable the development of methods to counteract fundamental issues, e.g. the uncontrolled generation of a microstructure at slow extraction. A major ongoing activity which needs to be completed in 2017 is the retrofit of the accelerator control system. The new control system architecture, including the new timing system, replaces the old VMS based controls hardware and will be implemented and tested for the first time for the recommissioning of SIS18. The successful completion of this effort is demanding and crucial for the machine operation in 2018. In parallel, upper level controls software, required for generating the set-values for all devices based on physics models and parameterized algorithms, will be completed. This software has been developed in collaboration with CERN, based on the LSA (LHC Software Architecture) over the last decade and is presently tested at commissioning of the new Cryring accelerator at GSI.

LINK EXISTING FACILITY – CIVIL CONSTRUCTION

In order to finalize the SIS18upgrade program and to enable the execution of major civil construction measures, the machine operation has been interrupted in 2017.

Figure 2: The soil shielding on top of the SIS18 tunnel is presently enhanced. This requires a table like construction, carrying the additional weight on top of the existing tunnel.

To cope for the operation with significantly increased average beam intensities, beside the machine upgrade, the SIS18 tunnel construction is presently receiving a major modification. The so called GAF (Gebäude-Anbindung-an-FAIR) civil construction project has been launched at the end of 2016 and shall be completed in January 2018. The project involves a) an enhancement of the soil shield-

DOI:10.15120/GR-2017-1

ing on top of the SIS18 tunnel, requiring a support structure to cover the additional load, b) a radioactive air management system, c) a fire protection system based on Nitrogen flooding, d) a reinforcement wall at the Northern arc of SIS18 and e) opening and modification of the Eastern building wall in the experimental hall, generating the interface to the FAIR tunnel 101. The underground pillars acting as foundation of the table are presently constructed (figure 2).

SIS100 STATUS

Major progress has been achieved in contracting of new components for SIS100 and developing FOS (First of Series) devices towards readiness for series-production.

After the successful manufacturing and cold testing of the FOS superconducting dipole magnet, the series production of 110 magnets has been released. The manufacturer, BNG, has just completed its move of the production line to a new dedicated building and released the series production of the steel for the yokes and the superconducting coils. Starting from August 2017, one sc. dipole magnet will be delivered per week to GSI for cold testing. Therefore, the set-up of the team for series testing of the dipole magnets over the three years production time is presently a major issue. The manufacturing of the superconducting quadruple magnets in Dubna has progressed towards two integrated units, consisting of two quadruple magnets, a steerer- and a sextupole magnet. In parallel, the preparation for cold testing of these units is progressing. The set-up of the dedicated NICA-FAIR superconducting magnet test facility could be completed end of November 2016. The commissioning of the test facility has been celebrated as an official ceremonial act. In terms of contracts, all deliverable of JINR for FAIR are covered up to the completion of the FOS devices. The production chain of superconducting units at JINR and the manufacturing and integration of the quadrupole modules is the critical path in the SIS100 schedule. Therefore, a major focus over the last year has been set onto the completion of the design of the cryogenic quadrupole modules and the preparation of the tendering for module production and integration. The design of the quadruple modules has been conducted together with industrial partners. The tendering of manufacturing and integration, which is one of the biggest technical efforts for the FAIR accelerators, could be launched recently. In parallel, possibilities for cryogenics testing of the integrated modules have been evaluated. The status of design and manufacturing of the radiofrequency systems, used for acceleration and compression of the beam has been progressed well. After successful completion and testing of the FOS bunch compression cavity by the company AURION, the series production of the remaining eight cavities has been launched. The company RI (Research Instruments) could complete the design and manufacturing of the FOS acceleration cavity. The cavity receives presently an intensive FAT (Factory Acceptance Test) including ramping with typical machine cycles [figure 3].

Figure 3: First of Series (FOS) SIS100 acceleration cavity at factory acceptance test at Research Instruments (RI).

The procurement of several other SIS100 components has been launched. The goal is to complete the procurement according to functional sections. All major components of the injection system, the injections kicker modules and the injection septum magnets have been tendered and awarded. As next large system, the components of the extraction system shall be procured, starting with the electrostatic extraction septum in summer 2017. The local cryogenics system is one of the most complex and unique technical systems of SIS100. Especially the bypass lines, bridging the warm sections of SIS100, differ from conventional cryogenic transfer line by the integrated superconducting bus bar system. A FOS bypass line has been manufactured and delivered by the Wroclaw University of Technology as Polish inkind contribution. Although the FOS bypass line has been accepted, the internal design had to be further improved for series production. The tendering process for the series production of the bypass lines has launched by WUST (Wroclaw University of Science and Technology). The design of the overall local cryogenics system, including the end boxes, current feed boxes and all bypass lines segments by WUST is progress very efficient. In order to finalize the (inkind) contracting of components of the local cryogenics system, it was necessary to complete and approve the specification for the feed boxes and feed-in lines. The local cryogenics system components are critical items in the overall SIS100 project schedule.

References

[1] P. Spiller et. al, Proc. of EPAC2004,1180(2004)
[2] P. Spiller et. al, Proc. of IPAC2014
[3] P. Hülsmann, Internal note Nr. 20.02.2017.RRF

DOI:10.15120/GR-2017-1

Status of the superconducting magnets for FAIR*

E. Fischer†, M. Becker, V. Bezkorovaynyy, A. Bleile, H. Bouillot, J. Ceballos, E. J. Cho, V. Datskov, N. Fischer, W. Freisleben, R. Jäger, F. Kaether, P. Kosek, V. Marusov, F. Marzouki, S. Mohite, J. P. Meier, A. Mierau, H. Müller, C. Roux, P. Schnizer, F. Seifert, K. Sugita, P. Szwangruber, and H. Weiss
GSI, Darmstadt, Germany

Introduction

Within this report the various and manifold activities and achievements of the superconducting magnets division (SCM) at GSI are summarized. In the context of superconducting magnet modules intended mainly for the SIS100 and Super-FRS, the spectrum of assignments of SCM ranges from the development of particular modules, their procurement, and follow-up of their production to the testing of the devices including the development of sophisticated methods and the set-up of test facilities.

Superconducting Magnets

Rapidly cycling magnets for SIS100

SIS100 Dipoles – status of the series production: In the course of an intensive series of tests of the First of Series (FoS) SIS100 main dipole delivered in 2014 showed excellent results with respect to e.g. quench behaviour, electric properties, powering, and ac losses. The nominal field was reached without any issues. However, the geometrical properties of the yoke aperture were found to be beyond the specified values caused by an inappropriate production technique chosen by the contractor. It was based on a standard welding technique of the yoke followed by the milling of the aperture. As a result the magnetic-field homogeneity showed characteristics which are insufficient for beam operation and the series production could not be released.
After a broad survey for alternative production techniques in cooperation between GSI and the contractor a second yoke was produced with lamination cut to the final cross section geometry, and with a novel laser welding technique (among other changes). Tests of the magnet with the new yoke were finalized in Q1/2016 with positive results. The aperture geometry was well improved with respect to the specified values. Consequently, the magnetic field provides properties suitable for beam operation proven by a sophisticated measurement system developed at GSI [1].
In parallel, about 140 issues between the FoS and the series dipoles concerning design, fabrication, and quality assurance issues were identified in a basic optimization process. With such alteration and the changes of the production technique the supplier's manufacturing concept of the series dipoles was successfully reviewed (FDR) and the series production was released in 07/2016.
In Q3 and Q4 of 2016 the manufacturer started to acquire the required material and tools, and first components of the series dipoles were manufactured. The delivery of the first series dipole is expected to be in 08/2017.

Quadrupole unit production: The Quadrupole units for the SIS100 will be built by Joint Institute for Nuclear Research (JINR) in Dubna as FAIR In-kind-contribution from Russia. The production of two pre-series quadrupole units has started at the beginning of 2016. The first one is the so-called VQD unit built from a defocusing quadrupole magnet (QD) with a vertically focusing sextupole (V) in a common unit assembly. The second one, the SF2B unit, is built from a focusing quadrupole magnet (F2) with a steering magnet (ST) joined in one unit assembly.
The yokes of all magnets have been produced by a subcontractor and delivered to JINR. The coils for both quadrupole magnets and for the sextupole corrector magnet have been manufactured at JINR. The production of the steerer coil, superconducting bus bars and the assembling of quadrupole units is scheduled for the beginning of 2017.
The design of the remaining components needed for the assembling of the quadrupole units – terminal boxes and cold terminals of the 250 A current leads – was finished and the engineering drawings were transferred to JINR. A prototype of the terminal box for the corrector magnets was tested at GSI and has shown reliable operation.

Quadrupole doublet integration: A first version of a SIS100 quadrupole doublet module (QDM) in its final configuration was finished in engineering design in 2016. This QDM located in the SIS100 arc section is named type 2.5 (QDM with type 2 focusing quadrupole magnet (QD) located in ion optical cell no. 5). It is equipped with two different superconducting quadrupole units in the so called VQD-CR-SF2B configuration. In between these two units, a cryo-collimator (CR) is located within the integrated cold mass. The unit SF2B is equipped with a beam position monitor (B). The full module also provides LHe supply for magnet cooling, main current supply for main quadrupole magnet operation, and local current supply for corrector magnet operation as well as the beam vacuum chambers.
The engineering design for the complete series of SIS100 QDMs was derived from the design of the QDM type 2.5. The series consists of four different module classes with, in total, eleven configurations including two special modules for injection and extraction of the beam with very special

* We acknowledge the support of the European Community-Research Infrastructure Activity under the FP7 program CRISP (Grant agreement no: 283745) Work Package 5. We acknowledge the support through the JINR–BMBF contract.
† e.fischer@gsi.de

DOI:10.15120/GR-2017-1

engineering design and configuration [2].
The type 2.5 QDM will be manufactured in 2018 as the first QDM in a series of 83 modules for SIS100. The procurement of the full series of SIS100 QDMs is planned in a process including multiple contractors for the various subsystems. All critical ultra-high vacuum components are planned to be procured separately by specialised manufacturers. For manufacturing of cryostat components and mechanical integration of the SIS100-QDMs a dedicated contractor shall be commissioned. The preparation work for tendering of the module integration was completed in 2016. An according contract for module integration is planned to be signed in 2017.

Magnets for the Super-FRS

The superconducting magnets of the Super-FRS comprises 33 multiplets (assemblies of quadrupole, sextupole and other corrector magnets) and 24 dipoles. The multiplets are being built by ASG, Genoa, Italy. The final design of the first of series multiplets has been approved in December 2016 and the production is about to start. The first multiplet will be available in spring 2018. The design of 21 standard superconducting dipoles by CEA Saclay is finished [3] and the tender has started. The contract signature with a manufacturer is planned for the end of 2017. The design of three special branching dipoles (i.e. dipoles with an additional straight exit) will also be carried by CEA, Saclay.

Magnet testing

Prototype test facilities

The prototype test facility (PTF) at GSI was upgraded to be able to power the high current superconducting dipoles. The new DC power converter is able to provide 20 kA at an output voltage up to 66 V with a current stability of 10^{-4}. Since the cooling power of the cryoplant is limited to 300 W the conventional vapour cooled copper current leads used before were replaced by 14 kA DC HTS-current leads in order to reduce the heat load and guarantee a reliable cooling of the magnet.

One of the main tasks running at the prototype test facility is the development of new and the adjustment of existing measurement systems for testing the SIS100 series dipole magnets.

The new system for magnetic-field measurements was developed in collaboration with CERN. It consists of a shaft of five rotating coil probes, a motor drive with an angular encoder and the data acquisition electronics. Next to this a system to measure the geometry of the magnet's aperture was developed and successfully tested during the measurements on the first of series dipole magnet for SIS100 [1].

Series test facilities

The GSI test facility for SIS100 series dipoles (STF) was built from 2014 to 2015 and is under commissioning. The main use of the STF is to execute the series tests of the SIS100 dipoles and the SIS100 string test, a short part of SIS100 consisting of one dipole and one quadrupole module together with local cryogenic components. Besides this the STF allows for testing of every type of superconducting magnet for SIS100, Super-FRS and later on of Heavy Ion Synchrotron SIS300. Moreover, it provides cooling capacity for operating a superconducting continuous-wave linear accelerator (cw-linac) later on.

The main supply systems such as a cryoplant with a cooling power of 1500 W and two power converters with 20 kA (at 66 V output voltage) were successfully commissioned during 2015 and 2016. The STF is expected to be ready for operating in May 2017.

SIS100 quadrupole unit testing

A facility for testing of superconducting magnets for FAIR and NICA projects has been commissioned and put in operation at Joint Institute for Nuclear Research in Dubna in November 2016. JINR and GSI shared the costs of building the facility. Three of six cryogenic test benches are foreseen for testing of quadrupole units for the SIS100 synchrotron. The testing program will include the power tests of the magnets at helium temperatures, measurements of the magnetic-field quality as well as the adjustment of the hydraulic resistance for each type of the quadrupole unit. Tested units will be shipped to the company responsible for the integration of the units to the Quadrupole Doublet Module (QDM). Cold testing of two pre-series quadrupole units is scheduled for the middle of 2017.

Testing of Super-FRS magnets

The Super-FRS dipoles and multiplets will be tested under cold condition (4 K) at a novel cryogenic test facility in CERN [4]. In accordance with a collaboration agreement between CERN and GSI, refurbishment of the facility and installation of the new infrastructures have been done. The commissioning of the facility is partly started. The handover of the facility from CERN to GSI is planned in the middle of 2017. For completion of the commissioning to be participated by GSI colleagues, and the pre-series multiplet testing starts from 2018.

Current leads

The four pairs of Main HTS Current leads have been delivered to the series test facility (STF) at GSI in 2016. The first pair of current leads in Feedbox1 at STF passed the high voltage tests up to 3 kV and a successful run with 14 kA DC current, 13.2 kA cycling current and up to 17 kA pulsed current. Such test program during two days of tests corresponds to the SIS100 requirements. The design of 250 A local current leads made from HTS was finished

DOI:10.15120/GR-2017-1

and two prototype current leads were tested during three runs at the prototype test facility (PTF). Those current leads with novel concept successfully passed tests with 250 A DC current, cycling of 0-250 A current at 1-3 Hz and training pulses of 0-300 A . For the γ_t-Jump-Quadrupole with 250 A pulses of 100 ms duration the design of conventional copper current leads has been finished and a prototype current lead has been successfully tested at PTF. For the Hedgehob collaboration a modern design of conventional copper current leads cooled by vapor was proposed due to the high risk for HTS with respect to magnetic field and radiation losses.

Quench detection system of SIS100

The quench detection system dedicated to survey the magnets of SIS100 against quench was recently redefined. In order to reduce the impact of parasitic capacitance introduced to the SC dipole and quadrupole circuits by a large number of voltage taps, it was decided to develop a new cabling concept that enables to compare two adjacent magnets of the circuit.
The new cable structure provides a high reliability level since each magnet is surveyed by two quench detectors. For the main magnets either a magnetic amplifier (MA) [5, 6] or classical bridges (BRD) will be utilised. MA provides galvanic insulation at the cryostat level while BRD cards require high voltage cabling between the magnet and quench detection cabinets. The R&D program on MA is ongoing. A number of transductor prototypes were manufactured and tested with a single dipole magnet. The results are very promising. The next experiment will consider a test of 10 identical transductor assembled in the overlapping structure.
For the corrector magnets, it is foreseen to use a new Mutual Inductance Detector. The first prototype was manufactured and successfully tested with the corrector magnet model (solenoid) at cryogenic conditions.

Conclusion

In 2016 many remarkable steps were taken in the various fields of activities of the SCM division. By the release of the series production of the superconducting dipoles a major milestone in the procurement of the components for SIS100 was passed. The start of the pre-series production at JINR, Dubna, complements this process on the quadrupole unit side. There, the unit's yokes are produced and other components are on the track. In parallel, the engineering design of the first quadrupole doublet module formed by an assembly of the quadrupole units was finalized and the further module designs were derived from this concept. Regarding the production of the Super-FRS magnets, the manufacturer's concept of the pre-series multiplet was reviewed and confirmed. The engineering design of the Super-FRS dipole was finished and the tendering for manufacturing will be started soon.
On the testing branch, a novel magnetic-field measurement system for the SIS100 dipole was developed. Moreover, a tool for the precise mapping of the yoke's aperture geometry as a crucial parameter for the field quality of the magnets was engineered. The series test facility for acceptance measures of the SIS100 dipoles is under commissioning at GSI. In parallel, the test facility for the quadrupole units was commissioned and successfully put in operation at JINR, Dubna. The installation and commissioning of the Super-FRS magnets testing site at CERN has partly started. The four pairs of main current leads for the STF successfully passed acceptance tests. Their design will be used for the main current leads for SIS100. Novel developments for local current leads were confirmed.
For the scope of quench detection and magnet protection, the planned system for SIS100 was redefined in terms of a novel cabling concept to minimize parasitic capacitances. A research program on magnetic amplifiers was started in order to open up alternatives to classical bridge detectors.
To summarize, the manifold activities under the responsibility of the SCM division yielded in many crucial milestones and set the basis for further steps to successfully realise the FAIR project.

References

[1] C. Roux et al., IOP Conf. Series: Materials Science and Engineering 171 (2017), 012108, doi:10.1088/1757-899X/171/1/012108

[2] J. Ceballos Velasco et al., IEEE TRANSACTIONS ON APPLIED SUPERCONDUCTIVITY, VOL. 26, NO. 3, APRIL 2016, http://ieeexplore.ieee.org/document/7433400/

[3] J. E. Munoz Garcia et al., IEEE Transactions on Applied Superconductivity 2017, Volume 27, Issue 4

[4] L. Serio and P. Schnizer et al., IEEE TRANSACTIONS ON APPLIED SUPERCONDUCTIVITY, VOL. 27, NO. 4, JUNE 2017

[5] K. H. Mess, Quench Protection at HERA, CH2387-9/87/0000-1474 IEEE, PAC, 1987.

[6] L. Coull, D. Hagedorn, V. Remondino, F. Rodriguez Mateos, LHC Magnet Quench Protection System, CERN Internal Note AT-MA/LC 93-81, July 1993.

Investigations on desorption using the single shot method *

Ch. Maurer[†1,2], *L. Bozyk*[2], *Sh. Ahmed*[2], *P. Spiller*[2], *and D.H.H. Hoffmann*[1]
[1]TU Darmstadt, Institut für Kernphysik, Germany; [2]GSI, Darmstadt, Germany

Introduction

Beam induced gas desorption is a key process that drives beam intensity limiting ionization losses in heavy ion synchrotrons in general and in the upcoming SIS100 in particular. Minimizing this effect by providing low desorption yield surfaces is an important part of maintaining a stable ultra high vacuum, which is required for accelerator operation with medium charge state heavy ions. This necessitates the measurement of beam induced desorption yields for various materials and thermal properties of the target in combination with energy and ion species of the beam. Due to the relevancy of high intensity beams for high energy density physics, previous iterations of this report have contained contributions about the results of these experiments [1] as well as novel methods for data analysis [2].

Experimental Setup

An experimental setup for desorption yield measurement has been devised, constructed and taken into commission at the SIS18 at GSI. Based on the experience gained during operation in the beamtime of 2014, it has been continuously improved and expanded. The new setup was used during a beamtime in 2016. Both versions have been used in single shot mode, since measurement in continuous bombardement mode is unfeasible when using a synchrotron. This technique relies on a time resolved measurement of the pressure peak after beam impact, known as the desorption peak. [3] explains both methods in context of a review of past results.

Data Analysis

The desorption yield η is defined as the relation between the number of incoming beam particles N_{beam} and the number of desorbed gas particles N_{des}. Expanding it with the height of the measured desorption peak Δp yields

$$\eta = \frac{N_{\mathrm{des}}}{N_{\mathrm{beam}}} = \frac{\Delta p}{N_{\mathrm{beam}}} \cdot \left(\frac{\Delta p}{N_{\mathrm{des}}}\right)^{-1}.$$

This way, η can be expressed as a product between two factors. $\Delta p/N_{\mathrm{des}}$ must be measured for every desorption event, while $\Delta p/N_{\mathrm{des}}$ is the pressure peak height caused by a single desorbed particle from the target, regardless of the way the desorption was caused. This value, the gas dynamics factor, is characteristic for the experimental setup and can be calculated in a variety of ways, including the ideal gas law. In this work, the ideal gas approach has been rejected in favour of a technique using 3D Monte Carlo gas dynamics syimulations to account for additional effects, like the pumping of the cryotarget.

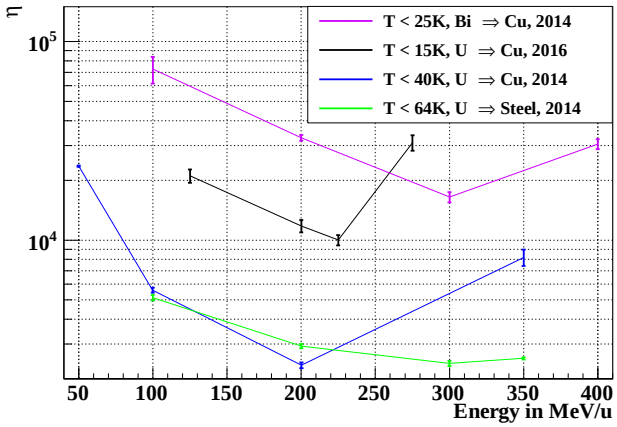

Figure 1: Energy dependance of desorption yields η, measured during the beam times in 2014 and 2016.

Results

Fig. 1 shows a heavily condensed summary of the results obtained with a cryogenic target. While room temperature results show a scaling of eta with the ion's energy loss at the target surface (i.e. a lowering of η with rising energy), the rise in η after a local minimum represents a deviation from this dependancy, which has been observed before [4]. A lower temperature also seems to cause a general rise of η, which suggests the existance of a temperature with a minimum desorption yield. Comparing the data taken with uranium beams suggests a relation between the strength of this deviation and the temperature. However, when taking into account the bismuth curve, one can see that the temperature does not seem to be the only responsible variable.

References

[1] Ch. Maurer et al., "Heavy Ion Induced Desorption on Cryogenic Targets", GSI annual report 2014

[2] Ch. Maurer et al., "Gas Dynamics Simulations for Heavy Ion Induced Desorption Measurements with the Single Shot Method", GSI annual report 2015

[3] E. Mahner, "Review of heavy-ion induced desorption studies for particle accelerators", Phys. Rev. Acc. Beams, Vol. 11, 2008

[4] L. Bozyk et al., "Development of a cryocatcher prototype and measurement of cold desorption", LPB, Vol. 34, 2016

* This report is also submitted to the HEDgeHOB-Report 2016

† christoph.maurer@skmail.ikp.physik.tu-darmstadt.de

DOI:10.15120/GR-2017-1

SIS100 Inspection robot – development and status report

N. Schweizer[*1] *and I. Pongrac*[2]
[1]TU Darmstadt RMR, Darmstadt, Germany; [2]GSI, Darmstadt, Germany

During maintenance work or upgrade measures of large particle accelerator vacuum systems, randomly as well as deliberately introduced foreign objects may inhibit the particle beam significantly, usually leading to a considerable high risk of a complete shutdown of the accelerator. Considering reported incidents from several different particle accelerator laboratories, where e.g. bottles, screws, dropped down inserts, and in the case of SIS18, a crumpled aluminum foil, have been found within the vacuum system, a novel platform for a mobile inspection device is currently being developed and is foreseen to be deployed in SIS100.

Development of the robot design

The vacuum system of SIS100 offers a challenging topography for any mobile inspection robot where a multitude of steps, deep gaps, as well as chambers with limited apertures have to be traversed reliably. Ideally, during each shutdown and prior to closing the vacuum system, the inspection robot shall traverse the complete vacuum system of the SIS100 and visually examine the beam pipe vacuum for any obstacles, damages or anomalies.

In order to design a suitable semi-autonomous robot to be used in the SIS100 vacuum system, the geometries of the different vacuum chambers and pipe sections have been analyzed. The robot is designed in such a way that steps and gaps can be detected and traversed in a safe way. In addition, the robot is able to move forwards and backwards in case an insurmountable obstacle is detected.

The ab initio modular concept of the robot where several modules can be attached successively to increase the total length ensures a high degree of flexibility for the inspection robot to be able to traverse most vacuum chamber topographies. Fig. 1 illustrates the current modular prototype design.

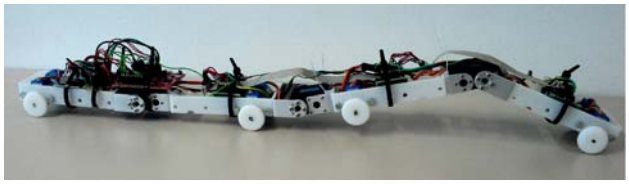

Figure 1: Fully functional prototype model of the SIS100 inspection robot.

* nicolai.schweizer@rmr.tu-darmstadt.de

Simulations and current status

After the determination of the fundamental robot design, extensive 3D simulations have been performed to test and to verify that the robot can traverse as many vacuum sections of SIS100 as possible. Thus, the probability of malfunctions (e.g. the robot gets stuck) can be minimized. Various locomotion strategies have been simulated in realistic test environments based on actual SIS100 CAD data. Additionally, several experiments have been successfully executed with real vacuum chambers or replicas. In Fig. 2 a typical simulation scenario is exemplarily illustrated.

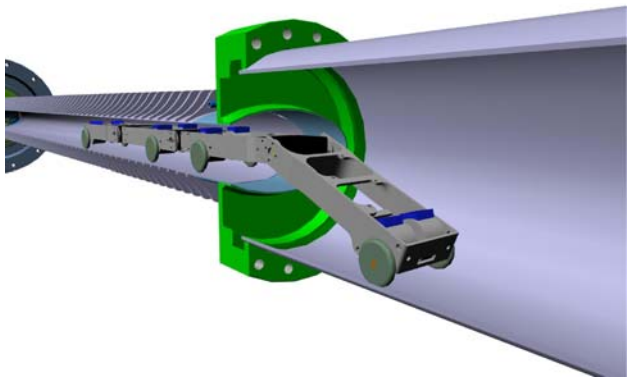

Figure 2: 3D simulation with the Gazebo [1] robotics simulator: A step is traversed as an example of a typical locomotion sequence of the inspection robot.

Outlook and further steps

Consideration of more complex chamber geometries (e.g. double steps), adaptations for curved vacuum chambers (dipole chambers) as well as ongoing maneuver strategy optimizations are currently under development. Battery management, communication possibilities and the implementation of a suitable on-board camera are the principal topics of ongoing work. Further experiments as well as simulations are crucial to allow the SIS100 inspection robot to become a universal tool for particle accelerators.

References

[1] N. Koenig and A. Howard, “Design and use paradigms for Gazebo, an open-source multi-robot simulator”, IEEE/RSJ International Conference on Intelligent Robots and Systems (IROS), pp. 2149-2154, vol. 3, 2004

DOI:10.15120/GR-2017-1

Mechanical interaction of the cryogenic piping system of SIS100*

M.C. Serna Moreno[1], *J. Ceballos Velasco*[† 1,2], *V. Datskov*[2], *and PBMT department*[2]
[1]Universidad de Castilla-La Mancha, Ciudad Real, Spain; [2]GSI, Darmstadt, Germany

The SIS100 superconducting magnetic system consists of different types of modules all along the ring perimeter, containing the main dipole and quadrupole magnets. The modules must be lined up under exigent displacement tolerances, accomplishing the challenging requests on the positioning of the cold masses and vacuum vessels [1]. Due to the hexagonal shape of the synchrotron, there are angular connections between adjacent modules. Traditionally, numerical studies analysing their structural response have been carried out isolating each module. However, the mechanical influence that they could have over each other should not be omitted. The join with a certain angle of modules with different geometries in combination with temperature changes and linkages for displacement compensation could lead to unexpected interaction forces. Their effect should be taken into account in order to avoid any source of misalignment.

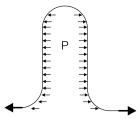

Figure 1: Resulting forces along the expansion joint axis transferred to the pipelines [3]

The piping installation that ensures the cooling to cryogenic temperatures of the magnets is vital to maintain superconducting conditions during the operating phase. In particular, within the conceptual engineering design developed in the Super Conductive Magnets & Testing department of GSI, the analysis of the relative displacements in the connection point between cryogenic pipes from different modules has been recently developed [2,3]. The study has taken into account the angular joint, the thermal shrinkage and the internal pressure withstood. The introduction of universal compensation junctions is essential to absorb the resulting interaction forces and to reduce the undesirable axial, lateral and angular deflections. But these bellows-type elements generate unbalanced loads over the piping system in the axial direction of the linkage (Fig. 1), proportional to the internal pressure and the surface of the crest, which have had to be also accounted in the analysis.

Simulations have been performed with the ANSYS® finite element software under license of GSI. Simplified models from the point of view of the geometry have been considered under the hypotheses of static and linear analysis. In order to assure that the physics of the problem was reproduced, a previous study of the elements accuracy has been performed. The correctness of the numerical estimations have been confirmed by means of comparing the simulation results with those of known situations with analytical solution. As well, sensitivity analyses to the element size have been carried out to ensure that the mesh was ine enough, finding an adequate balance between the computational cost and the degree of precision of the results. This work has been focused on studying the mechanical interaction of the piping systems that ensure the cryogenics of the magnets. As main scenario, the angle of the connection between the cooling tubes which belong to two contiguous modules has been assumed to be equal to 1.67° (Fig. 2). Both pipes have been modelled with the same cross-section and material properties but different lengths, working at temperatures of 4.5 K and supporting internal pressures of 1.1 bar. Besides, the existence of a displacement compensation joint has been considered for completing the definition of realistic conditions. The linear analyses have been developed with simplified 1D geometries, thanks to the use of PIPE188 and MPC184 elements for modelling, respectively, the tubes and the desired rigidity in the connection. Being the variable of interest the mid-point displacements of the system, the results have demonstrated the importance of the flexural deformation of the pipes caused by the angular joint and the induced horizontal movements due to the non-symmetric geometry. These effects could be transmitted to the body of the vacuum vessel at the attachment points, generating a loading hypothesis not contemplated in previous designs. Taking into account that the displacement tolerances of the modules are very restrictive, it is desirable to evaluate its influence at the analysis stage.

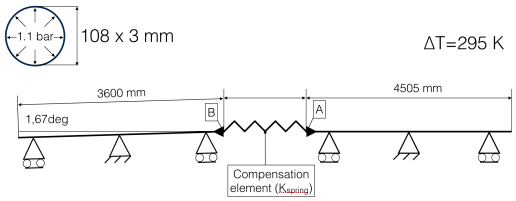

Figure 2: Reference simulation for coupled pipes with a displacement compensation linkage [3]

* Work supported by FAIR@GSI PSP code: G2.08.02.10, the University of Castilla-La Mancha and the grant DPI2016-77715-R from Ministerio de Economía y Competitividad (Spain).

† j.ceballosvelasco@gsi.de

DOI:10.15120/GR-2017-1

References

[1] J.P. Meier, A. Bleile, E. Fischer, G. Hess, J. Macavei, P. Spiller, “Cryo-technical design aspects of the superconducting SIS100 quadrupole doublet modules”, ICEC/ICMC 2014, July 2014, p. 1519.

[2] J. Ceballos Velasco, M.C. Serna Moreno, V. Datskov, E. Fischer, PBMT department, “First Steps of the Development of a Simplified FEM Model for an Arc Section of SIS100 Synchrotron”, GSI Scientific Report 2015, p. 357.

[3] J. Ceballos Velasco, M.C. Serna Moreno, V. Datskov, E. Fischer, “Evaluation of mechanical displacements in superconducting accelerator magnet arrays”, 14th Cryogenics 2017, Dresde, May 2017.

DOI:10.15120/GR-2017-1

Feasibility of RF feedback control loops in heavy-ion synchrotrons by means of derivative estimation *

B. Reichardt[†1], *J. Adamy*[1], *D. Domont-Yankulova*[1,2], *K. Groß*[2], *H. Klingbeil*[2,3], *and D. Lens*[3]
[1]TU Darmstadt RMR, Darmstadt, Germany; [2]TU Darmstadt TEMF, Darmstadt, Germany; [3]GSI, Darmstadt, Germany

Damping of longitudinal coherent bunched-beam oscillations is needed in SIS18 and SIS100 to stabilize the beam, prevent emittance growth and keep beam loss low during acceleration. In last year's work several approaches of digital filters for beam-phase control have been examined. An FIR (finite impulse response) filter with 3 taps, cf. [1], has been successfully used at GSI in several machine experiments for a beam-phase control system and a longitudinal feedback system. In this report an alternative FIR filter approach based on derivative estimation leads to better results as it damps dipole oscillations *within* one oscillation period whereas the former filter approach unveils its full potential only *after* one oscillation period.

Requirements and filter properties

A numerical differentiator approach [2] has been chosen as an alternative to the established 3-tap filter. Both filters share the same control topology, but have different coefficients. The results obtained so far indicate that the optimal filter gain is approximately a constant divided by the synchrotron frequency. Therefore the derivative estimation filter has to be adapted to varying synchrotron frequency.
A filter bank will be used to select different filters based on available parameters such as the synchrotron frequency and bunch length. Alternatively, a continuous tuning of the coefficients will be possible [3].

Experiment, simulations

Both the experiment and the nonlinear tracking simulations were performed for $^{238}U^{73+}$ as ion species at an energy of 300 MeV/u for a stationary operation with a linear synchrotron frequency of 422 Hz at h=2. The beam-phase measurement varies with white Gaussian noise with about $3\sigma = \pm 0.66°$. In this case the derivative estimator has a length of L = 10 non-zero taps without additional zero-taps and is tuned to a high damping rate.
Figure 1 shows the experimental and the simulated results where a disturbance of $2°$ on the beam phase is applied to intentionally excite a feedback reaction. The results indicate that the experiment is in very good agreement with the nonlinear tracking simulation for the derivative estimation approach. Compared to the 3-tap filter approach, there is no overshoot and the dipole oscillation is damped within one oscillation period for the derivative estimation approach. Also the RMS-emittance does not increase while using the derivative estimation approach, which is a second quality criterion besides the damping rate. Furthermore, this approach can be put into practice easily with the existing control topology.

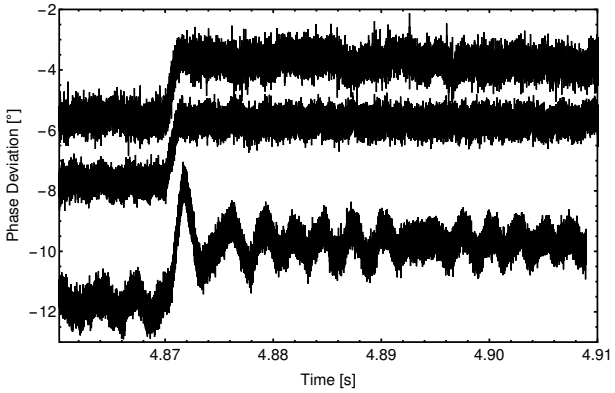

Figure 1: Beam-phase with respect to uncorrected Group-DDS: Experimental data (top), simulated data with arbitrary offset for a controller with derivative estimator (middle) and 3-tap filter (bottom) with a $2°$ distortion at 4.87s.

Outlook

Under current investigation is the critical signal to noise ratio (SNR), at which the derivative estimator approach delivers better results than the 3-tap filter. Another important investigation regards the implementation of the new approach for operation during acceleration ramps.

References

[1] H. Klingbeil et al., "A Digital Beam-Phase Control System for Heavy-Ion-Synchrotrons", IEEE Transactions on Nuclear Science Vol. 54, No. 6, December 2007

[2] M. Mboup et al., "Numerical differentiation with annihilators in noisy environment", Numerical Algorithms, Vol. 50, Issue 4, April 2009

[3] K. Möller et al., "FPGA Based Tunable Digital Filtering for Closed Loop RF Control in Synchrotrons", GSI Scientific Report, 2013

* Supported by the Helmholtz Graduate School for Hadron and Ion Research

† benjamin.reichardt@rmr.tu-darmstadt.de

DOI:10.15120/GR-2017-1

Measurements of incoherent synchrotron frequencies in dual RF bucket

O.Chorniy
GSI, Darmstadt, Germany

The knowledge of the so-called incoherent synchrotron frequencies may be used in different applications: for the RF voltage calibration or studies of the high intensity effects [1]. Future operation in FAIR synchrotrons includes regimes when beam is bunched using two RF harmonics. For such bunches, the incoherent frequencies were obtained using bunch profiles.

In Figure 1 the longitudinal bunch profiles measured using Beam Position Monitor every machine turn in SIS18 is shown. To create the bunch, two RF harmonics were used: one with 10 kV amplitude at h=5 and second 4.6 kV at h=10 (see Figure 1, lower plot). Measurements were done at injection energy of 6.75 Mev/u with 0.4 mA current of Xe^{43+} ion beam.

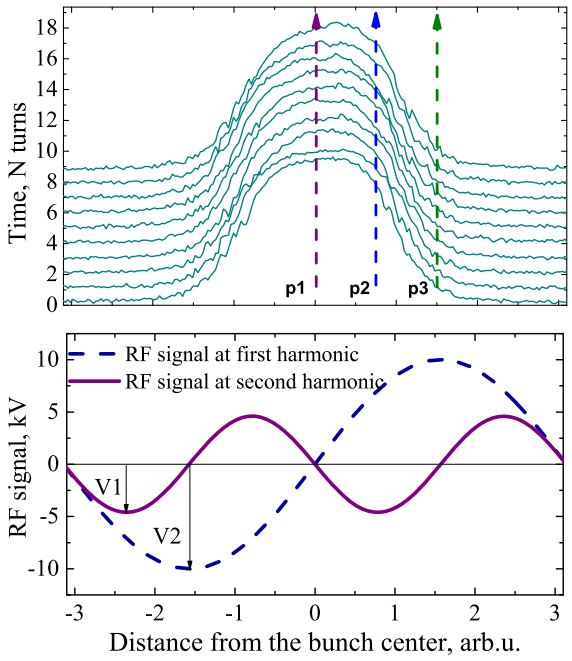

Figure 1: Waterfall of the measured buches (upper plot) created by two RF harmonics (lower plot)

It can be seen that the current at each coordinate of the bunch profile fluctuating with time (as example along the lines p1,p2,p3 on Figure 1). In [1] it was shown that the frequency spectra of these fluctuations must have maximum at specific frequencies (as example see spectra on upper plot of Figure 2). The position of the maximum depends on the bunch coordinate at which the current was measured. Therefore, calculating the current spectrum at different coordinates and correlating the spectrum peaks with these coordinates the incoherent synchrotron frequencies can be obtained. The measured frequencies compared with theory are presented on lower plot of Figure 2.

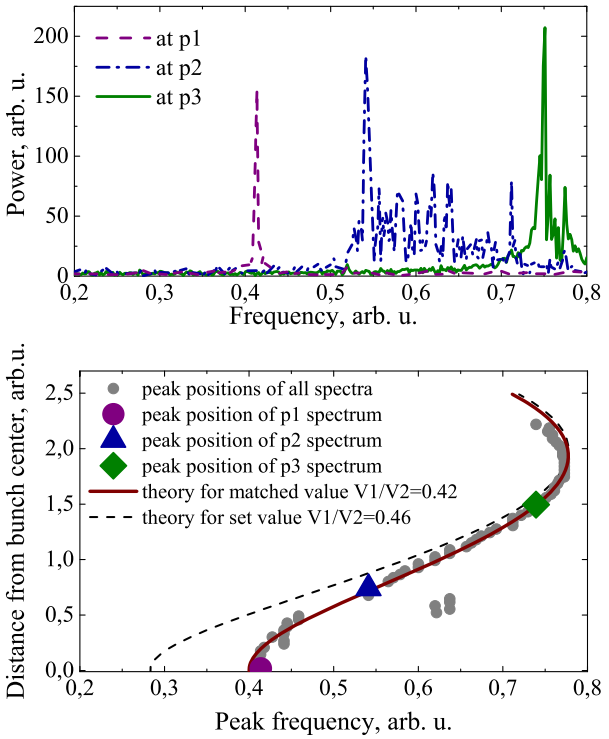

Figure 2: Spectra of current fluctuations measured at three coordinates (upper plot), position of the spectrum peak depending on the coordinate at which the spectrum was obtained and theorethical curves for two cases (lower plot)

In theory, the incoherent synchrotron frequencies can be obtained using formulas in [2]. One of the parameter influencing the incoherent frequencies is the relation of the RF voltage amplitudes. Despite this relation was set to 0.46, the measurements show that the value of 0.42 matches better to the measurements. The reasons for this deviation will be investigated during next beam times.

References

[1] Oleksandr Chorniy and Hansjörg Reeg, A Method To Measure The Incoherent Synchrotron Frequencies In Bunches., Proc. of HB2012, Beijing, China, 2012

[2] S.Y. Lee. Accelerator Physics. World Scientic Publishing Co. Pte. Ltd., second edition, 2004, pages 327-331

DOI:10.15120/GR-2017-1

The SIS100 laser cooling facility*

D. Winters[†1], *T. Beck*[2], *G. Birkl*[‡2], *O. Boine-Frankenheim*[‡1,2], *M. Bussmann*[3], *C. Egelkamp*[4], *L. Eidam*[2], *V. Hannen*[4], *D. Kiefer*[2], *Th. Kühl*[1,5], *M. Löser*[3,7], *X. Ma*[§6], *U. Schramm*[‡3,7], *M. Siebold*[3], *Th. Stöhlker*[1,5,8], *Th. Walther*[‡2], *W. Wen*[6], *D. Winzen*[4], *and P. Spiller*[1]

[1]GSI Helmholtzzentrum, Darmstadt, Germany; [2]Technical University Darmstadt, Germany; [3]Helmholtz-Zentrum Dresden-Rossendorf, Germany; [4]Münster University, Germany; [5]Helmholtz Institute Jena, Germany; [6]Institute of Modern Physics-CAS, Lanzhou, China; [7]Technical University Dresden, Germany; [8]Jena University, Germany

Within POFIII ARD 'Matter and Technologies', the project group 'SIS100 laser cooling' is setting up a laser cooling facility at the FAIR heavy-ion synchrotron SIS100. With the aid of this facility, intense beams of relativistic heavy highly charged ions will be laser-cooled to lowest temperatures, thus providing worldwide unique beams. The project group that deals with this task consists of scientists from GSI and the collaborating partner universities and research centers in Dresden-Rossendorf, Darmstadt, Jena, Münster, and Lanzhou (China) [1].

The laser systems are being developed by the HZDR/TU-Dresden and the TU-Darmstadt, with strong support from the BMBF. These laser systems can be operated at 257 nm or 514 nm, and produce about 100 mW of coherent radiation. The TU-Darmstadt will provide a fast scanning cw-laser system [2], and a pulsed laser system with long (up to 1 ns) pulses and a high repetition rate (up to 1.5 MHz) [3]. The HZDR will provide a pulsed laser system with short pulses (∼ps) and a high repetition rate up to 1 MHz [4]. The Münster group will provide an XUV/X-ray detector for the SIS100, again supported by the BMBF.

The laser lab at the SIS100 will be located 18 m underground in the service tunnel, spatially separated from the accelerator tunnel where the ions circulate. We will need a dedicated laser beamline with sophisticated laser beam steering, stabilization, and diagnostics to ensure an optimal transport and overlap (in space and time) of the laser beam with the ion beam. Currently, we are designing a prototype for the laser beamline, which will have complete laser beam steering and diagnostics. Important components for this beamline, such as a complete set of doubly-coated (257 - 266 nm and 514 - 532 nm) mirrors of the highest quality (reflectivity >99.5%), in 1", 2", and 3" sizes [LayerTec], are already available. These mirrors are compatible with the required vacuum of 10^{-6} mbar of the beamline. The same is true for an entire set of high-quality mirror mounts and prism holders [Liop-Tec]. The mounts incorporate fast piezo drivers, which can be remotely controlled. The new 1" polarizing beam splitter cubes also work for both wavelength ranges [MPO]. Two small green (532 nm) laser systems will be used for tests of the laser beamline. Figure 1 shows a collage of some of the new components.

Figure 1: Collage showing a selection of the components purchased in 2016. Top row, polarizing beam splitter cube and doubly-coated mirrors. Middle row, mirror mounts (vacuum, 2", prism). Bottom row, $\lambda/4$-plate, green laser.

Finally, also two test beamtimes for laser cooling have been performed in 2016: one in April at the CSRe of the IMP in Lanzhou, China, and one in July at the ESR in Darmstadt [5]. The pulsed laser system from the HZDR was shipped over especially for the beamtime at the CSRe. At the ESR, the pulsed laser system was also used, and uniquely exhibited a clear and effective interaction with the stored and bunched ion beam. The cw-laser system from the TU-Darmstadt was also very successfully applied and delivered great results, also for laser spectroscopy of $^{12}C^{3+}$. In addition, the new XUV detector system from Münster university was successfully used for the first time during an experiment [6]. A similar detector is foreseen for the SIS100 vacuum chamber, where also the laser will be coupled in. The design of this vacuum chamber is ready and the chamber can hopefully be delivered in 2017.

References

[1] D. Winters *et al.*, Phys. Scr. **T166** (2015) 014048.

[2] T. Beck *et al.*, Opt. Lett. **41** (18) (2016) 4186.

[3] D. Kiefer *et al.*, GSI scientific report 2015.

[4] M. Siebold *et al.*, Opt. Expr. **20** (2012) 21992.

[5] D. Winters *et al.*, GSI scientific report 2016.

[6] D. Winzen *et al.*, GSI scientific report 2016.

* Work supported by HGF POFIII ARD-ST2.

† d.winters@gsi.de

‡ Work supported by BMBF.

§ Work supported by BMBF-WTZ.

DOI:10.15120/GR-2017-1

Optimization of the multi-turn injection

S. Appel[1], O. Boine-Frankenheim[1,2], L. Groening[1], Y. El Hayek[1], M. Maier[1], C. Xiao[1]
[1] GSI, Darmstadt, Germany, [2] TU, Darmstadt, Germany

The multi-turn injection (MTI) into the SIS18 is one of the bottlenecks for providing ion beams of unprecedented intensities and qualities for FAIR. An optimized injection is also crucial for an excellent interfacing between injector linac and synchrotron. The loss-induced vacuum degradation and associated life-time reduction is one of the key intensity limiting factors for SIS18. Beam loss during injection can trigger the pressure bump instability. An optimized injection can relax the dynamic vacuum problem, but is also crucial to reach the synchrotron intensity limit by a large multiplication of the injected current. For the SIS18 the optimization with genetic algorithms (GA) resulted in a significant improvement of MTI performance and subsequent transmission for intense beams [1]. A loss-free or low-loss injection over many turns were identified. The dependence between gain factor and injection loss is shown in Fig. 1. GA optimization found a much better MTI performance than the previous simulation studies in [2]. Space charge results in a similar MTI performance, but with different injection settings. Using a global residual gas pressure and beam lifetime model together with the optimized multi-turn injection a range of injector brilliance could be defined. This crucial information gives more flexibility for the injector upgrade layout for FAIR [3] and allow an excellent interfacing between injector linac and synchrotron.
One consequence of the single-plane MTI is that the required injection emittance for the injection plane (usually the horizontal one) is very demanding; to the other plane not. Re-partitioning of the injected beam emittances, i.e. round-to-flat transformation would increase the injection efficiency. This benefit effect to the MTI performance of a smaller emittance has been measured as a function of the amount of flatness of the beam. The injection performance has increased significantly up to about 30% shown in Fig. 2. An excellent agreement between simulation and measured injection performance as a function of the injected emittance was achieved thanks to fast adjustment of the beam flatness without changing other beam parameters [4]. The flat beam injection scheme is a scenario for an additional upgrade of the existing UNILAC which may be necessary if the other upgrade measures [3, 5] including a well optimized injection turn out to be not sufficient to reach the beam parameters imposed by FAIR.
Further opportunity to enhance the MTI performance is to injected into both space phase planes. One possibility is to used skew quadruples during injection to couple both planes. The other is to rebuild the SIS18 injection section and transfer channel for the advantage of two-plane injection. Injection optimization simulation studies with this mentioned methods are ongoing. After the undergoing

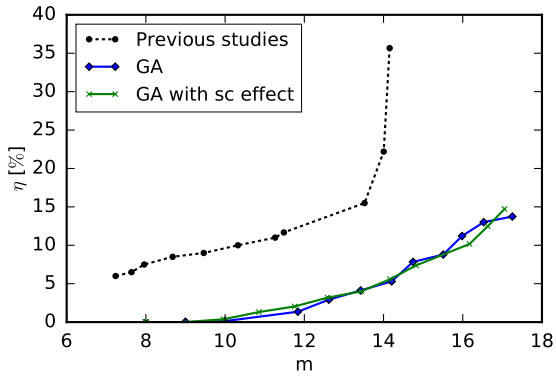

Figure 1: The GA optimization found much better MTI performance than the previous simulation studies [2].

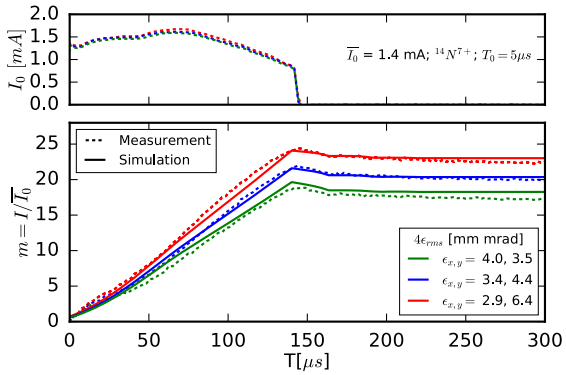

Figure 2: MTI optimization through emittance transfer.

construction work at SIS18 has been finished, it is planned to test an online injection optimization with the new implement and more flexible control system. First online GA optimization test as been already performed at CRYING injector [6].

References

[1] S. Appel, el al, Nucl. Instr. and Meth. A 852 7379 (2017), http://dx.doi.org/10.1016/j.nima.2016.11.069.

[2] S. Appel, O. Boine-Frankenheim, arXiv:1403.5972 (2014).

[3] L. Groening et al, PRL 113, 246802 (2014)

[4] S. Appel, et al, Injection optimization through generation of flat ion beams, submitted to Nucl. Instr. and Meth. A (2017).

[5] L. Groening et al, Upgrade of the Universal Linear Accelerator UNILAC for FAIR, Proc IPAC2016 (2016).

[6] S. Appel et al, Automatized Optimization of Magnet Settings using Evolutionary Algorithms, Proc IPAC2017 (2017).

DOI:10.15120/GR-2017-1

The cryosorption pumps of the SIS 100 – acceptance tests of the first-of series units

St. Wilfert[1] and I. Pongrac[1]
[1]GSI, Darmstadt, Germany

Abstract

The article gives an overview on the production of the SIS100 series cryosorption pumps and their acceptance tests. We also present simulation results on time and position dependent hydrogen density profiles in a SIS100 sector which show why the use of localized cryosorption pumps is crucial for keeping the hydrogen partial pressure in the cryogenic section at an acceptable low level for sufficiently long times.

Introduction

The cryogenic beam vacuum system of SIS100 will be operated at wall temperatures between 5 … 15 K. At such low temperatures, with the exception of hydrogen and helium, all vacuum relevant gas species can effectively be cryopumped by the cold chamber walls with practically infinitive pumping capacity. However, while H_2 can be cryosorbed by the bare chamber walls at least with a limited pumping capacity at these temperatures, no pumping speed is available for He at 15 K. Consequently, additional pumping speed for these both gas species is of crucial importance for long-term maintenance of sufficiently low beam vacuum pressures. Local cryosorption pumps (CSP) are predestined for this purpose and will therefore be used in the cryogenic sections of SIS100 as auxiliary pumps. In total, 14 CSPs are required for each SIS100 sector, 11 of them will be distributed in the cryogenic arc. They will be installed in ~ 13 m intervals between each superconducting (sc) dipole doublet. In addition, each one pump will be integrated in the sc quadrupole doublets on the straight beam line sections of the ring.

In [1] we reported on a prototype of the CSP developed and tested at GSI. The pump was specially designed according to the space and installation conditions in the SIS100 magnet cryostats. The pumping elements are formed by 6 circular charcoal-coated cryopanels, which are uniformly cooled-down to 4.2 K by an axially running liquid helium (LHe) cooling tube. In contrast to the prototype pump described in [1], however, minor technical modifications have been made to the series pumps. First, all panels of the series pumps have the same diameter of 9 cm, achieving a higher pumping capacity. Second, instead of the charcoal type SC2 by Chemviron Carbon, all panels are now coated with the adequate charcoal type Aquacarb 208C (particle size 12x30 US mesh) also produced by Chemviron Carbon. The cryosorption properties of the alternative charcoal type were investigated experimentally in advance, no significant differences in pumping characteristics were found. Each panel is coated with approximately 5 g, i.e. 2.5 g charcoal per panel side. This corresponds to an average coating density of approx. 0.04 g/cm^2. In total, approximately 30 g charcoal contains one pump. The coating was done using a suitable low temperature-resistant epoxy. The central cooling tube was manufactured from a threaded Cu rod. In operation, pressurized liquid helium with a mass flow of minimum 1.0 g_{LHe}/s (at 4.2 K, 2 barg) will be led through the cooling tube. The pump is mounted on a standard D100CF base flange, its housing is formed by a standard stainless steel DN100CF full nipple. In order to avoid charcoal particles from falling out of the pump, a commercially available turbo pump splinter shield with a high optical transparency will be mounted at the pump inlet flange. Figure 1 shows the series pump to be used in the cryogenic beam line sections of the SIS100.

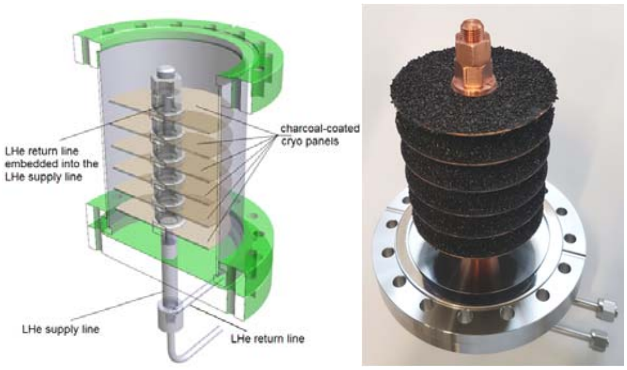

Figure 1: Series cryosorption pump produced by ILK Dresden, Germany.

Acceptance Tests of the First-of Series Units

The production order of the series pumps was granted to ILK Dresden, Germany. The first two pumps, denoted to as first-of-series (FoS) pumps, were subjected to intensive tests at the manufacturer and GSI. Of particular importance is the leak tightness of the central cooling circuit. As the LHe cooling circuit runs through the pump housing and faces directly the beam pipe vacuum system, absolute leak tightness was mandatory. LHe leaking into the pump may disable completely the pumping action of the pump due to rapid He saturation of the panels. In order to prove the leak tightness of the axial cooling tube, the leak test has been conducted for 30 min while the tube circuit was pressurized with 28 barg gaseous helium (GHe). In addition, a GHe flow rate test and a residual moisture test have been carried out successfully. Another important aspect of CSP production was their dust release. Since turbulences can generate and disperse dust from the charcoal-plated panels during roughing, it was crucial to

DOI:10.15120/GR-2017-1

analyse the dust release of the CSP to make sure that no dust contamination of the beam vacuum may occur. Thanks to the optimization of the coating process by means of an epoxy, however, the producer was able to demonstrate experimentally that no dust or charcoal particles with a size of > 100 µm were released from the panels while the pump was roughed. The pumping speed measurements of the FoS pumps were carried out at GSI using a standardized PNEUROP vacuum dome. It was mounted on a test cryostat where the cryosorption pump was built in and cooled down. Details on the measuring procedure can be found in [2]. The tests were carried out with the aforementioned splinter shield which reduces the pumping speed by of about ~ 10%. Results of the measurements are shown in Figure 2.

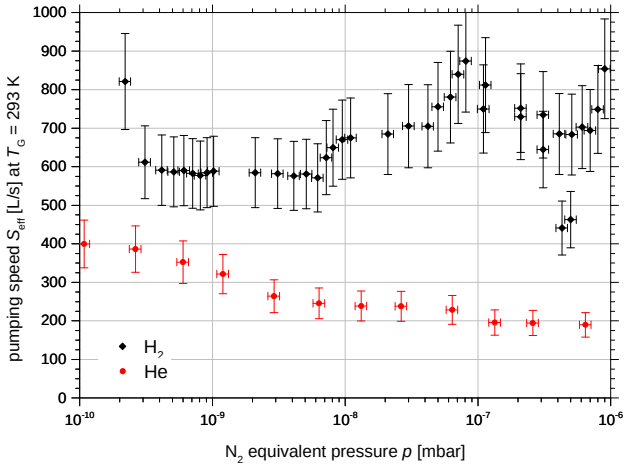

Figure 2: Measured pumping speed, S_{eff}, for H_2 and He

One can clearly see that the CSP provides high pumping speeds for both hydrogen and helium. For H_2 an averaged effective pumping speed of $S_{eff} \approx 600$ ℓ/s was measured in the lower UHV range and for He $S_{eff} \approx 300$ ℓ/s. It must be noted that the real pumping speed of the pump, S, however, is significantly higher than its measured S_{eff} as it is reduced by the conductance of the splinter shield and an upstream installed radiation baffle needed for thermal screening the cold pumping panels during measurement. Both were not taken into account yet in the above presented S vs. p characteristics. Moreover, since the test gas injected was at room temperature, the measured effective pumping speed only holds for $T_G = 293$ K. But what will be the pumping speed of CSP under cryogenic conditions, i.e. at $T_G = 5$ K? From the kinetic gas theory it is known that the pumping speed of a surface, S, depends on the Maxwellian mean velocity of impinging gas molecules, $\bar{c}$,

$$S = \frac{\bar{c}}{4} sA = \frac{1}{4}\sqrt{\frac{8k_B T_G}{m\pi}} sA, \qquad (1)$$

where s is the sticking coefficient, A the surface area, k_B is Boltzmann's constant, T_G the gas temperature, and m the mass of the gas particle. Assuming the sticking probability is temperature-independent, it follows that S is only a function of gas temperature, T_G, and one gets as an approximation

$$\frac{S(T_G = 5\text{K})}{S(T_G = 293\text{K})} = \sqrt{\frac{5\text{K}}{293\text{K}}} \approx 0.13. \qquad (2)$$

Consequently, the pumping speed at $T_G = 5$K is only ~ 1/8 of that at $T_G = 293$ K. Thus, the pump provides under cryogenic conditions a pumping speed for H_2 of $S \geq 78$ ℓ/s and for He $S \geq 40$ ℓ/s.

The effect of CSPs on hydrogen density profile in time in one SIS100 sector

In order to verify the advantage of using the CSPs in the cryogenic beam vacuum system of SIS100, calculations on the long-term hydrogen density distribution in one 180m long sector have been carried out using the novel simulation tool TRANSVAC also developed at GSI [3]. The simulation results are shown in Figure 3. In this Figure, the positions of the CSPs within the cryogenic sections are indicated by blue arrows. The red arrows represent the position of the conventional pumps ($S_{H2} = 2200$ ℓ/s) in the room temperature (RT) sectors. A constant and non-capacity limited H_2 pumping speed of $S_{H2} = 78$ ℓ/s per cryosorption pump was assumed in the simulation. The results indicate that the use of the pumps positively influences the hydrogen density distribution in time. It is interesting to note that the pumping action of the SPCs in the arc (section position $48 \leq l \leq 180$ m) come into real effect particularly in long time scales of a few years, rather than in short time scales. At these times, the H_2 cryosorption capacity of the bare chamber walls has already decreased gradually. Furthermore, the SPCs also limit the H_2 density rise in the cryogenic vacuum system of the sc quadrupole modules on the straight ring sections (section position $0 \leq l \leq 48$m) to nearly the same H_2 density level expected in the adjacent RT sections.

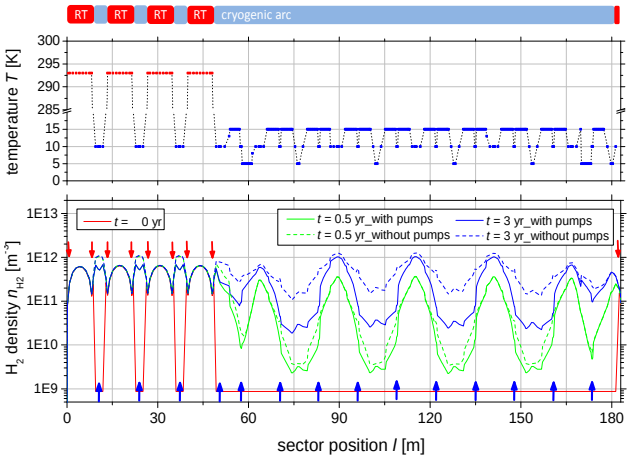

DOI:10.15120/GR-2017-1

Figure 3: Temperature profile of one SIS100 vacuum sector (upper chart) and simulated time and position dependent hydrogen density profiles (chart below).

The simulation neglects any beam dynamical vacuum effects.

The CSPs have an additional advantage. With their installation, a possible small He leak in the cryogenic beam vacuum system can be accepted several times longer as without their use.

References

[1] St. Wilfert, T. Hackler, M. Wengenroth, GSI Scientific Report, PHN-FAIR-16 (2012), 241
[2] International Standard ISO 21360-1
[3] to be published

DOI:10.15120/GR-2017-1

Collimation of primary ion fragments in SIS100

I. Strasik
GSI, Darmstadt, Germany

Introduction

The halo collimation system in the SIS100 synchrotron of Facility for Antiproton and Ion Research (FAIR) must be capable to collimate various ion species from protons up to uranium [1]. For protons and fully stripped ions, a conventional two stage betatron collimation system [2] is going to be applied. The collimation of the primary halo particles is summarized in Ref. [3].

The halo particles, except the scattering and momentum losses, undergo also the inelastic nuclear interaction with the primary collimator. It results in a production of secondary particles due to two processes: (1) hadronic fragmentation and (2) electromagnetic dissociation (EMD).

Probability of inelastic nuclear interaction

The probability P_{in} for the inelastic nuclear interaction (hadronic fragmentation and EMD) of the halo particles with the primary collimator material was calculated using FLUKA code [4]. The P_{in} for various primary ions with magnetic rigidity 18 and 100 Tm, pertaining to injection and extraction in SIS100, are presented in Fig. 1.

The P_{in} shows a substantial increase with increasing mass and atomic number of the primary ions especially taking into account the EMD. A significantly higher growth rate of the P_{in} is observed at 100 Tm with the EMD switched on.

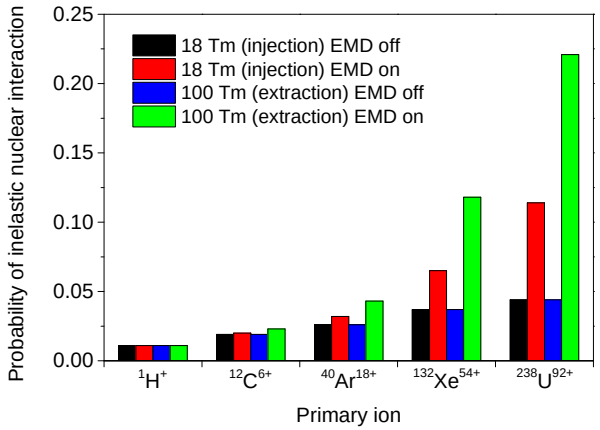

Figure 1: Probability P_{in} for the inelastic nuclear interaction of the halo particles with the primary collimator.

Fraction of the primary ion fragments

Inelastic nuclear interaction of the halo particles with the primary collimator and consequently production of individual secondary fragments was simulated again using FLUKA. A fraction of the individual fragments produced from ^{238}U primary ions after the interaction with the primary collimator is shown in Fig. 2.

The values are normalized by A/238, where A and 238 are the nucleon numbers of the fragment and primary ion, respectively. It can be seen that only the fragments corresponding to the EMD products (isotopes with the lowest and the highest nucleon numbers) have the abundance higher than 10^{-4}.

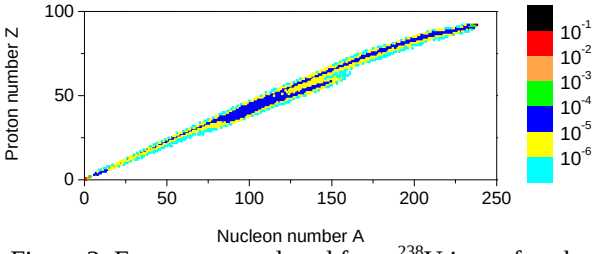

Figure 2: Fragments produced from ^{238}U ions after the interaction with 1 mm tungsten primary collimator.

Collimation of primary ion fragments

Particle tracking simulation in SIS100, for the fragments with the abundance > 10^{-4}, was performed using MAD-X code [5]. The beam loss map of the $^{238}U^{92+}$ halo primary particles together with the secondary fragments is presented in Fig. 3. In general, the calculated collimation efficiency with and without [3] the secondary fragments differ from each other by only a few percent.

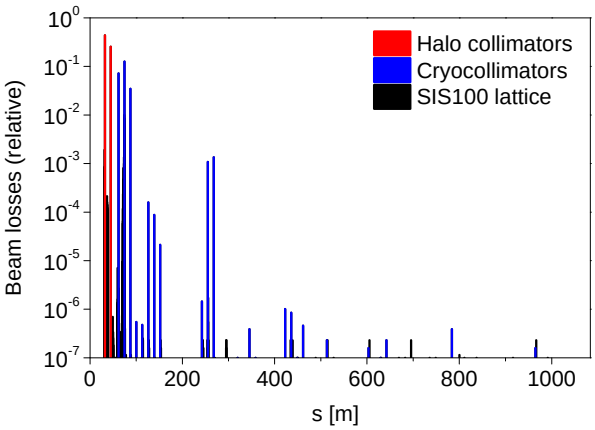

Figure 3: Distribution of the lost $^{238}U^{92+}$ primary beam particles including their secondary fragments in SIS100.

Conclusions

By comparison with the collimation of primary ions in Ref. [3] was shown that the fragmentation in the primary collimator has no significant effect on the efficiency.

References

[1] P. Spiller et al., IPAC'13, Shanghai, China, p. 3782.
[2] J.B. Jeanneret, PhysRev ST AB 1 (1998) 081001.
[3] I. Strasik et al., PhysRev ST AB 18 (2015) 081001.
[4] http://www.fluka.org
[5] http://mad.web.cern.ch/mad

DOI:10.15120/GR-2017-1

Phase calibration of synchrotron RF signals

A. Andreev[*1], *D. Lens*[2], *and H. Klingbeil*[1,2]
[1]TEMF, TU Darmstadt, Germany; [2]GSI, Darmstadt, Germany

Introduction

The RF reference signals for the FAIR synchrotron RF cavity systems are generated by direct digital synthesis modules mounted in so-called Group DDS crates which allow to perform various multiharmonic operations [1]. This means that each DDS unit operates in a certain mode defined by the harmonic number that is generally independent of the module and can be changed during operation. Different harmonic numbers of the DDS modules lead to a different phase response of each module, which results in a phase shift between reference DDS RF signals.

Absolute phase calibration

In the formerly used Group DDS calibration procedure the harmonic numbers of DDS modules are fixed and the calibration is done with respect to the highest harmonic number. If the harmonic number of the DDS module is changed, calibration data stored in calibration electronics modules (CEL) are no longer valid and one has to repeat the process for the new value. With the new proposed method phase correction values stored in CEL stay valid independent of the harmonic number realized by the DDS.

The BuTiS T_0 signal with a 10 μs period is used as one of the clock signals for DDS modules to ensure that reference RF signals are synchronized [2]. Therefore the measurement procedure is synchronized with the T_0 pulse train in order to increase the accuracy of the results. The measurement setup includes (Fig. 1):

- DDS module under calibration
- Scalable Control Unit (SCU) controlled by the PC[1]and forwarding data with the frequency tuning word to the corresponding modules via the backplane
- BuTiS reference signal generator and distributor

All the traces are measured by an oscilloscope and the acquired data are transferred into the PC which performs the subsequent analysis. The resulting phase correction data can finally be stored in a CEL module, which receives telegrams with the DDS frequency via optical fiber link and provides optical telegrams with phase corrections. The first pre-condition to arm the oscilloscope is the output trigger signal of the DDS module, marking the moment when the new frequency tuning word is received by the DDS. The oscilloscope is triggered on one of the next periods of the T_0

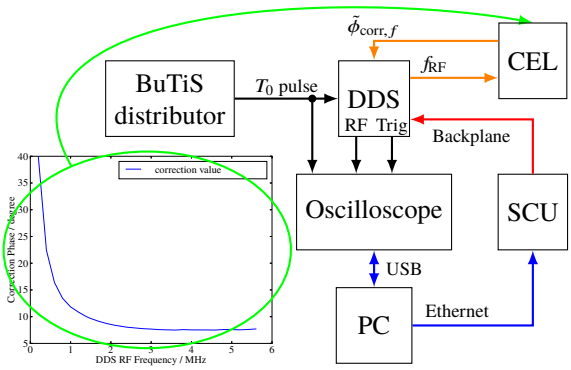

Figure 1: Measurement setup layout.

pulse N_{T_0} and the DDS RF signal portion after the trigger is used for the subsequent analysis.

The DDS RF output signal phase $\hat{\phi}_f$ is precisely estimated with a four-parameter sine wave fit algorithm [3] for each measurement. The phase correction value $\tilde{\phi}_{\mathrm{corr},f}$ for each frequency under calibration is obtained with

$$\phi_{\mathrm{corr},f} = \hat{\phi}_f - 2\pi f\,(N_{T_0} \times 10\mu\mathrm{s} - \tau_\delta)$$
$$\tilde{\phi}_{\mathrm{corr},f} = [(\phi_{\mathrm{corr},f} + \pi) \bmod 2\pi] - \pi,$$

where τ_δ is the dead time of the DDS unit after a T_0 slope to realize the new frequency tuning word settings at the analog RF output, including the delays of digital processing, PCB, filters and cables. The resulting phase correction table can be stored into the CEL module and applied during regular operation. The standard deviation of the obtained phases doesn't exceed 0.2°, allowing to meet the desired phase accuracy requirements.
The measurement as well as the data analysis procedures are automatized by means of Python scripts allowing to perform calibration quickly and comfortably.

References

[1] H. Klingbeil *et al.*, "New digital low-level rf system for heavy-ion synchrotrons", *Phys. Rev. ST Accel. Beams*, vol. 14, p. 102802, 2011.

[2] B. Zipfel and P. Moritz, "Recent progress on the technical realization of the bunch phase timing system BuTiS", in *Proc. IPAC'11*, pp. 418–420.

[3] P. Händel, "Properties of the IEEE-STD-1057 four-parameter sine wave fit algorithm", *IEEE Trans. on Instr. and Meas.*, vol. 49, no. 6, pp. 1189–1193, 2000.

* andreev@temf.tu-darmstadt.de
[1]During regular operation the SCU receives the data from the Central Control System

DOI:10.15120/GR-2017-1

Simulating particle loss for slow extraction from SIS-100*

S. Sorge†[1]
[1]GSI, Darmstadt, Germany

Slow extraction of heavy ion beams will be one of the most important operation modes of SIS-100. The minimisation of uncontrolled particle loss is essential for avoiding damages and irradiation of the machine. For that reason, expected particle losses are estimated with particle tracking simulations. The special focus of the studies is on the impact of magnet imperfections.

Slow extraction from SIS-100 is based on the excitation of the third integer resonance given by $3 \cdot Q_x = 52$ with six resonance excitation sextupoles, leading to the formation of a triangular stable area in the horizontal phase space plane. Rf knock-out (KO) extraction will be applied, where the beam is excited with horizontal rf noise which results in a slow growth of the phase space area of the beam beyond the stable phase space area so that particles will successively become unstable, travel towards the electro-static septum (ESS), and enter the extraction channel after passing the ESS.

Essential for minimising uncontrolled particle loss during slow extraction from SIS-100 is to reduce the large horizontal chromaticity which is

$$\xi_{x,nat} = -20, \tag{1}$$

according to the definition $\Delta Q_x = \xi_x Q_x$, to

$$\xi_{x,corr} = -1 \tag{2}$$

with chromaticity correction sextupoles in order to fulfil the Hardt condition [1]. In doing so, the trajectories of the particles can be adapted to the extraction septa independently of their momenta.

Superconducting dipole and quadrupole magnets will be used which have field errors characterised by the series [2]

$$B_y + \mathrm{i}B_x = B\rho \sum_{n=0}^{\infty} (k_n + \mathrm{i}j_n) \frac{(x+\mathrm{i}y)^n}{n!} \tag{3}$$

of the normal and skew multipole coefficients $k_n = (\partial^n B_y)/(\partial x^n)|_{x=y=0}$ and $j_n = (\partial^n B_x)/(\partial x^n)|_{x=y=0}$. The sextupole contribution k_2 to the field error of the dipole magnets is important because it is relatively strong and induces a significant change of the chromaticities as well as of size and orientation of the stable phase space area. k_2 is as all other coefficients a function of the magnet's excitation current and, consequently, of the beam rigidity $B\rho$, see Figure 1. The resulting horizontal chromaticity without correction for $B\rho = 100$ Tm is $\xi_{x,uncorr} = -27$ and, hence, strongly deviates from the natural chromaticity in Equation (1). Therefore, stronger chromaticity correction sextupoles are necessary for achieving the required horizontal chromaticity of Equation (2) resulting in a decreased stable phase space area and unacceptably high uncontrolled particle loss. By performing particle tracking simulations with 5000 test particles tracked for 15000 turns for conditions of a U^{28+} beam at $E = 2.7$ GeV/u, particle losses ~ 10 % in places anywhere in ring except the ESS [4] were obtained. Applying new settings for the resonance sextupoles, essentially generated by reducing their strengths in order restore the size of the stable phase space area and to re-adjust its orientation, reduced these losses to less than 1 %. In addition, particles losses of about 3 % due to collisions with the ESS were obtained without and with modifications of the settings which is acceptable. Similar amounts of lost particles could be achieved in ongoing tracking studies also for beams of lower energies, where the sextupole settings always had to be adapted to the actual magnet errors. The results indicate that finding proper sextupole settings for each rigidity will be essential for enabling slow extraction from the real machine.

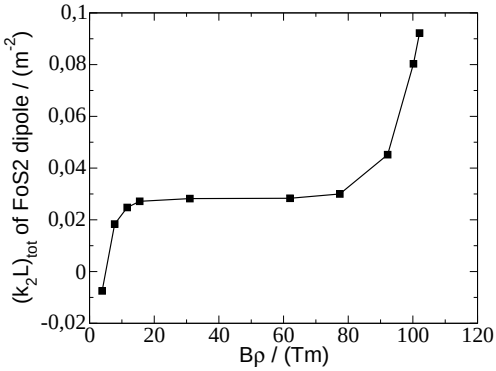

Figure 1: Total integrated coefficient of the sextupole error in the field of the FoS2 dipole [3].

References

[1] W. Hardt, "Ultraslow extraction from LEAR", PS/DL/LEAR Note 81-6, CERN, Geneva, 1981.

[2] A. Wolski, "Maxwell's equations for magnets", arXiv:1103.0713v1 [physics.acc-ph] 3 March 2011.

[3] P. Schnizer, private communication.

[4] S. Sorge, "Slow extraction issues of SIS-100", talk at the Slow extraction workshop, Darmstadt, June 1-3, 2016.

*This report was also submitted to the Annual Report "News and Reports from High Energy Density generated by Heavy Ions and Laser Beams 2016"

† s.sorge@gsi.de

Behavior of the planned RF feedback loops under beam loading during a reference SIS100 cycle*

D. Mihailescu-Stoica[†1], *J. Adamy*[1], *D. Domont-Yankulova*[1,2,3], *H. Klingbeil*[2,3], *and D. Lens*[3]
[1]TU Darmstadt RMR, Darmstadt, Germany; [2]TU Darmstadt TEMF, Darmstadt, Germany; [3]GSI, Darmstadt, Germany

It is well known that beamloading effects in accelerating cavities can have a serious impact on the beam quality. In order to prevent emittance growth and to keep beam loss low during acceleration, detailed simulations are necessary to evaluate the effects on the cavity and its low level RF feedback systems. This situation is aggravated by the fact that in a SIS100 scenario two out of ten buckets have to stay empty. Up to now the closed loop performance of the overall cavity system is still an open topic. Therefore a detailed study has been started.

Planned architecture and requirements

For most operating conditions ferrite-cavities can be well modeled as parallel, time variant RLC-circuits [1]. In order to analyze the influence of beamloading and empty buckets a simulation model has been set up consisting of the cavity itself, its attached control loops and a macro-particle nonlinear tracking simulation. The LLRF systems consist of the amplitude control loop, the resonance frequency control and the cavity synchronization. The amplitude control loop is planned as a linear PI controller in order to achieve stationary accuracy. The resonance frequency controller is as well a PI element and possesses additionally a feed-forward path which maps the desired resonance frequency to the desired bias current. Finally the cavity synchronization is a P-type controller with inherent integral type behavior.

It can be shown that all three control loops are influenced by beam loading. As a phase accuracy of better than $\pm 3^\circ$ and an amplitude accuracy of $\pm 6\%$ are intended to guarantee a satisfactory beam quality [2], beam loading effects must not be neglected. Especially the induced parasitic frequencies due to empty buckets are an open topic up to now and the planned control architecture has to be validated with respect to this issue.

Simulation of the RIB $^{238}U^{28+}$ 2.7GeV cycle

Nonlinear tracking simulations of the full acceleration cycle were performed for 5×10^{11} $^{238}U^{28+}$ ions with an injection energy of 1.976×10^8eV/u and an extraction energy of 2.7×10^9eV/u according to the official SIS100 cycle document [3]. The maximum synchronous phase during the cycle is 59.28° with a maximum gap voltage of 372.53kV. The bunches are injected in groups of two, letting the last two buckets of in total ten empty. The shape of two bunches during acceleration, near flat top, is shown in Fig.1, where the peak beam current reaches about 6 A . The emittance growth depends on the bunch position. While the first bunch growth by 2.1% the sixth bunch shows an emittance growth of 8.4%. Particle losses are hardly noticeable and will be dominated by other effects. The objective of the simulation is to serve as a proof of principle for the closed-loop control systems planned for SIS100. There is still the possibility to improve the beam quality, for example by temporarily de-activating individual cavities.

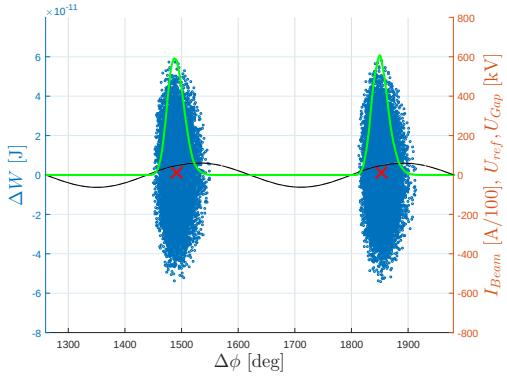

Figure 1: Two filled buckets during acceleration: particles (blue), beam current (green), gap voltage (black) and center of gravity (red)

Outlook

The results obtained in the detailed simulation study described in this contribution show that the planned low level RF control loops are able to deal with beam loading effects during the extremal RIB $^{238}U^{28+}$ cycle and maintain the RF accelerating voltage at the desired set point. Current work focuses on the influence of beam loading on the LLRF systems during a bunch-to-bucket-transfer from SIS18 to SIS100 and the arising transient effects. In future the influence of dipole beam oscillations on the stability and performance of the controlled cavity dynamics is going to be analyzed.

References

[1] H. Klingbeil, U. Laier, D. Lens, "Theoretical Foundations of Synchrotron and Storage Ring RF Systems", Springer, 2015

[2] H. Klingbeil et al., "New digital low-level RF system for heavy-ion synchrotrons", Physical Review Special Topics - Accelerators and Beams, 2011

[3] H.Liebermann, D. Ondreka, "SIS100 Cycles 3.0", Tech. rep. GSI, 2016

* Work supported by GSI
† dinu.mihailescu-stoica@rmr.tu-darmstadt.de

DOI:10.15120/GR-2017-1

Signal processing development for the SIS100 bunch-by-bunch longitudinal feedback*

D. Lens†[1], *M. Hardieck*‡[3], *K. Groß*[2], *H. Klingbeil*[1,2], *M. Kumm*[3], *K. Möller*[3], *and P. Zipf*[3]
[1]GSI; [2]TU Darmstadt, TEMF; [3]University of Kassel, Digital Technology Group

Overview of the System

The bunch-by-bunch longitudinal feedback planned for SIS100 is a broad-band feedback system (BBFB) that will help to stabilize the beam, keeping longitudinal emittance blow-up low and minimizing beam losses [1]. The low-level RF (LLRF) topology of the signal processing part of the system is mainly based on hardware and software components that have already been successfully tested in several machine experiments at SIS18, e.g. [2, 3]. However, some new components have to be developed such as a de-multiplexer and multiplexer (MUX). Here, the progress on the development of the digital MUX is reported.

Digital Multiplexing and Amplitude Modulation

The signal processing chain of the BBFB system is planned in principle as follows. First, the beam current signal is de-multiplexed into 10 channels each representing a single bunch (two channels will be zero for SIS100). For each channel, a DSP system with analog pre-processing is used to detect the bunch phase and amplitude and to calculate correction values (phase and amplitude). The correction values for all channels are converted to in-phase and quadrature components (I/Q) and then forwarded to the MUX. As the BBFB system will use dedicated broad-band kicker cavities, a driver signal for these cavities has to be generated. Therefore, the MUX has to convert the I/Q corrections of all channels into a single analog driver signal. Since the corrections of each channel must act on a particular bunch, it is mandatory that the driver signal is synchronized with the beam. Thus, the MUX also needs reference RF signals as inputs.

Figure 1 shows the inner functionality of the MUX. The signals with the correction values for each bunch are transmitted over a so-called Optical Direct Link (ODL, [4]). They consist of a stream of optical telegrams that contain the I/Q components. The new values are stored in buffers before they are used to avoid parameter switching during operation. The MUX performs a unique bucket numbering by counting periods of two reference RF signals (sine) which correspond to the bunch frequency (analog inputs) and the revolution frequency (harmonic number $h = 1$, Trigger input), respectively. Using these signals, the multiplexer selects the correct pair of I/Q values for the current

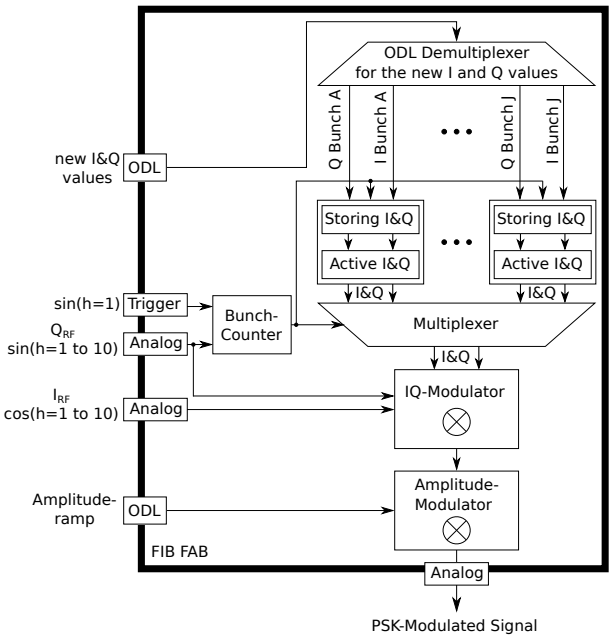

Figure 1: Functionality of the planned MUX module.

bunch and modulates the two analog signals with $h \geq 1$ (sine and cosine) according to I and Q. To obtain the necessary phase and amplitude correction of the beam, the gap voltage of the kicker cavities has to be scaled with respect to the total gap voltage of all other SIS100 cavities. Therefore, a subsequent modulation with an optical amplitude ramp is needed. Finally, the driver signal is generated as an analog signal at the output.

Outlook

The MUX firmware is currently under development and will be tested in a laboratory environment first. As a next step, a machine experiment with beam at SIS18 using one of the h=2 magnetic alloy cavities as dedicated kicker cavity will be necessary to evaluate the setup.

References

[1] K. Groß et al., GSI SR 2014, FG-SIS100-10 (2015).

[2] H. Klingbeil et al., "A digital beam-phase control system for heavy-ion synchrotrons", IEEE Trans. Nucl. Sci. 54(6)2604:2610 (2007).

[3] D. Lens et al., GSI SR 2014, FG-GENERAL-29 (2015).

[4] H. Klingbeil et al., "Generic Data Format for Optical Links", Rev. 1.42, 18.01.2017.

* Work supported by GSI.
† d.e.m.lens@gsi.de
‡ Hardieck@uni-kassel.de

A new bunch-to-bucket transfer technology for FAIR*

T. Ferrand†[1], *H. Klingbeil*[1,3], *O. Bachmann*[1], *and J. Bai*[2]

[1]Technische Universität, Darmstadt, Germany; [2]Goethe Universität, Frankfurt, Germany; [3]GSI Helmholtzzentrum für Schwerionenforschung GmbH

Introduction

In the continuity of [1] and [2], this paper reports the status stand of the Bunch-to-Bucket transfer topology development for FAIR as well as some key results obtained recently. The Bunch-to-Bucket topology for FAIR relies on the BuTiS absolute time frame and White Rabbit high-speed synchronous Ethernet packet exchange.

Implementation

The position of the beam's first bucket is locally and asynchronously measured at the source and at the receiving synchrotron by means of a DSP-based phase measurement system [3].

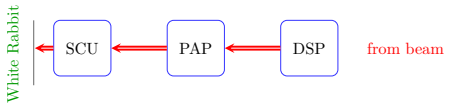

Figure 1: Functional flow of the new Bunch-to-Bucket transfer acquisition chain for FAIR.

As shown in Fig. 1, the Phase Advance Prediction (PAP) module uses the measured phase values to extrapolate a re-synchronized phase value and time-stamp it before it shares it through a separated Virtual LAN of the White Rabbit network by means of a Scalable Control Unit (SCU) [4].

According to the latest measurements, the transfer of synchronized Ethernet packets via the White Rabbit costs less than 30 μs per switch layer. The maximum amount of switch layers depends on the tolerable frame loss rate. The firmware of the White Rabbit switches is still under development at CERN.

New functions such as the PAP function require the development of a new FPGA-based Multi-purpose Hardware Unit (MHU), which is under development in cooperation with the IES Institute at the TU-Darmstadt. The MHU benefits from a modular design and a variety of interfaces, which make it a key stone for a variety of applications foreseen in the framework of the FAIR development.

Phase advance prediction

The DSP-based phase measurement device delivers phase difference values between a RF signal and a BuTiS-based synchronous reference signal through optical telegrams every 3.22 μs with an accuracy of 0.1 ^{o} [5]. According to the technical concept, the maximum absolute frequency difference between the measured signal and the reference signal is 50 kHz.

Phase prediction algorithms have been developed in Python and tested off-line with real phase measurements performed in February 2017 at GSI. The equation

$$\bar{\bar{X}} = \frac{1}{M}\sum_{n=0}^{M-1}\bar{X}_n = \frac{1}{MN}\sum_{n=0}^{M-1}\sum_{i=n}^{N+n-1}X_i. \qquad (1)$$

enables to use a minimum amount (N) of required samples (X_i) to achieve the required prediction stability of 1 ^{o} over the expected 10 ms of synchronization time (see fig. 2). M defines a second averaging window.

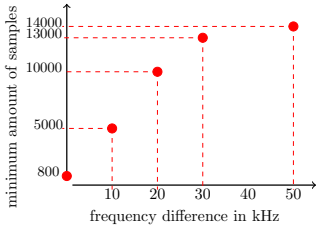

Figure 2: Summarized results of PAP code simulation as function of the frequency difference.

Outlook

Recent results confirm that the averaged phase advance converges towards a final value. The minimum amount of samples that is required to reach the required accuracy is very large but can be optimized.

The phase advance prediction accuracy and the systematic errors must still be investigated.

References

[1] T. Ferrand and J. Bai, "System Simulation of Bunch-to-Bucket Transfer Between Synchrotrons", *GSI SCIENTIFIC REPORT 2014*, 2015.

[2] T. Ferrand, H. Klingbeil, J. Bai and O. Bachmann, "Development of a topology for the bunch-to-bucket Transfer for FAIR", *GSI SCIENTIFIC REPORT 2015*, 2016.

[3] H. Klingbeil *et al.*, "New Digital Low-Level RF System for Heavy-Ion Synchrotrons", *Phys. Rev. ST Accel. Beams*, vol. 14, p. 102802, 2011.

[4] J. Bai and T. Ferrand, "Technical Concept of the Bunch-to-Bucket Transfer for FAIR", EDMS 1514162v.6.

[5] H. Klingbeil, "A Fast DSP-Based Phase-Detector for Closed-Loop RF Control in Synchrotrons", *IEEE Transactions on Instrumentation and Measurement*, vol. 54, no. 3, pp. 1209–1213, 2005.

* Work supported by GSI

† ferrand@temf.tu-darmstadt.de

DOI:10.15120/GR-2017-1

Beam position measurement during multi-turn injection in SIS-18

R. Singh, P. Forck, A. Reiter, and Y. El-Hayek
GSI, Darmstadt, Germany

New asynchronous algorithm for beam position evaluation [1] provided online measurement of beam position of each injected beamlet during the multi-turn injection in SIS-18. Injection bump and decoherence of injected beam were clearly visible. Further, horizontal and vertical tune at injection were measured.

Experiment and results

The multiturn injection in SIS-18 involves painting the UNILAC beam into horizontal transverse phase space by means of injection bumper and appropriate horizontal tune setting over several revolution periods of SIS-18 [2]. The exact temporal length of injection is regulated by the time window of electrostatic chopper. Figure 1 shows the pick-up data recorded immediately after injection. Nine beamlets with 108 MHz structure are injected which decoheres in roughly 1 turn. Since the "chopper window" is not exactly matched to revolution time, an additional longitudinal structure with revolution frequency and harmonics stay for 100-500 turns depending on the exact beam momentum spread. Presence of such a longitudinal structure due to the injection process allows for position calculation in these periods after injection and could be utilized to tune the injection.

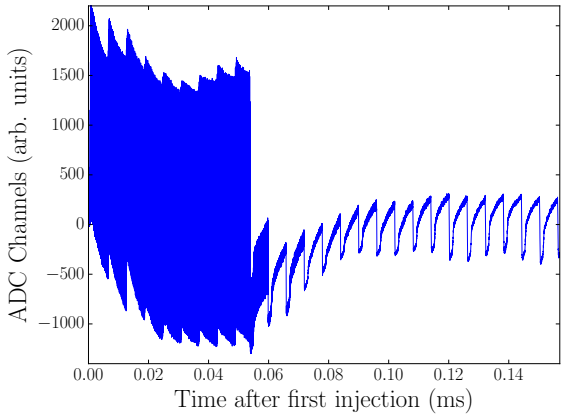

Figure 1: Raw data from top plate of the BPM 3 immediately after the start of multi-turn injection.

Figure 2 shows the horizontal and vertical positions at BPM 3 as a function of number of turns. The horizontal oscillations are expectantly much larger than vertical oscillations and the initial horizontal position at BPM 3 is ≈ 18 mm confirming the injection bump design. An "Injection orbit" is calculated by taking an average of initial 2 turn positions. It is plotted as a function of section number in Fig. 3. BPM 12 was unavailable between 3rd and 40th turn while capacitor charging and discharging transients were observed. The vertical BPM in section 7 was malfunctioning during this experiment and the corresponding data point should be ignored. The orbit bump matches well with designed orbit bump shown in Fig. 7.4 of reference [2]. Further tune was measured by spectral analysis of turn-by-turn data in both planes and the results compared well with the set values during the experiment.

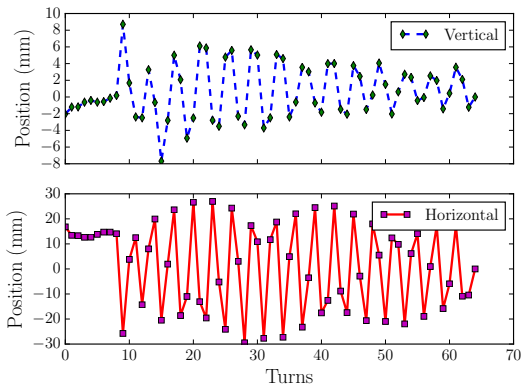

Figure 2: Vertical and horizontal beam oscillations after injection at BPM 3.

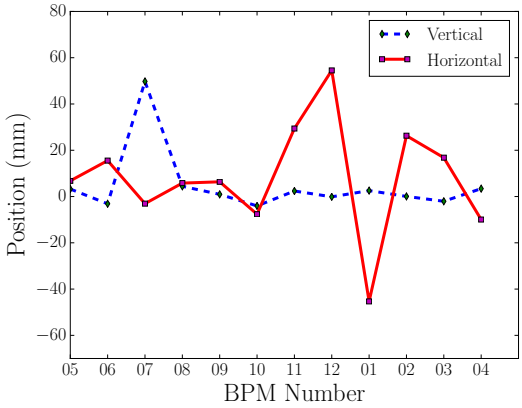

Figure 3: The orbit bump created during injection.

References

[1] A. Reiter et al., "Statistical Treatment of Beam Position Monitor Data", https://arxiv.org/abs/1609.01332 2016.

[2] Y. El-Hayek, "Minimierung der systematischen Anfangsverluste im SIS18", Goethe UNiversity Frankfurt, PhD-Thesis, 2013.

DOI:10.15120/GR-2017-1

Pressure measurement in low temperature vacuum systems – Advances in the development of an extractor ion gauge with CNT cathodes

M. Lotz[1,2], St. Wilfert[1], and O. Kester[1,2]
[1]GSI, Darmstadt, Germany; [2]Goethe University, Frankfurt

Abstract

Pressure measurement in cryogenic UHV and XHV environments is non-trivial. Basically, commercially available hot-filament ion gauges can be used in cryogenic vacuum systems [1], however, one has to accept disadvantages. The operation of their thermionic filament is always associated with a huge heat development. The heat-produced radiation disturbs the thermal equilibrium of the ambient gas and makes the pressure reading erroneous. In a cryogenic environment, moreover, such additional heat load is absolutely unwanted as it must be countered by a higher cooling effort. The problem of thermionic cathodes in ion gauges can be overcome by using non-thermal field emitter cathodes instead. For this reason, we studied a conventional extractor ion gauge type IE514 (INFICON) with a single CNT emitter cathode. Our investigations published in [2-4] confirmed the general functionality of this gauge with a field emission cathode in low temperature vacuum systems. In order to improve the gauge performance by extending its measuring range towards lower pressures, a gauge design with multiple field emitter cathodes was developed and evaluated in numerical simulations [5]. In this gauge design small-sized field emitter cathodes were arranged around the anode grid. Two different emitter types have been tested consecutively with this design: gated field emitter arrays (FEA) and CNT cathode spots.

Gated Mo field emitter array-based gauge

The gated molybdenum field emitter array chips were provided by the Vacuum Nanoelectronics group of PSI, Switzerland. The emission properties of these emitters were studied in [6] and showed emission currents > 1mA at relatively low gate voltages, making their use in an ion gauge interesting. However, during conditioning at GSI, short circuits between substrate and gate occurred in every tested FEA. The reasons are not known. We suppose a chemical reaction of the Mo field emitter tips with the residual gas or a dust particle effect. Also, the emission currents extracted before breakdown were insufficient for the application in our gauge. If they cannot be significantly increased by appropriate measures, these emitters seem to be unsuitable for the use in our modified gauge.

CNT cathode-based gauge

Due to our positive experience with CNT cathodes during our previous studies [2-4], we decided to examine the use of CNT cathodes instead of FEAs in the advanced extractor gauge design. Since CNT cathodes need substantially higher extraction voltages than micro-structured FEAs to generate comparable emission currents, numerical simulations have been carried out first to investigate the impact of the higher potentials on the electron trajectory length and thus on the gauge sensitivity. The results obtained have shown that the electron trajectory length decreases only slightly. This finding suggested that the gauge with 3 individual emitter arranged around the anode grid (each rotated by 120 degrees) can also be used for a gauge with CNT cathodes. However, a new miniature CNT housing had to be developed which fits into the tight space between the anode grid and the surrounding vacuum tube. Furthermore, the housing had to be as small as possible in order to keep the additional gas load due to the outgassing to a minimum. In addition, the housing design had to be such that the extraction potential (< 1kV) is safely insulated against the ground potential (substrate). The gap distance between emissive CNT layer and extraction grid was set to 200 µm. The final CNT housing and its integration into the gauge are shown in Figure 1.

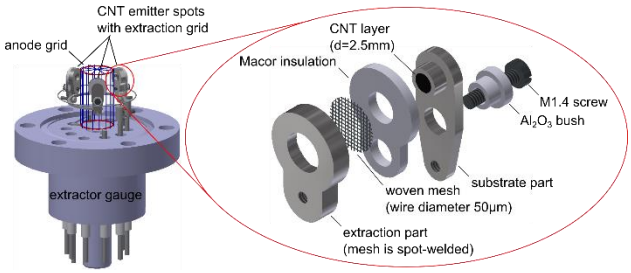

Figure 1: Advanced extractor ion gauge with parallel-wired miniature CNT cathode spots.

The CNT layer deposition and the final assembly of the customized CNT cathodes have been contracted out. The CNT emitter spots were tested and showed sufficient emission current to be suited for the use in an extractor gauge at the expected extraction voltages. Preliminary measurements of the gauge characteristic show a higher gauge sensitivity compared to the former gauge design, as predicted by the numerical simulations.

References

[1] Rao, M. G.: Advances in Cryogenic Engineering Bd. 41, p. 1783 (1996).
[2] Lotz, M. *et al.*, GSI Report 2012, p. 263 (2013).
[3] Lotz, M. *et al.*, Proceedings of IPAC2014, p. 2320 (2014).
[4] Lotz, M. *et al.*, Vakuum in Forschung und Praxis (VIP) 27 (2015), p. 34 (2014) (in German).
[5] Lotz, M. *et al.*, GSI Report 2014, p. 515 (2014).
[6] Kirk, E. *et al.*, J. Vac. Sci. Technol. B 27, p. 1813 (2009).

DOI:10.15120/GR-2017-1

Study of SIS-18 spill structure by introducing external ripples

R. Singh, P. Boutachkov, P. Forck, P. Kowina, P. Schmid, A. Stafiniak, and H. Welker
GSI, Darmstadt, Germany

The slow extraction spill structure from SIS-18 suffers from ripples of the main magnet power supplies which results in a duty factor significantly below the theoretically achievable level given by the Poisson statistics. External ripples were introduced into dipole and quadrupole power supplies and their effect was observed in the spill structure in order to estimate the magnitude and frequency of inherent power supply ripples.

The duty factor within in the time period Δt of the spill is defined as,

$$F(\Delta t) = \frac{\langle N \rangle^2}{\langle N^2 \rangle} = \frac{\langle N \rangle^2}{\langle N \rangle^2 + \sigma^2}$$

where N is the particle count in each measurement bin δt and σ is the std. deviation. It can also be described as the ratio of "DC power" to total power in the spill frequency spectrum. In our measurements, Δt and δt were chosen 10 ms and 10 μs respectively. Figure 1 shows the change in the spill duty factor for bunched and unbunched beams as a function of ripple currents introduced in dipole and quadrupole power supplies at 137 and 177 Hz respectively. The frequencies were chosen such that no overlap happens with harmonics of 150 Hz inherently present in the power supplies. Bunched beams are known to be more robust to power supply ripples as explained in [1].

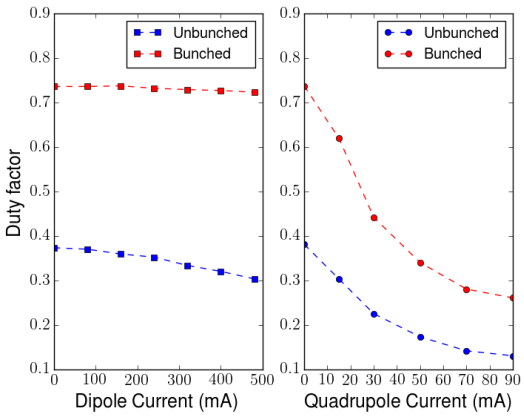

Figure 1: The change in duty factor for increase in ripple amplitude for dipole and quadrupole magnet power supplies.

The quadrupole ripples modulate the tune and therefore the stable phase space area at slow extraction and leads to a strong influence on the spill duty factor. Dipole ripples on the other hand affect the extraction process via change in dispersion and mean orbit which do not strongly translate into spill structure variations. Figure 2 compares the temporal variation of duty factor along the extracted spill

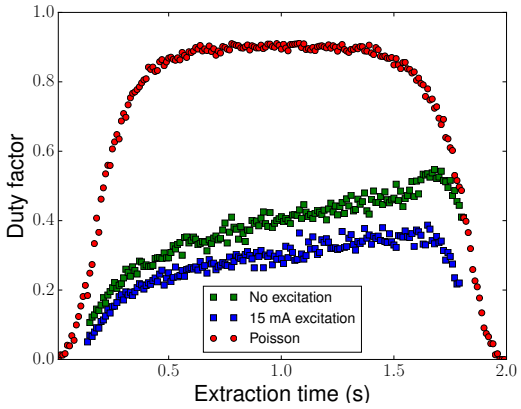

Figure 2: Duty factor of an unbunched beam with no excitation and 15 mA ripple introduced in the quadrupole.

for an unbunched beam without any excitation to the case with 15 mA ripple introduced in the quadrupole. It can be compared to the theoretical "Poisson spill" which also indirectly represents the actual extracted spill profile. Figure 3 shows the spectra of the spill in previous figure. The relative heights of peaks at 177 Hz and 600 Hz gives an estimate of inherent ripple of $\approx$ 5mA present at 600 Hz in the quadrupole power supply. Since the magnet current was set to 500 A at the time, the inherent ripple to total current ratio is 10^{-5}. The full scale dipole current is 3.5 kA and for quadrupoles is 1.75 kA.

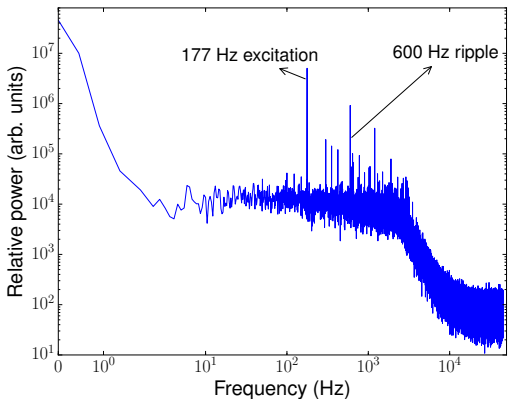

Figure 3: FFT of the spill with 15 mA ripple at 177 Hz introduced in the quadrupole for unbunched beam.

References

[1] P. Forck et al., Proceedings of EPAC 2000, Vienna, Austria (2000)

DOI:10.15120/GR-2017-1

Rf based bunch detection for position calculation in SIS-18

R. Singh, K. Lang, D. Lens, P. Forck, P. Kowina, and A. Reiter
GSI, Darmstadt, Germany

For the calculation of synchronous bunch-by-bunch transverse beam position in SIS-18, the temporal position of the bunches in the pick-up (PU) data stream has to be accurately identified. At present, a bunch detection method based on double threshold crossing of the PU data is used [1]. However, this data based bunch detection approach led to operational issues when the bunches were very short during proton operation (only 1 or 2 ADC samples) or when misformed bunches or unexpected amplifier spikes occur. To overcome these shortcomings, an rf frequency based bunch detection was attempted where the cable lengths and amplifier delays between PU cables and rf signal cables were matched.

The rf signal is strongly correlated to the PU signal due to the fact that bunches are formed as a result of cavity action. The rf cavity feedback system guarantees that the DDS source and cavity phases are precisely matched [2]. Usually the rf cavity signal is required by the BPM acquisition system to convert absolute time into units of synchrotron revolution turns. The signal paths from rf cavity and PUs to the acquisition system are shown in Fig. 1. The

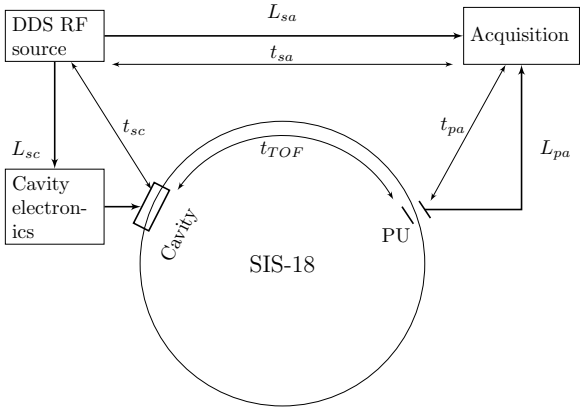

Figure 1: Principle of rf based bunch detection.

time difference Δt between the two paths is a function of rf frequency given by,

$$\Delta t(f_{rf}) = t_{sa} - (t_{sc} + t_{pa} + t_{TOF}) \quad (1)$$

where t_{TOF} denotes the time required by beam to traverse between cavity and PU and scales with beam velocity, t_{pa} and t_{sa} are the path delays between the components highlighted in Fig. 1 taking cables, amplifiers and switching electronics into account and t_{sc} represents the synchronous phase and phase ramp set by the control system. If represented in terms of the phase slip between the two paths,

$$\omega_{rf} \cdot \Delta t(f_{rf}) = \omega_{rf}(t_{sa} - t_{pa}) - \phi_{ramp} - \frac{\alpha \cdot h}{2\pi} \quad (2)$$

where $\alpha \in [0, 1]$ denotes the distance between cavity and the PU normalized to synchrotron circumference, h is the harmonic number. ϕ_{ramp} is assumed to be independent of rf frequency for SIS-18 ramp. However, since the rf frequency changes during acceleration ramp to account for increase in beam velocity, a linear frequency dependent phase slip is expected between rf signal and PU signal unless the condition $\omega_{rf}(t_{sa} - t_{pa}) = 0$ is satisfied. A fixed phase offset which is function of relative locations of cavity and PU denoted by α and frequency harmonic h in accordance to Eq. 2 needs to be individually set at each BPM.

The cavity rf ($h = 6$) for SIS-18 ramps from 850 kHz to 5 MHz. In our experiment, we varied the length mismatch between rf and PU signal cables to compensate the path delay mismatch in order to eliminate the phase slip as a function of frequency for a selected PU. Figure 2 shows

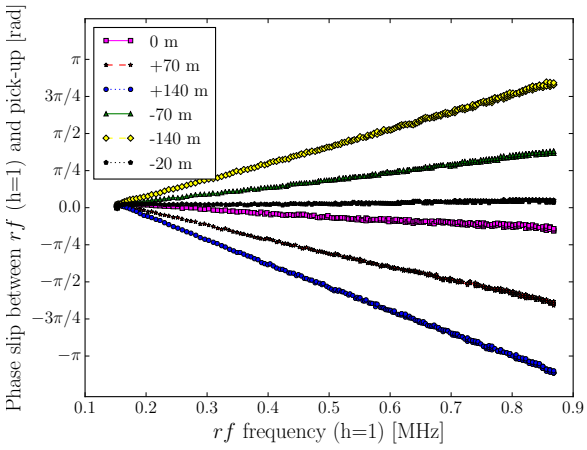

Figure 2: The measured phase slip as a function of frequency for different cable length variations.

the measured phase slip as a function of rf frequency for several variations of relative lengths of rf and PU cables ($t_{sa} - t_{pa}$). The phase slip was minimized when PU cable was appended by a 20 m cable. With this compensation in place, robust bunch detection independent of PU data deformations can be performed under most operational scenarious.

References

[1] U. Springer, "High resolution of betatron tune at SIS-18", PhD thesis, Goethe University Frankfurt (2010)

[2] B. Zipfel et al., Proceedings of IPAC14, Dresden, Germany (2014)

DOI:10.15120/GR-2017-1

Observation of SIS-18 spill structure by systematic parameter variations

R. Singh, P. Boutachkov, P. Forck, P. Kowina, and P. Schmid
GSI, Darmstadt, Germany

Typical slow extraction parameters such as chromaticity, momentum spread, sextupole strength and spill extraction length were systematically varied individually to see their effects of spill structure for the quadrupole driven resonance extraction.

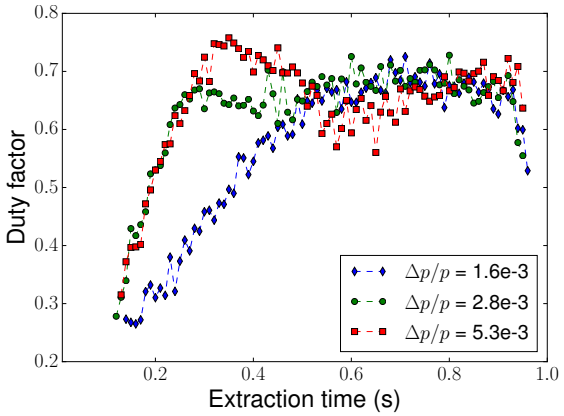

Figure 1: The effect on duty factor for change in momentum spread variation.

Chromaticity and momentum spread of the beam affect the spill structure via their effect on tune spread of the beam. A changed tune spread is not expected to have a significant effect on the spill duty factor for our extraction method where the tune of the beam is moved into resonance using fast quadruples. Thus, any power supply ripples will have a similar effect on the beam irrespective of tune spread. Figure 1 shows the duty factor [1] for three values of beam momentum spread confirming the assertion.

Figure 2 shows the duty factor along the extracted spill for various set sextupole strengths. A clear trend of spill structure improvement as a function of sextupole strength is seen. Figure 3 shows the corresponding spill spectra, where the high frequency components are seen to be drastically reduced for lower sextupole strength. The stable phase space area is inversely proportional to the sextupole strength, and therefore a smaller sextupole strength has two major effects countering the tune ripple. First, it reduces the ability of tune ripple from completely ”squeezing” the phase space area, and second, a larger stable phase space area corresponds to a larger range of transit times for the extracted particles i.e. the time between when they become unstable till the time when they exit the septum. These larger range of transit times are expected to suppress the effect of high frequency ripples on duty factor [2]. One should note that sextupole strength cannot be arbitrarily reduced since the resulting smaller ”spiral step” and ”spiral kick” would lead to higher losses in the septum. Further

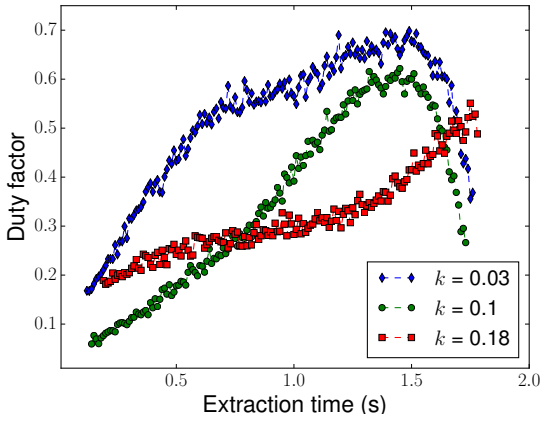

Figure 2: The change in duty factor for variation in sextupole strength. Note: The non uniform shape of duty factor curve do not represent the spill profile/structure.

simulation studies are required to understand these results.

Reduction of spill length is effectively a faster tune movement towards resonance and should reduce the the effect of ripples and improve the duty factor [2]. This was also clearly observed during the experimental campaign.

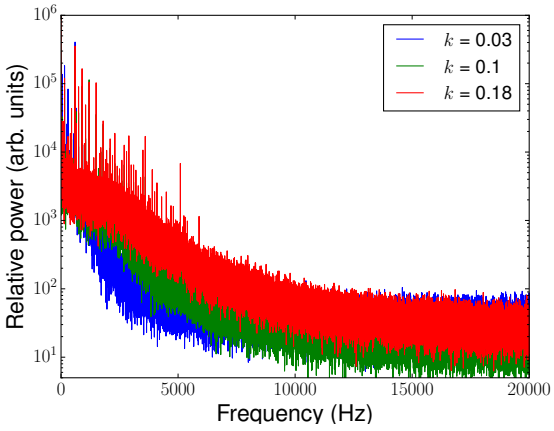

Figure 3: Spectra of the the spill data used in Fig.2.

The observations will be further studied by means of simulations to determine the relative importance of each parameter and obtain hints on their operational usage.

References

[1] R. Singh et al., Proceedings of this annual report (2017)

[2] “PROTON-ION MEDICAL MACHINE STUDY (PIMMS) PART I”,CERN/PS 99-010 (DI), Geneva (1999)

DOI:10.15120/GR-2017-1

DOI:10.15120/GR-2017-1

Super-FRS design status report

M. Winkler[*1], *S. Althoff*[1], *F. Amjad*[1], *K.-H. Behr*[1], *A. Bergmann*[1], *T. Blatz*[1], *E.J. Cho*[1], *W. Freisleben*[1], *H. Geissel*[1,2], *C. Karagiannis*[1], *A. Krämer*[1], *A. Kratz*[1], *J. Kurdal*[1], *H. Leibrock*[1], *H. Müller*[1], *G. Münzenberg*[1], *I. Mukha*[1], *C. Nociforo*[1], *S. Pietri*[1], *A. Prochazka*[1], *S. Purushothaman*[1], *M.V. Ricciardi*[1], *P. Rottländer*[1], *C. Scheidenberger*[1,2], *F. Schirru*[1], *C. Schlör*[1], *H. Simon*[1], *C. Schlör*[1], *P. Szwangruber*[1,3], *K. Sugita*[1], *F. Wamers*[1], *H. Weick*[1], *A. Wiest*[1], *J.S. Winfield*[1], *and Y. Xiang*[1]

[1]GSI, Darmstadt, Germany; [2]JLU Giessen, Germany

System design

The LEB cave could be integrated into the Civil Construction planning to its full extend which includes in particular the floor plan of the beam lines and their technical infrastructure as well as the arrangement of the various experimental areas. A rather short and thus cheap connection of the local cryogenic into the LEB could be found by linking it directly to the separator tunnel. This avoids to install the previously planned long cryo transferline into the supply building. In fact by introducing an additional distribution box in the LEB cave also a simplified and direct cryo connection from the LEB cave to the HEB Cave could be realized.

Magnets

During 2016 an extensive design phase of the SC multiplets was conducted. Our provider ASG Superconductors SpA, Genoa, concentrated on the design of the two pre-series multiplets (one short multiplet and one long multiplet). The long multiplet is the most complex cryo module and contains altogether 9 individual magnets including two types of quadrupoles with superimposed octupole coils, sextupole magnets, and y-steerer magnets. It has a total length of approximately 7 m, a diameter of almost 2.7 m and a total weight of 60 tons. In summer we could release the Preliminary Design Review (PDR) which included the complete magnetic design of all individual magnets, a manufacturing sensitivity analysis, a preliminary mechanical design, as well as the assembly concept. This design was then detailed and in beginning of December we could also release the Final Design Review (FDR) for the pre-series multiplet. The FDR included detailed calculation reports on all relevant subsystems, the quality assurance documentation, the 3D model and the main 2D drawings, a Factory Acceptance Test (FAT) Plan, and the report on already prepared mock-ups and specimen of various sub-components.

The technical documents for the superconducting dipole magnets were approved and also all further tender documents were established. At the time of writing this report the tender of these magnets is running (qualifying phase done already) and tender award is expected for end of 2017.

All revised remote connectors (water, power, etc.) of the radiation resistant pre-series dipole were taken into operation and tested successfully [1] such that the concept will be included into the design of all remaining radiation resistant magnets. The power dissipation of that magnet into air was tested once more in order to be able to finalize the technical infrastructure of civil construction planning (the total electrical power of all NC magnets in the heavily shielded target area tunnel is expected to be about 1 MW).

Local cryogenics

The technical discussions with our In-Kind provider (WUST, Wroclaw, Poland) were initiated. As a result the conceptual design of the feedboxes was modified such that we are turning towards a modularized design (see Fig. 1). In this case each cryo-module is operated by an individual feedbox which increases the feasibility for series production and thus reduces design effort and production time.

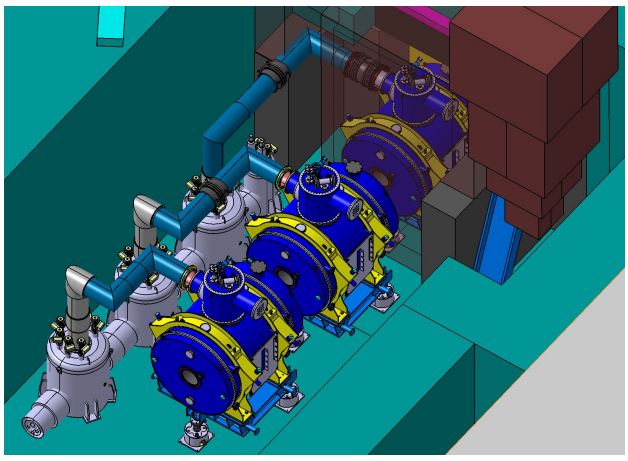

Figure 1: Each cryo-module is operated by an individual feedbox as shown for some short multiplets located in the Pre-Separator.

Beam instrumentation

The detailed specification for various types of detectors could be finalized and approved. This includes the SEM grids (beam profile monitors), the time-of-flight detectors (ToF), the energy-loss detectors (MUSIC) and the plastic

* m.winkler@gsi.de

DOI:10.15120/GR-2017-1

scintillates. For these systems the contract preparation with our In-Kind providers were initiated.

Several prototypes of various detector systems could be tested during the beamtime in 2016. This comprises in particular the GEM-TPC (tracking detector) including its corresponding read-out electronics [2] and silicon detectors which are intended to be used as ToF systems [3].

The slit systems are produced by our collaboration partner KVI-CART. The contract to manufacture 26 blocks of heavy tungsten alloy has been awarded to Plansee. Meanwhile all blocks have been produced and were delivered to KVI. Most of the remaining x-slit purchase parts have been ordered and the manufacturing of the x-slit series is continuing. The prototype of the y-slit has been manufactured, too, and the FAT test of this system is in preparation.

Vacuum

The vacuum system design has been detailed and is described in [4].

The specification of the SC dipole vacuum chambers as well as the specification of the focal plan chambers have been established. Altogether 20 focal plan chambers will be installed in the Super-FRS. These chambers contain all Super-FRS beam instrumentation such as various beam detectors, slit systems, degrader stations, etc. (Fig. 2 shows the focal plane chamber at FPF2, i.e. the midplane of the Pre-Separator). The chambers have a cross section of approximately 1x1 m^2 and a length of up to 4.5 m.

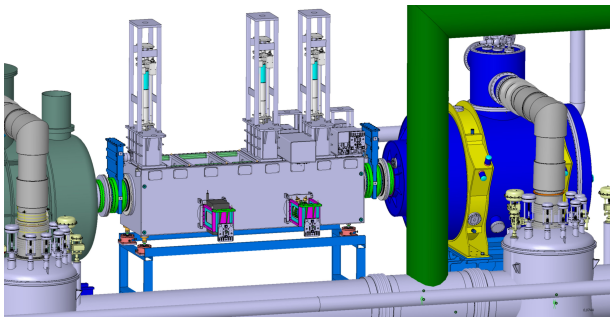

Figure 2: Focal plane chamber at FPF2 with some of its beam instrumentation inserts.

Target area / handling system

In summer 2016 we signed a collaboration contract with KVI-CART to design the Super-FRS target chamber and its plug inserts. A preliminary design of the target chamber is already available and shown in Fig. 3. The chamber will be approximately 2.1 m long and it will comprise five plug inserts including the production target which is a rotating carbon wheel. Each plug insert consists of a functional unit which is shielded to the top by a 1.6 m high iron block. The weight of one plug is up to 4.0 t.

All plug interfaces (electrical power, cooling water, etc.) are located on the top of the plug which will be accessible

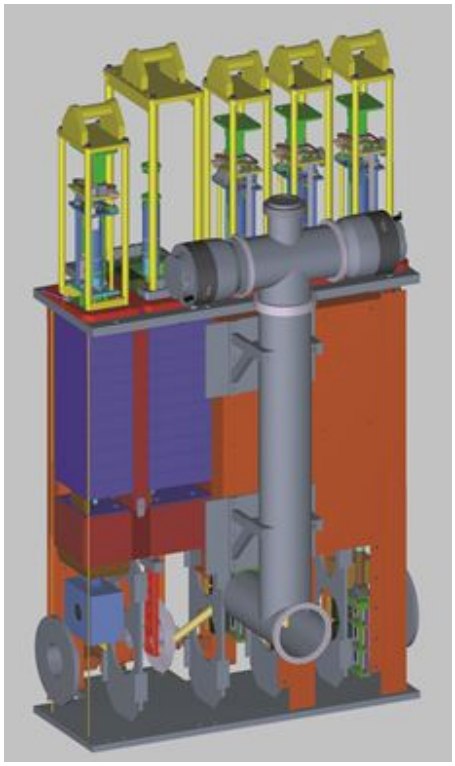

Figure 3: Preliminary design of the Super-FRS target chamber.

by a maintenance tunnel. Here also vacuum pumps will be placed which are coupled to the target chamber by a knee in backward direction to minimize the radiation level on the top of the chamber. The plugs will be inserted into the target chamber from the top by means of a special transport flask (not part of this work package) and must then be guided into the chamber. To demonstrate the feasibility of the plug-guidance system a 1:1 mock-up is in preparation, too. Another feature is the integration of a thermal imaging system for diagnostic purposes of the beam spot on the target. Basically it will consist of a mirror system which will guide the light out of the high-radiation zone where it will be coupled to an IR camera.

References

[1] H. Leibrock et al., “Upgrade of the prototype of a radiation resistant Super-FRS dipole to an operational FAIR-magnet”, this report

[2] F. Garcia et al., “Twin GEM-TPC Prototype (HGB4) Beam Test at GSI – a Tracking detector for the Super-FRS”, this report

[3] O. Kiselev et al., “Performance tests of the Si detectors for TOF beam diagnostics of the Super-FRS”, this report

[4] J. Kurdal et al., “Pressure simulation for the Super-Fragment Separator (Super-FRS) of the GSI future accelerator facility FAIR with various pumping configurations”, this report

DOI:10.15120/GR-2017-1

Upgrade of the prototype of a radiation resistant Super-FRS dipole to an operational FAIR-magnet

H. Leibrock, C. Mühle, T. Blatz, C. Will, A. Bergmann, R. Lotz, O. Zurkan and M. Winkler #
GSI, Darmstadt, Germany .

The areas after the production target of the Super-Fragment-Separator (Super-FRS) will be exposed by high radiation. Integral doses up to $2.8 \cdot 10^8$ Gy (mainly neutrons) within 20 years of operation are expected. Special magnets only consisting of non-organic radiation resistant materials like mineral insulated cables (MIC) must be used to ensure the functionality.

After the operation of the Super-FRS is started, direct access to the magnets is impossible because of the high radiation. Misalignment of the magnets due to settlement must be corrected with remote alignment of the adjustable support frame below the magnet. The remote alignment will be done per hand with rods and angle gears through a 1000 mm thick steel/concrete screen in a service tunnel above the magnets.

A prototype of a radiation resistant dipole has been made in cooperation with the Budker Institute in Novosibirsk [1] (Figure 1). It was successfully tested in the year 2009. The required field quality is achieved. The coils and the yoke of the magnet will withstand the hard conditions in the Super-FRS tunnel. Due to the results of the tests it was decided to use the prototype as one of the three necessary dipoles in the Super-FRS target area.

Figure 1: Prototype of the radiation resistant Super-FRS dipole after delivery to GSI.

Unfortunately not all parts of the prototype of the adjustable support frame below the magnet fulfil the requirements of radiation resistance and operability so a new adjustable support frame has been designed and manufactured (Figure 2). One important requirement besides the radiation resistance is that the adjustment in all directions must be possible with hand wheels. The required torque for adjustment in all directions must be less than 100 Nm. Three feet stand on a 3 m ×3 m baseplate. Roller bearings allow individual horizontal movements of each foot. The top of the feet are fixed on a steel support frame which carries the 90 tons magnet.

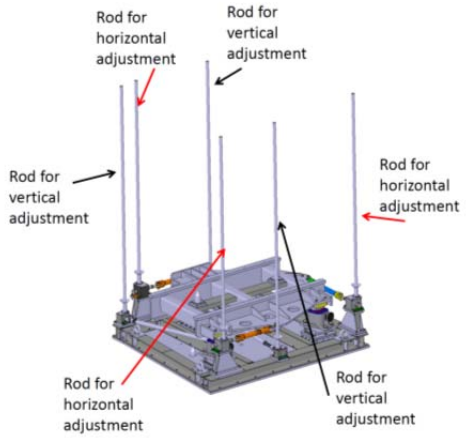

Figure 2: One adjustable support frame for one dipole with the six adjustment rods. This system allows an adjustment for all six degrees of freedom.

The horizontal movement is based on a three strut system. These three struts are connected on one side with an angle gear; the other side is fixed on the support frame (Figure 3).

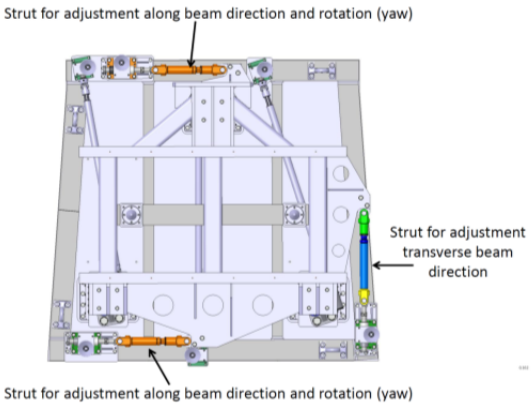

Figure 3: Top view on the support frame. A 3-strut system is used for horizontal adjustments.

The vertical adjustment is based on the principles of the feet of the prototype but with 100 % non-organic material. An angle gear and a gear inside each foot connected with a cardan shaft reduce the required torque for vertical movement to less than 100 Nm. It appeared that the combination of heavy weight (100 tons) and greaseless gears (grease is not radiation resistant) is still a challenge. But after several tests with different materials and coating the problems were solved.

In parallel to the work on the new adjustable support frame new connections for cooling water and electrical current have been designed and manufactured. Long term

DOI:10.15120/GR-2017-1

tests with the 100% powered magnet (140 kW) verified the full functionality of the new connections.

References

[1] C. Muehle et al., “Radiation Resistant Prototype Dipole for the First Stage of Super-FRS”, IEEE Trans. Appl. Supercond., vol. 22, p. 4003304, 2012

DOI:10.15120/GR-2017-1

Pressure simulation for the Super-Fragment Separator (Super-FRS) of the GSI future accelerator facility FAIR with various pumping configurations *

J. Kurdal[1], *A. Bergmann*[1], *and E. Renz*[1]
[1]GSI, Darmstadt, Germany

The Super-FRS will be the most powerful in-flight separator for exotic nuclei up to relativistic energies [1]. These calculations are mandatory to estimate the number of pumps, their pumping speed and the position in the Super-FRS [5].

Simulated Beamlines FMF1 - FMF2

The simulated beamlines consists of multiplet, dipole and focal plane chambers (Figure: 1).

Figure 1: Drawing from FMF1 - FMF2: From left to right, Multiplet, 3 Dipoles, Multiplet, Focal Plane Chamber, Multiplet, 3 Dipoles, Multiplet, and a Focal Plane Chamber.

The Simulation Software

For simulations Molflow+ [2] was used, which is a Test Particle Monte Carlo (TPMC) [3] Software. The code generates a total number of $N_{virtual}$ test particles, each of them represents the number of real particles.

$$K_{\frac{\text{real}}{\text{virtual}}} = \frac{\sum \mathrm{d}N_{\text{real}}/\mathrm{d}t}{N_{\text{virtual}}} \qquad (1)$$

The cosine law of Knudsen is applied as $ds = \frac{d\omega}{\pi} \cdot \Theta$, where ds is the probability that a molecule leaves the surface, $d\omega$ the solid angle and Θ the polar angle. Both angles can be generated in the following way: $\Theta = sin^{-1}\sqrt{r}$ and $\delta = r \leq 2 \cdot \pi$. Where δ is measured from x-axis in xy-plane in spherical coordinates. The random number **r** is uniformly generated in the real interval from (0,1). Fast gas molecules cross more frequently transparent **facets** [2] into the volume as slower ones [4]. If $f(v)_{(gas)}$ is the probability density function in volume (**pdf**), then it's possible to calculate the **pdf** of molecules colliding with the wall in a certain period $f(v)_{(coll)}$ [3,4].

$$f(v)_{coll} = f(v)_{gas} \cdot \nu \cdot C \qquad (2)$$

C is the normalizing factor (the integral of **pdf** must be unitary [4]). The following is obtained after a number of mathematical transformations and simplifications:

$$C = \frac{1}{f(v)_{(gas)}} \Rightarrow f(v)_{(gas)} = \sqrt{\frac{8 \cdot R \cdot T}{\pi \cdot m}} \qquad (3)$$

Results

The results diagrammed in (Figure: 2) reveal that both concepts should work for the Super-FRS (pressure in the range of 10^{-7} mbar is required). Momentary there are mechanical collisions with the 4 ion getter pumps between the multiplets (Figure: 2) blue (diamonds). At the moment 3 ion getter pumps with a pumping speed of 300 l/s each between the multiplets seems to be the best solution [5] (Figure: 2) red (dots).

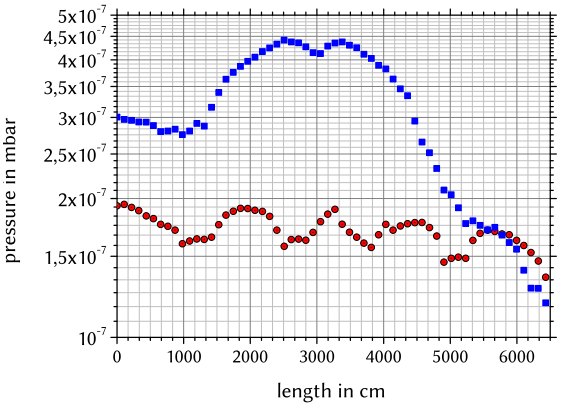

Figure 2: Pressure Profile from FMF1 - FMF2: Blue (diamonds) 4 IGPs between multiplets S=200 l/s per IGP, 1 TMP in the first focal plane and 2 in the second S=1000 l/s each. Red (dots) 3 IGPs between multiplets S=300 l/s per IGP and 1 TMP with S=1000 l/s per chamber.

References

[1] H.Geisel et al., Nucl.Instr. and Meth. in Phys.Res.B 204 (2003) 71-85

[2] M.Ady "Molflow+" https://test-molflow.web.cern.ch

[3] R.Kersevan, J. L. Pons, Journal of Vacuum Science Technology A 27, 1007 (2009)

[4] R.Kersevan, 13th IUVSTA School on Vacuum Gas Dynamics, Thessaloniki, Greece (2015)

[5] J.Kurdal, et al, 14th EVC, Portoroz, Slovenia (2016)

* PSP-Code: 2.4.7

DOI:10.15120/GR-2017-1

Twin GEM-TPC prototype (HGB4) beam test at GSI – a tracking detector for the Super-FRS

F. García[*1], *R. Turpeinen*[1], *J. Äystö*[1,2], *T. Grahn*[1,2], *S. Rinta-Anttila*[1,2], *A. Jokinen*[1,2], *B. Voss*[3], *J. Kunkel*[3], *V. Kleipa*[3],*H. Risch*[3], *C. Caesar*[3], *C. Simons*[3], *A. Prochazka*[3], *C. J. Schmidt*[3], *J. Hoffmann*[3], *I. Rusanov*[3], *N. Kurz*[3], *H.Heggen*[3]

[1]Helsinki Institute of Physics, University of Helsinki, 00014 Helsinki, Finland
[2]University of Jyväskylä, Department of Physics, 40014 Jyväskylä, Finland
[3]GSI Helmholtzzentrum für Schwerionenforschung, Darmstadt 64291, Germany

INTRODUCTION

The GEM-TPC detector will be part of the standard Super-FRS detection system, as tracker detectors at several focal diagnostic stations along the separator and its three branches.

GEM-TPC DETECTOR DEVELOPMENT

A group was created in 2009 for the development of a tracking detector to be located along the Super-FRS. Since then a series of prototypes were built and tested at GSI[1] The main requirements for the operation of those chambers are: close to 100% tracking efficiency at 1 MHz rates and position resolution less than 1 millimeter in the full acceptance on each diagnostic station. In order to, achieve such requirements a new configuration was proposed with two GEM-TPCs enclosed in one vessel; in such a way that one is flipped in the middle horizontal plane against the other one, thus the electric field of the field cages will be in opposite directions. Therefore, constraining the time of arrival of the hits in each GEM-TPC can drastically reduce the ambiguity of association of hits to a single track and therefore achieving the desired tracking efficiency.

BEAM TEST AT GSI & JYVÄSKYLÄ

The twin prototype 2 called HGB4-2, is shown in Fig. 1 was tested at GSI in cave S4 and in Jyväskylä.

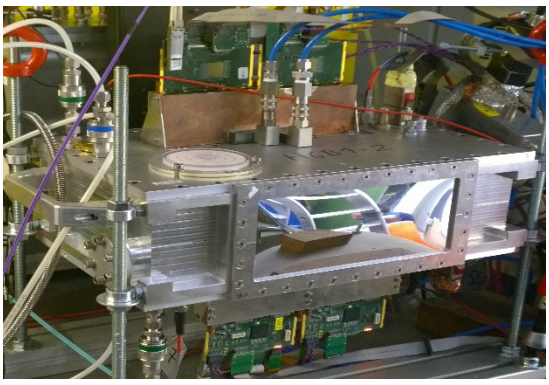

Fig. 1. Super-FRS GEM-TPC prototype HGB4, equipped with four GMX-NYXOR cards.

During these campaigns the readout system was the GMX-NYXOR cards, which contains two n-xyters chips to readout a total of 256 channels per card.

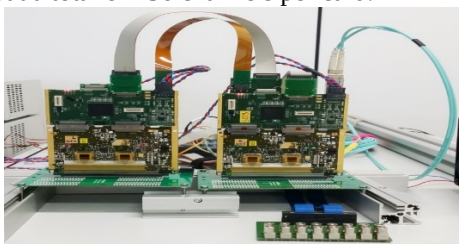

Fig. 2. The readout system GMX-NYXOR cards during testing in the laboratory.

Below is shown a correlation plot of the two GEM-TPCs X-axis projection of the HGB4-2 chamber.

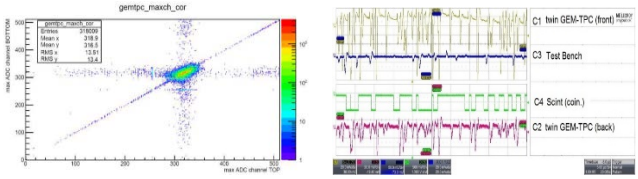

Fig. 3. Position correlation of the Top and Bottom GEM-TPCs of the HGB4-2 prototype for ^{124}Xe projectiles (left) and signals from the Bottom of both GEM #3 at 2.20 MHz rate under Protons at Jyväskylä.

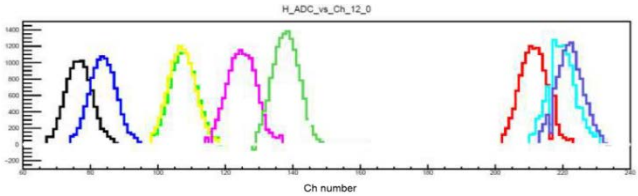

Fig. 4. Single clusters for primary ^{124}Xe @ 660 MeV/u beam.

Results from the test Beam campaign at Jyväskylä and GSI has shown that twin GEM-TPC (HGB4-2) has operated very stable in continuous mode and the concept has been proven to be the final one.

REFERENCES

[1] F. Garcia et al., 2011 IEEE Nuclear Science Symposium conference record, ISSN: 1082-3654, pp. 1788-1792.

DOI:10.15120/GR-2017-1

Performance tests of the Si detectors for TOF beam diagnostics of the Super-FRS*

O. Kiselev[1#], A. Bezbakh[2,3], N. Egorov[4], I. Eremin[5], V. Eremin[5], N. Fadeeva[5], A. Fomichev[2], M. Golovkov[2], S. Golubkov[4], A. Gorshkov[2,3], C. Konkov[4], D. Kostyleva[1,2,6], S. Krupko[2,3], D. Mitina[5], C. Nociforo[1], R. Slepnev[2], P. Sharov[2], Y. Tuboltsev[4] and E. Verbitskaya[5]

[1]GSI, Darmstadt, Germany; [2]JINR, Dubna, Russia; [3]FSBI NRC "Kurchatov Institute" - ITEP, Russia; [4]Research Institute of Material Science and Technology, Zelenograd, Russia; [5]Ioffe Institute, St. Petersburg, Russia; [6]JLU Giessen, Germany

The Time of Flight (ToF) information about the heavy-ion beam is one of the key aspects for the successful ion identification. It is also true for the Super-FRS setup and it's ToF system being designed now. The key parameter of the ToF system is the time resolution ≤30 ps (rms) for the ^{238}U ions. The active area of the largest station should be up to 380 x 60 mm^2 requiring the size of individual sensors to be at least 60 x 60 mm^2. In addition, similar detectors are needed for the experiments within the project EXPERT (EXotic Particle Emission and Radioactivity by Tracking) which is a part of the physics program of the Super-FRS Experiment Collaboration [1]. These experiments are aimed at studies of the unknown exotic nuclear systems beyond the proton and neutron drip-lines and will use the first half of the Super-FRS as a radioactive beam separator and its second half as a high-resolution spectrometer. The ToF information on the secondary ion beam and triggering on certain ion type will absolutely be required.

In summer 2016 a beam test of the few Si strip detector prototypes has been performed using ^{124}Xe and ^{12}C at energy of 600 MeV/u beams. One prototype had an active area 64 x 64 mm^2 and the strip pitch of 1 mm (Fig. 1).

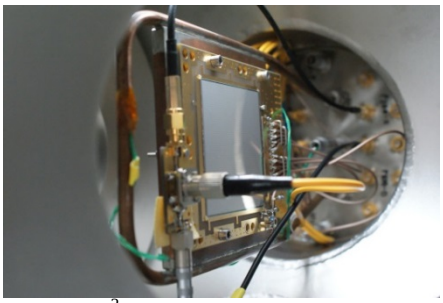

Figure 1: Photograph of the Si strip detector in the vacuum chamber. The small Si pad detector and the fiber-optic cable mounted on the top of it are also visible.

The second prototype had the same strip length but a different strip topology - the strips were arranged in 3 groups of 5 strips in each – with the pitch of 1 mm (2 groups with different width of interstrip gap) and one group with 1.5 mm pitch. A thickness of each detector was 300 µm. A quadrant detector built with 4 pads of 5x5 mm^2 each, was used as a start detector.

In addition, a thin scintillator detector LOS read out by 4 PMTs was provided by the R3B group as a reference start detector. One small Si pad detector illuminated by the red laser via the fiber-optic cable was also mounted for controlling the readout electronics based on the PADI-6 [2] preamplifier/discriminator and FPGA TDC VFTX2.

The time resolution of the large detector prototype has been already measured with U and Au ion beams; this time the main goals were the measurement of the ToF resolution with lighter ions beams, plus testing a different strip topology and confirmation of the previous measurements with U ions. More details about the detectors and setup can be found in [3].

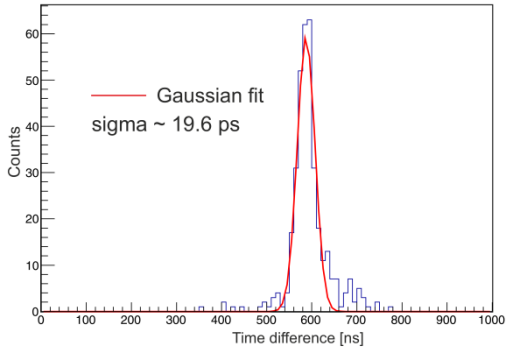

Figure 2: TOF resolution of the Si strip detector with ^{124}Xe beam.

The measured time resolution of the full-size detector prototype with Xe beam was close to 20 ps, including the resolution of the quadrant detector. This fully satisfies the requirements to the ToF system of the beam diagnostics of the Super-FRS. The analysis of the ^{12}C run is still in progress. It is already clear that the time resolution with ^{12}C beam will be worse due to the lower signal to noise ratio. This is not a real problem because the light ions identification is much easier and the requirements to the detector systems are not so severe as in the case of heavy ion beams.

References

[1] J.Aysto et al., NIM B376 (2016) 111.
[2] M. Ciobanu et al., *IEEE Trans. Nucl. Sci.* **61**(2014)1015.
[3] V. Eremin et al., *2017 JINST 12 C03001.*

*Work was carried out with partial support by RSF (project No. 17-12-01367), A.B., A.G. and S.K have been also supported by FAIR-Russia Research Center.
#o.kiselev@gsi.de

Implementation and test of a setting generator for the GSI fragment separator FRS in the LHC Software Architecture LSA*

J.P. Hucka[1,2], J. Enders[1], J. Fitzek[2], H. Huether[2], H. Liebermann[2], D. Ondreka[2], S. Pietri[2], and H. Weick[2]

[1]TU Darmstadt, Darmstadt, Germany; [2]GSI, Darmstadt, Germany

The LSA [1] framework from CERN is used to implement a new control system for accelerators and beam transfers. The fragment separator FRS [2] and - at a later stage - also the superconducting fragment separator Super-FRS at FAIR will be controlled within this framework. The challenge posed by the implementation of the control system for the FRS arises from the interaction of the beam with matter in the beamline and the beam's associated energy loss. This energy loss is determined using input from ATIMA [3] and has been included into the code of the LSA framework. The implemented setting generator was simulated and benchmarked by results of earlier measurements.

Benchmark Setup

The Benchmark was performed with data from the beamtime in October 2014 with 2 beam fragment settings and ^{238}U $^{73+}$ as the primary beam with an energy of 1 GeV/nucl. The used fragment settings are as follows:

- ^{238}U $^{92+}$ on a Cu-target with $90(2)$ mg/cm^2 at TA and degrader with 4200 mg/cm^2 at S2
- ^{134}Te $^{52+}$ on a Be-target with $6333(1)$ mg/cm^2 and Nb-Stripper with $233(1)$ mg/cm^2 at TA and degrader with 4200 mg/cm^2 at S2

Detectors (ionisation chambers, multi wire proportional chambers, TPCs and scintillators) were also taken into account at the positions of S2 and S4. TA means FRS target area, S2 and S4 mean middle and final focal plane respectively.
From given focussing strengths of quadrupole magnets and bending angles of dipole magnets the resulting currents for every single ion-optical element was calculated and compared to the experimental value and the calculated value of the simulation software LISE++ [6].

Results: Simulation vs. Experiment

From the given parameters the resulting values of magnetic rigidity Bρ and current I are used to find the relative deviation from the experimental values. Uncertainties in the calculation are only given by the uncertainty of the thickness of the different targets. It gives the biggest contribution to the resulting energy-loss calculation and delivers a relative deviation in the order of 10^{-5}. The beam energy was taken as given without uncertainty. Other input parameters were taken from MIRKO [7] with the inherent uncertainties, which was negligible.

* Work supported by HIC for FAIR and BMBF (05P15RDFN1).

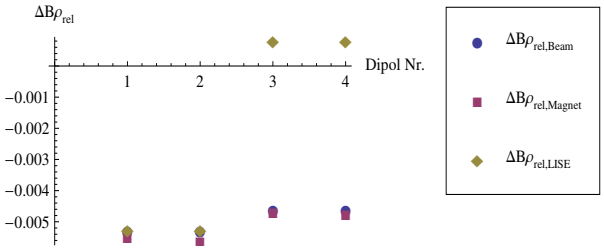

Figure 1: $\Delta B\rho_{rel}$ for $^{238}U^{92+}$ setting

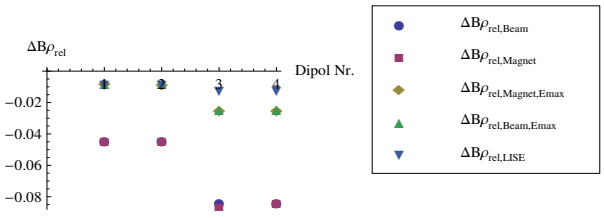

Figure 2: $\Delta B\rho_{rel}$ for $^{134}Te^{53+}$ setting

Conclusion

The machine model was benchmarked in the LSA framework with experimental data, which showed that LSA is better or in accordance with LISE++ calculations for single particle beams, whereas for beams containing secondary particles from fragmentation reactions, the quality of LSA suffers as there are no nuclear reaction models implemented which help the adjustment of the ion optical elements.

References

[1] M. Lamont et al., LHC Project Note 368
[2] H. Geissel et al., NIM B 70, 286 (1992)
[3] H. Weick et al., NIM B 164/165 (2000) 168
[4] J. Lindhard, A.H. Soerensen, Phys. Rev. A53 (1996) 2443
[5] J.F. Ziegler, J.B. Biersack, U. Littmark, The Stopping and Range of Ions in Solids, Vol.1, Pergamon Press (1985)
[6] LISE++ home page, http://lise.nscl.msu.edu/lise.html
[7] B. Franczak, simulation programme MIRKO, GSI Darmstadt. Siehe auch http://www-linux.gsi.de/~redelbac/MIRKO/.

DOI:10.15120/GR-2017-1

Design and production of klystron modulators for the pLINAC

S. Pütz, A. Schnase, G. Schreiber
GSI, Darmstadt, Germany

The pLINAC will be driven by seven identical klystron amplifier systems, each supplying the RFQ and CH accelerating structures with up to 2.5 MW of unsaturated RF-power [1].

Klystron modulators have been designed at GSI to generate pulsed high voltage for the klystron cathode. At their nominal operating point (-115 kV, 54 A, 4 pulses per second), the modulators produce a useable flat-top width of 360 µs (1% droop).

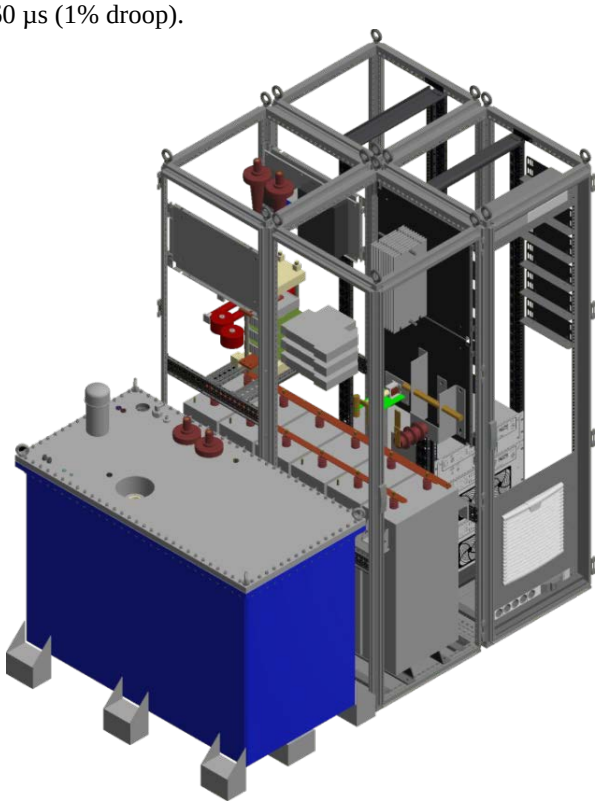

Figure 1: Electromechanical system layout

The modular construction of the power train with simple, well defined interfaces between function blocks provides excellent interchangeability. Components from alternative sources can be easily substituted, should the original component become obsolete or otherwise unavailable over the course of the operational life of the system. Function blocks of the pulse forming system are built from commercial off the shelf components.

Figure 2 shows the principal system structure of the klystron modulator. A capacitor charger supplied from 400 V mains recharges the capacitor bank between pulses to a user-defined voltage. The semiconductor switch assembly generates the output pulse and protects the klystron load in the event of internal arcing.

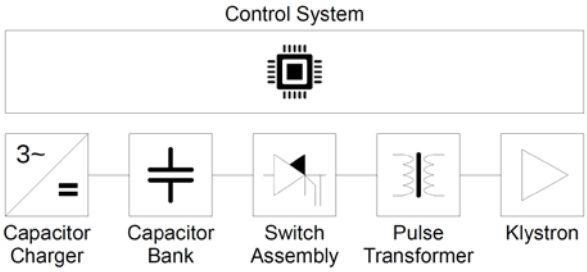

Figure 2: Function block diagram

The pulse transformer sets the intermediate voltage level of the pulse forming system to approx. 3.6 kV, an operating point at which cost optimal power semiconductor devices are available. Its parasitic series inductance limits the rate of rise of current in case of a load short circuit (i.e. klystron arc).

The control system consists of a PLC in combination with in-house designed fast analogue and digital electronics to control the switch assembly and implement active load protection.

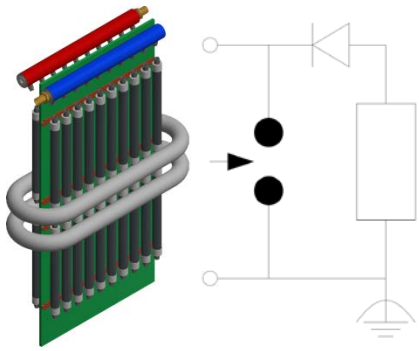

Figure 3: Resistive test load (left);
Arc simulator equivalent circuit (right)

A resistive test load has been designed to replace the klystron during the commissioning phase. A triggered spark-gap simulates a klystron arc which allows practical evaluation of the modulator's load-fault protection performance.

Component procurement for the prototype system is ongoing. Commissioning of the prototype is planned for 2018. Pending successful operation in the GSI RF test stand [2], the series production will follow with the first of series device anticipated ready for installation in the pLINAC building in 2020.

References

[1] "Detailed Specification on the FAIR pLINAC RF Systems", F-DS-RF-01e, 2012

[2] "Progress of the 325 MHz Rf Test Stand at GSI in 2015", FG-GENERAL-25, 2016

DOI:10.15120/GR-2017-1

Status of the modulated 3 MeV, 325 MHz Ladder-RFQ*

M. Schuett†, *U. Ratzinger, and M. Syha*
IAP, Frankfurt, Germany

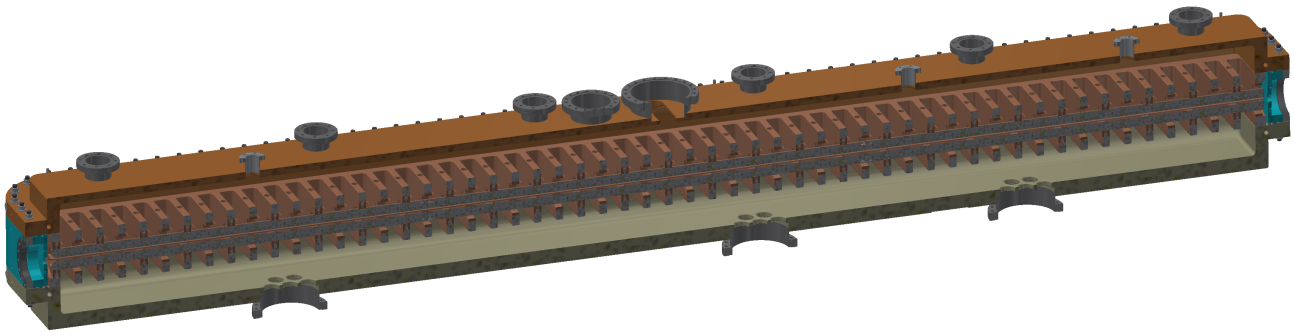

Figure 1: Isometric view of the 3.3 m modulated Ladder-RFQ prototype. The copper carrier-rings guarantee the electrode positioning as well as the RF contact. The ladder structure consists of bulk copper components. Any brazing or welding processes were avoided for the assembly of the main components. For more details cf. [1]. The successful high power tests of the unmodulated prototype motivated the development of a new beam dynamics with an increased electrode voltage of 96 kV [2].

Abstract

Based on the positive results of the unmodulated 325 MHz Ladder-RFQ from 2013 to 2016, a modulated 3.3 m Ladder-RFQ (s. Fig. 1) is currently under construction and will be tested with beam at GSI FAIR, Darmstadt. The 325 MHz RFQ is designed to accelerate protons from 95 keV to 3.0 MeV according to the design parameters of the p-linac at FAIR. The basic design and tendering of the RFQ has been successfully completed in 2016.

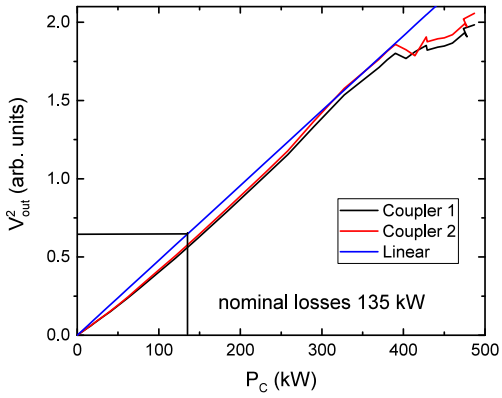

Figure 2: Results of the high power tests of the unmodulated prototype. The forward power up to 487 kW is shown in black. The RFQ accepted the power as the reflected power is stable along the flat top being lower than 3.34 kW.

* Work supported by BMBF 05P12RFRB9, 05P15RFRBA.
† schuett@iap.uni-frankfurt.de

High Power Measurements of the unmodulated Prototype

At the GSI 325 MHz klystron test stand the unmodulated Ladder-RFQ prototype with an electrode length of 630 mm was tested with a forward power up to 487 kW (s. Fig. 2) [3]. That exceeds the designed RF power at an electrode voltage of 80 kV during normal operation by a factor of 3.6. The averaged power reached 200 W, which is about 50% more than the thermal loss during normal operation.

Conclusion

All measurements of the unmodulated Ladder-RFQ such as frequency spectra, tuning, field flatness are in a good agreement with the simulations. The vacuum properties and pump ability has been verified. The design and construction of a full length modulated Ladder-RFQ, which will be tested with beam at GSI, is currently on-going. The completion of manufacturing is aimed until the end of 2017, to be ready for first RF tests in early 2018.

References

[1] M. Schuett, M. Obermayer, U. Ratzinger, M. Syha "Status of the modulated 3 MeV 325 MHz Ladder-RFQ", Proc. of IPAC2017.

[2] M. Syha, M. Obermayer, U. Ratzinger, M. Schuett, "Beam Dynamics for a high Current 3 MeV, 325 MHz Ladder-RFQ", Proc. of IPAC2017.

[3] G. Schreiber, E. Plechov, J. Salvatore, B. Schlitt, A. Schnase, M. Vossberg, "First High Power Tests at the 325 MHz RF Test Stand at GSI", Proc. of LINAC2016, East Lansing, USA, p. 3745.

DOI:10.15120/GR-2017-1

Beam Position Monitor design for the FAIR proton Linac

T. Sieber[1], P. Forck[1], W. Kaufmann[1], M. Almalki[2], C. Simon[3] and A. Bechtold[4]
[1]GSI Darmstadt, Germany; [2]KACST, Riyadh, Saudi-Arabia; [3]CEA, Saclay, France; [4]NTG, Gelnhausen, Germany

In order to achieve a significant intensity increase in the FAIR antiproton chain, the planned FAIR proton Linac will deliver a 70 mA, 70 MeV proton beam with a repetition rate of max. 4 Hz for injection into the SIS18 synchrotron. The 30 m Linac consists of an RFQ, followed by a number of cross-bar H-mode cavities (CH), which are partially combined to doublets, mechanically as well as rf-wise [1].

A key diagnostics for beam alignment during commissioning and also for verification of reproducibility during standard operation is an arrangement of 15 beam position monitors (BPM), which are distributed along the beamline. Nine of them are so-called 'inter-tank' versions (s. fig. 1), designed to be mounted directly to the magnetic triplet housings in between the CH tanks, while the other six are regular 'beamline' BPMs with CF100 flanges for the HEBT section. Both BPM types comprise four button-type capacitive pickups.

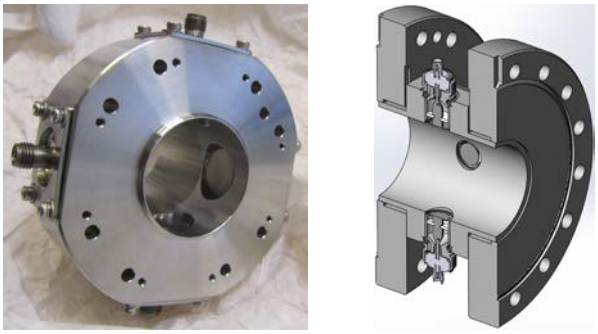

Figure 1: Left: inter-tank BPM prototype (tube radius 15 mm), right: beamline BPM (tube radius 25 mm).

A prototype of the inter-tank version has been built at CEA, using buttons from Kyocera. After extensive simulations [2, 3], and lab tests at GSI, a new button type was developed together with NTG company. The main difference between this button and the so far considered buttons (Kyocera, VACOM) is - besides the smaller button diameter of 12 mm instead of 14 mm - the conical increase in diameter of the inner conductor, starting directly at the SMA type rf-feedthrough.

Figure 2: Button pickup from NTG. Diameter 12 mm, gap width between button and housing 1.5 mm.

This type of geometry leads to a less drastic impedance jump at the position of the button, where the 50 Ω geometry is - unavoidably - no longer preserved. To investigate the effect of this change, time domain reflector (TDR) measurements were performed and compared to earlier results. Figure 3 shows the result of such a TDR measurement.

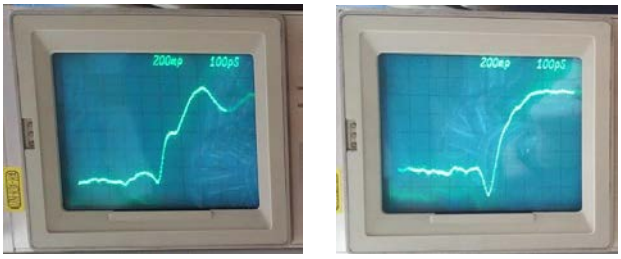

Figure 3: TDR measurements. Left: NTG, right VACOM.

The TDR shows that the new button has a significantly smaller reflection at the button position (negative peak in the curve). At the same time it seems to be more prone to oscillations, which probably derive from the smaller capacitive load.

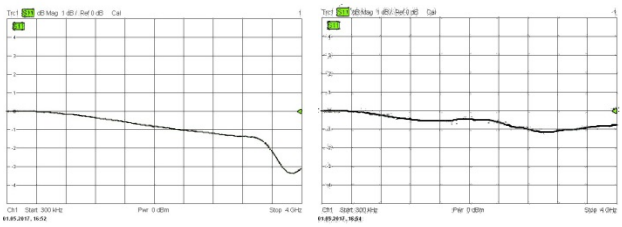

Figure 4: NWA measurement of S_{11}. Left NTG, right VACOM (scaling 1dB/div, span 300 MHz to 4 GHz).

To investigate the frequency range of these oscillations, both buttons were connected to a network analyzer and S_{11} was measured. Figure 4 shows again the comparison between the two buttons. In the frequency range below 3 GHz they show quite similar behavior, while above this value the NTG button has stronger return loss. Since the given measurement range is < 3 GHz, oscillations above this value are considered to be non-critical.

References

[1] L. Groening et al., "Status of the FAIR 70 MeV Proton LINAC", LINAC 2012, p. 927 (2012)
[2] C. Simon et al., "Numerical calculations for the FAIR Proton Linac BPMs", IBIC'14 (2014)
[3] M. Almalki, PhD Thesis, IAP, University of Frankfurt, 2016

DOI:10.15120/GR-2017-1

Status of CH-Cavity Design for the FAIR p-Linac

Ali M. Almomani[#1], Marco Busch[1], Ulrich Ratzinger[1] Carl M. Kleffner[2] and Florian D. Dziuba[2]
[1]IAP – Frankfurt University, Germany, [2]GSI – Darmstadt, Germany

Abstract

The FAIR proton linac will serve as an injector to provide a 70 mA, 68 MeV proton beam. The main acceleration will be performed by six room temperature "Crossbar H-type" CH-cavities which will be operated at 325 MHz. The beam dynamics had been revised by IAP – Frankfurt in collaboration with GSI-FAIR in Darmstadt to further optimize the design. This step was followed by cavity RF design. The mechanical cavity design will begin in 2017, while the quadrupole lenses are under production already. In this paper, an overview of the cavities RF design with integrated focusing triplets will be a main focus.

FAIR Proton Linac

The main accelerator section in the proton linac consists of six room temperature “Crossbar H-type” CH – cavities operated at 325 MHz. Figure 1 shows an overview of the proton linac from the RFQ exit down to the end of the last CH cavity.

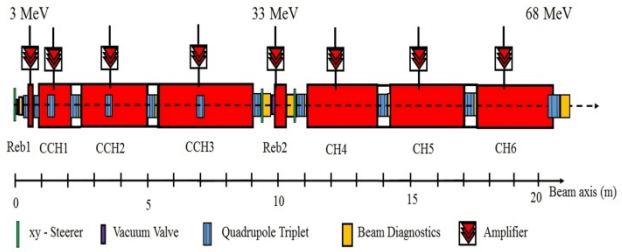

Figure 1: An overview of the FAIR proton linac from the RFQ exit down to the last CH cavity including the positions of the triplet quadrupoles, diagnostics and vacuum elements.

The CH – cavities consist of two sections: the first one is composed of three coupled CH – cavities (CCH1, CCH2 and CCH3) that will accelerate the beam from 3.0 to 33 MeV. The second part will be the high energy section-which consists of three lens-free CH – cavities. This helps to simplify the mechanical design and to tune the cavities besides reducing the total cost.

The main parameters of the CH – cavities are summarized in Table 1.

All cavities have been designed in order to fulfill the revised beam dynamics [1]. This includes the number of gaps, voltage distribution, coupling cell lengths, additional spaces for diagnostic and vacuum elements and the total length.

The Coupled CH – Cavity CCH2

As an example for the cavity RF design, the final layout of the second coupled cavity (CCH2) is presented here. Figure 2 shows a 3D – view on the cavity.

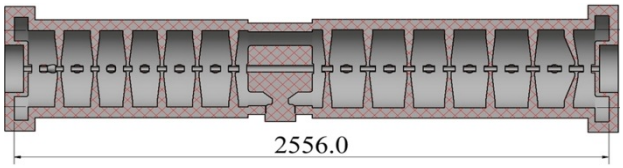

Figure 2: A cross sectional view on the second coupled CH – Cavity.

Table 1: Main Parameters of the FAIR Proton Linac CH – Cavities at 75 mA operation.

Cavity	L (m)	P_{tot} (MW)	Z_{eff} (MΩ/m)	Energy (MeV)	Gap No.
CCH1	1.44	1.33	53.5	3.0 - 9.9	21
CCH2	2.56	1.87	53.2	9.9 - 21.1	27
CCH3	3.66	1.92	44.6	21.1 – 33.0	30
CH4	2.67	2.14	42.4	33.0 - 44.6	20
CH5	3.02	2.12	38.5	44.6 - 56.3	20
CH6	3.31	2.06	36.7	56.3 – 68.0	20
Magnetic Quadrupole Triplets					
Effective Length (mm): 2 units 10 units				38, 60, 38 52, 95, 52	
Effective Gradients (T/m)				45 – 62	
Aperture Diameter (mm)				30	

The rf simulations have shown that an effective coupling is achieved with this geometry as shown in Figure 3.

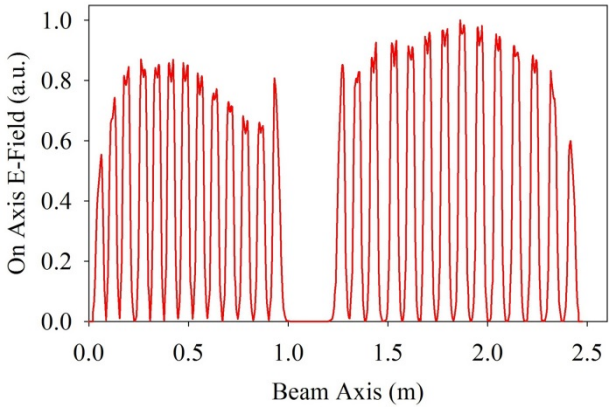

Figure 3: On axis electric field for the second coupled cavity.

Similarly, the final layout for the cavities has almost been finished and the results will be used as the basis for the mechanical layout and cavity construction [1].

References

[1] R. Tiede et al., Proceeding of LINAC16, East Lansing, MI, USA, MOPRC018 (2016).

[2] A. Almomani et al., Proceeding of IPAC17, Copenhagen, Denmark, TUPVA064 (2017).

[#]a.almomani@iap.uni-frankfurt.de

DOI:10.15120/GR-2017-1

Developments for the CR stochastic cooling system

C. Dimopoulou, R. Böhm, M. Bräscher, R. Hettrich, J. Krieg, C. Peschke, A. Stuhl, and S. Wunderlich
GSI, Darmstadt, Germany

Further progress was made in 2016 on in-house developing, engineering and testing for the demanding CR stochastic cooling system in the frequency band 1-2 GHz.

Cryogenic pickup with plunging electrodes

The first metallised ceramic (Al_2O_3) electrode plates have been delivered and tested (Fig. 1), confirming the demanding manufacturing concept. A redesign in-house is now necessary so as to ease the mechanics and reduce the cost of the series.

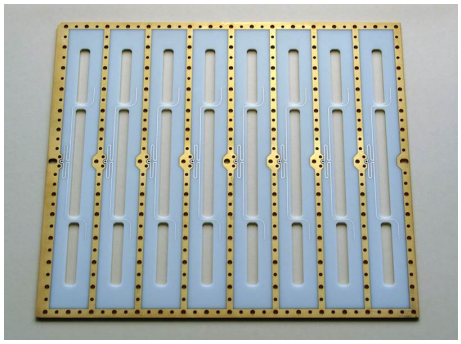

Figure 1: Prototype slotline electrode plate (signal side).

Progress was made towards an improved concept for the critical plunging Ag/BeCu sheets (geometry, manufacturing process). The pure BeCu sheets now sustain several million cycles in the test. Intensive optimization of the silver-plating procedure with the company is underway in order to reach such reliability with the $\approx$ 80 μm Ag layer on the BeCu sheets.

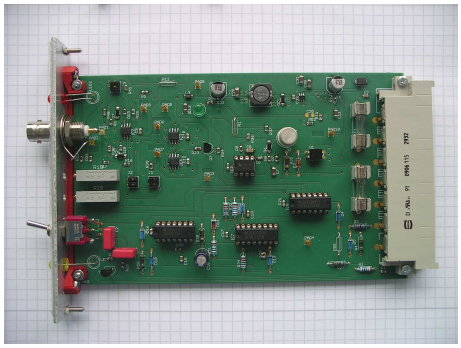

Figure 2: In-house designed comparator electronics ensuring the interlock function in case of over-acceleration of the motor drive units.

In the special chamber for testing motor drive units under pre-vacuum conditions, at room temperature, one linear motor drive unit with the dummy weight of the electrode module was mounted and tested in all 3 possible orientations of movement i.e. horizontal, vertical upwards, vertical downwards. In each case, appropriate springs have thus been specified, the static forces have been measured and benchmarked against theoretical calculations and the corresponding real-time code for the module movement was finalized. Special care is taken for machine protection and personnel safety (e.g. against mechanical crushing): The signal from the accelerator sensor mounted on the motor drive unit is fed into a specially designed comparator (Fig. 2). If the acceleration is beyond a specified range, the comparator initiates an emergency function of the servomechanism of the motors. The latter switches off the electrical power of the motor unit within 4 ms.

RF signal processing components 1-2 GHz

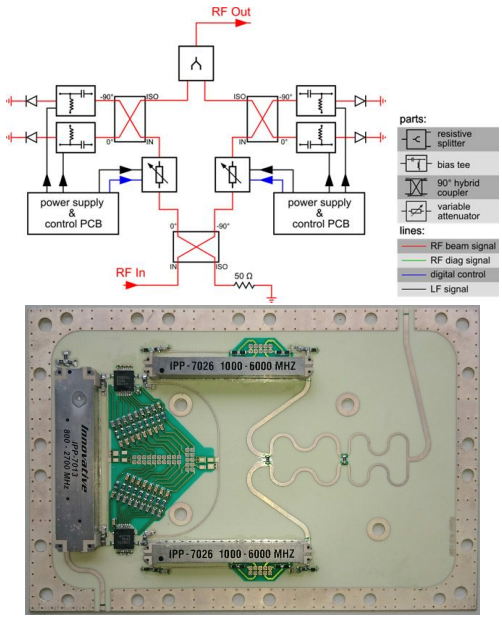

Figure 3: Block diagram and prototype RF PCB of the variable phase shifter.

The in-house design of demanding RF components has been continued: The pickup module controller and the versatile power supply and control unit are under development. The series of variable attenuators has been ordered. A functioning prototype of the variable phase shifter is now

DOI:10.15120/GR-2017-1

available (Fig. 3). The measured data show that the critical values: constant signal delay (1.818 ns $\pm$ 7 ps), high phase resolution ($< 1^0$), minimal phase distortion ($< \pm 3.5^0$), flat amplitude response and fast rampability (>10 kPoints/s) are within acceptable limits. Therefore, the device is only a small imperfection to the signal path.

The preseries unit (mw power 250 W in the 1-2 GHz band, water cooled) of the ordered power amplifiers at the kickers has been tested. The device demonstrates the design concept, nicely complies with the demanding RF properties and the full electrical specification (Fig. 4). However, it is not reliable for long-time operation and not yet mature for series production. Improvements are under way at the manufacturer to meet these reliability goals. A new round of factory and site acceptance tests is planned in 2017.

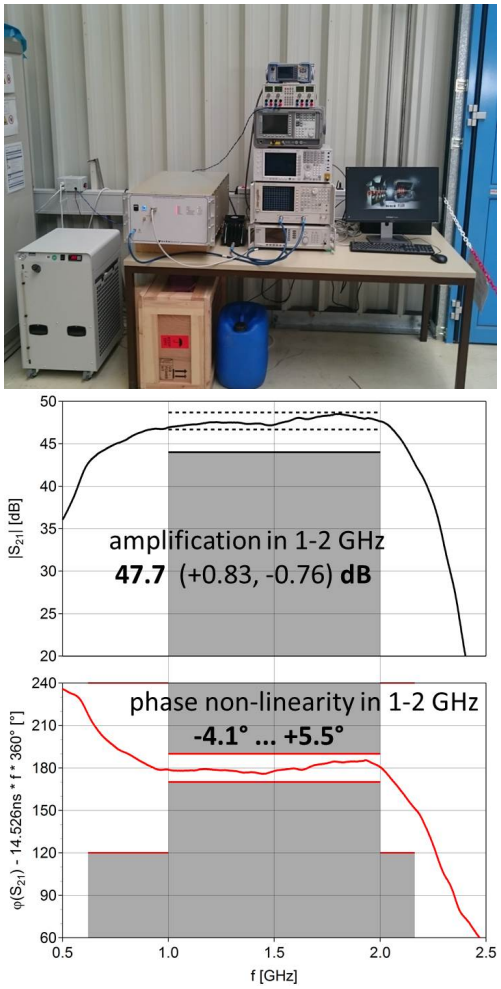

Figure 4: SAT (Site Acceptance Test) of the prototype power amplifier at GSI: test set-up and measured amplitude and phase response compared with the specification.

Expected stochastic cooling performance

New simulations of the stochastic cooling performance for the most demanding case of 10^8 antiprotons at 3 GeV in the CR have been performed taking into account the finalized lattice parameters and the realistic response of the designed slotline electodes. Cooling in all 3 phase space planes, with constant power gain of 150 dB in the longitudinal plane (notch filter momentum cooling with the pickups in sum mode) and constant power gain of 138 dB in both transverse planes (horizontal and vertical betatron cooling with the pickups in difference mode) has been studied, assuming no plunging of the pickup electrodes (Fig. 5). Already with the simple pessimistic assumption of constant transverse gain and no pickup plunging, simultaneous cooling in all 3 planes for 10 s leads to phase space quality close to the design limits for the HESR downstream.

Plunging the pickup electrodes reduces the diffusion in all 3 phase space planes from the beginning. The final emittances and momentum spread are lower by a factor 2-3 compared to the non-plunging case.

Therefore, the demanding pbar momentum spread budget between CR and HESR should be within reach by optimizing the interplay among the long. and transv. cooling in the CR and the rebunching/debunching procedures of the transfer. However, longitudinally there seems to be no safety margin, the high power requirement remains.

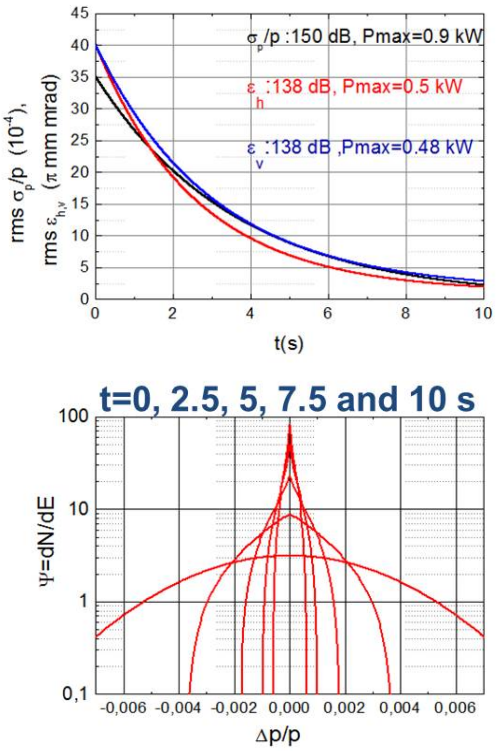

Figure 5: Reference case for stochastic cooling of 10^8 antiprotons at 3 GeV in the CR with the conservative assumption of no plunging. Four times (i.e. accounting for statistical beam signal fluctuations) the total maximum cw power is just within the installed microwave power of 8 kW.

DOI:10.15120/GR-2017-1

In-beam tests of the new secondary electron detector for FAIR*

P. Boutachkov[1], *C. Dorn*[1], *P. Forck*[1], *H. Graf*[1], *C. Müller*[1], *H. J. Reeg*[1], *A. Reiter*[1], *S. Schwarz*[1], *and B. Walasek-Höhne*[1]

[1]GSI, Darmstadt, Germany

The task of the Particle Detector Combination (PDC) detectors is to measure the beam intensity of slowly extracted ion beams. The complete range of possible beam intensities at FAIR cannot be covered by single detector type. At GSI this task is accomplished by a combination of three detectors, a plastic SCintillator (SC), an Ionization Chamber (IC) and a Secondary Electron Monitor (SEM).

The GSI-SEM detector has an active area of 80x80 mm^2, and is build from three 100 μm Al foils. For FAIR a larger and thinner detector is required. The new FAIR-PDC-SEM detector is shown in Fig. 1. The active area is a circle with a diameter of 107 mm. It is built from three 24 μm aluminum foils mounted 5 mm apart on ceramic isolators. The foils are shaped in order to remove mechanical vibrations. The outer foils were positively biased, collecting the secondary electrons knocked out by the ion beam. The central foil was connected via a short cable to the current-to-frequency converter described in Ref. [1]. The presented study investigates the response of the new FAIR-PDC-SEM detector.

Electrons are excited during the passage of charged particles through matter. Some of these electrons will have sufficient energy to migrate to the material surface and escape. The SEM detector measures the amount of these secondary electrons under controlled conditions. The beam current is calculated based on the measured secondary electron current and the experimentally determined secondary electron yield for a single beam ion. The yield for relativistic ions from thin foil is proportional to the energy lost in the material, for Al foil it is in the order of 30 electrons per $MeV/(mg/cm^2)$ [2]. It depends on the foil material and the surface condition. Assuming that the surface of the foil is saturated with defects created during manufacturing, shaping and cleaning, one expects similar yields for different foils from the same material.

The secondary electron yield is experimentally determined by first calibrating the IC detector relative to the SC. In a second measurement the SC detector is removed and the beam current is increased. The SEM secondary electron current is measured as a function of the beam intensity, determined by the IC.

A comparison between the data obtained in this work and the measurements by P. Forck et al. [2] is shown in Fig. 2. The derived secondary electron yields agree for the measurements performed with C, Xe and U beams.

In summary, secondary electron yields from different Al foils were compared. The data supports the idea that surfaces saturated with defects have similar secondary electron yields.

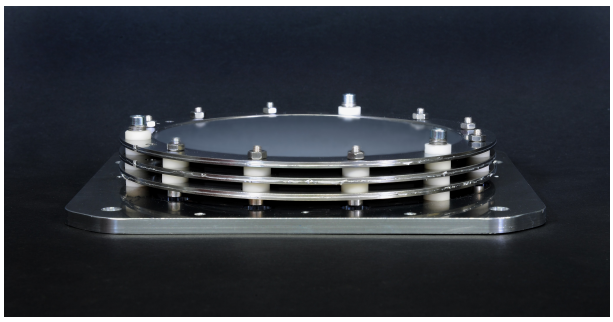

Figure 1: A photograph of the FAIR-PDC-SEM detector. The rings holding the Al foils have an inner diameter of 107 mm.

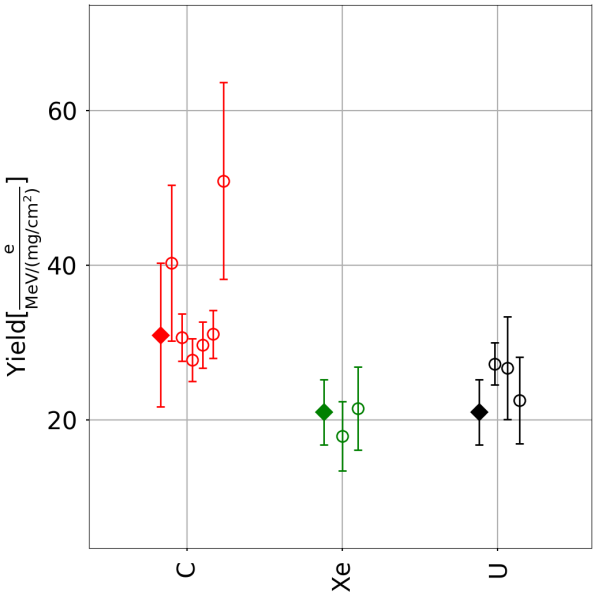

Figure 2: Secondary electron yields, measured with C, Xe and U. Filled-Rhombus: Data from the new FAIR-PDC-SEM, obtained at 300 MeV/u. Open-circles: Data from the GSI-SEM, Ref. [2], obtained at energies between 270 MeV/u and 1095 MeV/u.

References

[1] H. Reeg, DIPAC99, Chester, p. 147 (1999)

[2] P. Forck, P. Heeg, A. Peters, AIP Conf. Proc. 390, 422 (1997)

* It is pleasure to acknowledge the members of the GSI operating team for their support during the experiments.

Pressure profiles simulations of HEBT vacuum system for the FAIR project

P.M. Suherman, L. Urban, A. Kraemer, J. Cavaco, F. Hagenbuck
GSI, Darmstadt, Germany

Introduction

To achieve the aimed operating pressure (10^{-8} mbar), the pressure profiles of the HEBT (High Energy Beam Transport) beam lines for the FAIR project have been simulated. The simulation of pressure profiles are used to optimise the amount and specifications of the required pumps at specific locations along the beam lines. This report only presents the T1S beam line of the HEBT system. T1S beam line consists of 4 consecutive beam line sections, i.e. T1S1, T1S2, T1S3, and T1S4. T1S1 is the first incoming beam line to the HEBT system from existing synchrotron SIS18 (after TE1 section), whereas, T1S4 beam line section is an injection beam line from HEBT to a new built synchrotron SIS100.

Pressure Profile Simulations

The pressure profile reported in this work was calculated based on an analytical model [1]. Figure 1 shows a comparison of pressure profiles of T1S beam line calculated using different nominal pumping speeds (200, 400, and 800 l/s). As shown in Figure 1, there is no significant difference in pressure profiles for different nominal pumping speeds. This demonstrates that the constraint in the pump optimisation for the HEBT system is conductance limited. Since the chambers are conductance limited, adding more pumps with different pumping speed at more positions may be one of the alternatives to improve the pressure profile distribution. The addition of more pumps, however, is sometimes restrained by the available space. Some beam lines are mostly occupied by quadrupole, dipole, and steerer magnets.

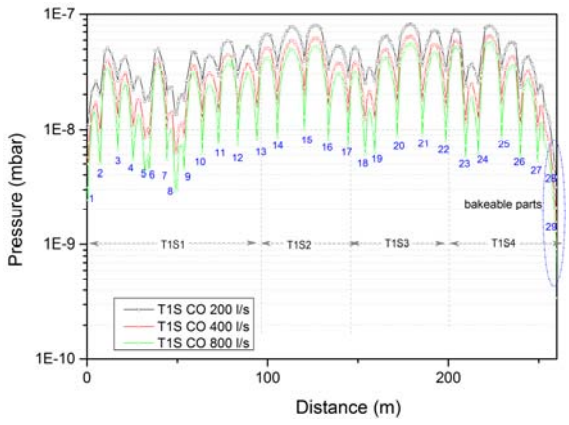

Figure 1: Pressure profiles for T1S beam line for CO based conductance. The numbers in sequence show positions for vacuum pumps.

Figure 2 shows pressure profiles for T1S beam line calculated based on CO conductance, with a combination of various pumping speeds and additional pumps at some locations at the beam line. The 200 l/s pumps were used as additional pumps, which were located in the middle of long straight chambers. The additional pumps of 400 l/s and 800 l/s were also introduced at the end of the T1S4 section that is connected to the synchrotron SIS100. As shown in Figure 2, the pressure profile distribution improved slightly with the use of additional pumps. The improvement was more pronounced at the end of T1S4 section, where the bakeable parts that are connected to the synchrotron SIS100 can now achieve the required pressure range of approximately 10^{-11} mbar.

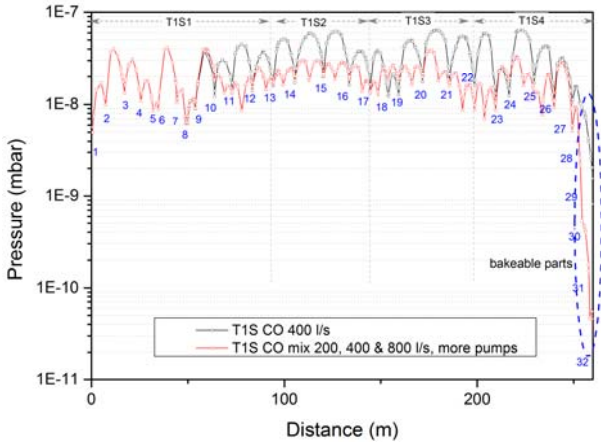

Figure 2: Pressure profiles for T1S beam line for CO based conductance with additional pumps. The numbers in sequence show positions for vacuum pumps. The positions of extra pumps are not all numbered.

The pressure profile presented in this work is only a guideline to estimate the specification and the amount of vacuum pumps needed for the HEBT vacuum system. There are many other factors that are not considered in the calculation, such as the use of partial pressure in the calculation, gas dependence for nominal pumping speed, dynamic gas loads in the system and the 'beam effect' on the chamber materials that may affect the desorption yield and conductance.

Note:

- The simulation in this work was based on the beam line from CATIA® drawing for HEBT in 2014. Based on this calculation, the pump distributions for some of the HEBT beam lines have been slightly changed, in order to reach a better operating pressure.
- Part of this work has been published in [2].

References

[1] V. Ziemann, http://ziemann.web.cern.ch/ziemann/
[2] P.M. Suherman, et. al, Vacuum, 2015, v. 122, p. 268

DOI:10.15120/GR-2017-1

Tests of ZnO, fast inorganic scintilators for Counting Applications at FAIR*

P. Boutachkov, C. Andre, A. Reiter, and B. Walasek-Höhne
GSI, Darmstadt, Germany

In the FAIR High Energy Beam Transport (HEBT) lines scintillation counting detectors will be used to measure the absolute beam intensity and spill structure as a function of time. The measurements will be performed with an organic plastic sintilator inserted into the path of the ion beam. The same type of detectors are used at GSI, see Reference [1] for further details. Due to radiation damage, the routinely used scitillators are exchanged yearly. The presented study was started in order to find a radiation hard scintillation material to be used in the HEBT particle counters. We investigated the response to heavy ions and the radiation hardness of ZnO:Ga and ZnO:In ceramic scintillators. The samples are described in Reference [2].

A photograph of the experimental setup is shown in Figure 1. The heavy ion beam from SIS-18 comes from the right. It is collimated to a spot with a diameter of 5 mm by the Aluminum collimator, indicated as COL in the picture. An ionization chamber (IC) is used to determine the dose deposited by the beam into the studied samples. The samples are inserted into the beam with a remotely controlled manipulator, indicated as SCI. A photo-multiplier (PMT) detected the scintillation light.

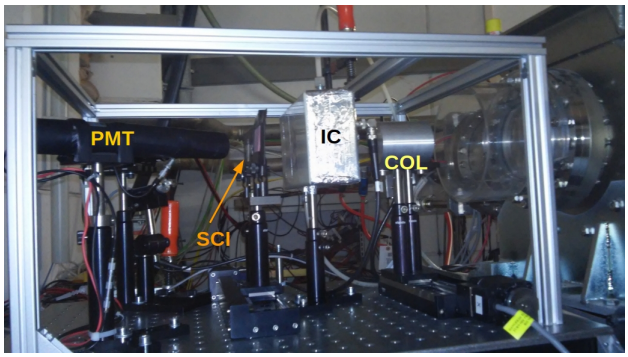

Figure 1: A photograph of the experimental setup. See the text for details.

The response to 300 MeV/u ^{238}U ions of 1 mm thick BC400 plastic scintillator and 0.4 mm thick ZnO:Ga and ZnO:In ceramics is shown in Figure 2. The measurement demonstrates that the fall times of the different scintillating materials is similar. In contrast, the light yield of the ZnO ceramics was about 2 times lower compared to the one of the BC400 scintilator. Hence, in terms of counting capability the ZnO ceramics can be used as a replacement of the plastic scintilators as the lower light yield can be compensated by a higher PMT gain.

The radiation hardness of the ZnO samples was studied with 300 MeV/u U, Xe beams. The ions punched through the material. The preliminary data analysis showed that the ZnO:In and ZnO:Ga generate usable signals for particle counting at 1000 higher integral particle number than the number of particles sufficient to damage a BC400 plastic scintillator.

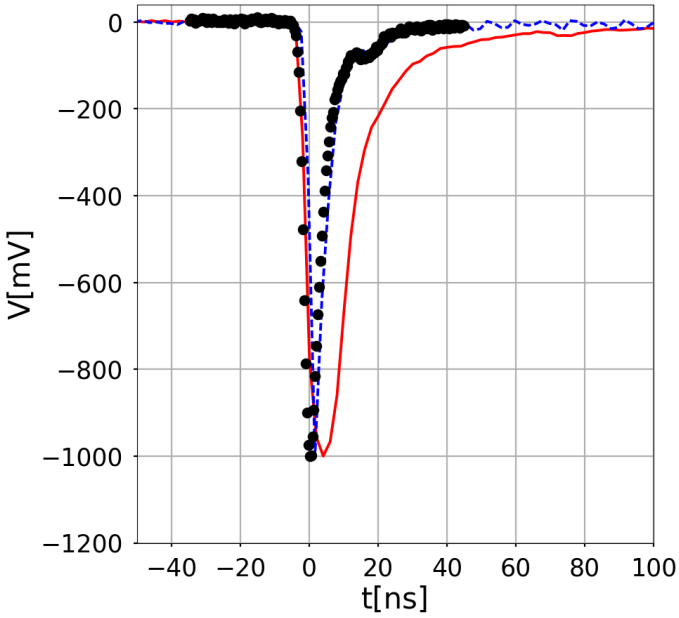

Figure 2: Comparison of the rise and fall times of the studied materials. The signals are scaled to 1V. Red line: BC400 signal. Blue-dotted: ZnO:Ga signal. Black-circles: ZnO:In signal.

In summary, ZnO:In and ZnO:Ga are promising substitutes of the plastic scintilators used in the HEBT particle counting detectors. Further investigations of these promising materials and the construction of large size detectors for heavy ions are planned.

References

[1] P. Forck, P. Heeg, A. Peters, AIP Conf. Proc. 390, 422 (1997)

[2] P. A. Rodnyi, K. A. Chernenko, E. I. Gorokhova, S. S. Kozlovskii, V. M. Khanin, IEEE Trans. Nucl. Sci. 59, 2152 (2012)

* It is pleasure to acknowledge the members of the GSI operating team for their support during the experiments.

DOI:10.15120/GR-2017-1